# Stratigraphic revision and remapping of the Mathinna Supergroup between the River Tamar and the Scottsdale Batholith, northeast Tasmania

Department of Infrastructure, Energy and Resources
Mineral Resources Tasmania

Tasmania
Explore the possibilities

*Cover: Overturned thick-bedded sandstone sequence of the Stony Head Sandstone in a disused quarry on the eastern shore of the Curries River Reservoir near Lefroy.*

Mineral Resources Tasmania
Department of Infrastructure, Energy and Resources

Tasmania
Explore the possibilities

## *1:25 000 Scale Digital Geological Map Series — Explanatory Report 4 —*

# Stratigraphic revision and re-mapping of the Mathinna Supergroup between the River Tamar and the Scottsdale Batholith, northeast Tasmania

## Explanatory report for parts of the 1:25 000 scale Low Head, Tam O'Shanter, Weymouth, Retreat, Lilydale, Bridport, Bowood, Nabowla, Lisle and Patersonia map sheets

***by D. B. Seymour, I. R. Woolward, M. P. McClenaghan and R. S. Bottrill***

**June 2011**

Mineral Resources Tasmania PO Box 56 Rosny Park Tasmania 7018
Phone: (03) 6233 8377 ● Fax: (03) 6233 8338
Email: info@mrt.tas.gov.au ● Internet: www.mrt.tas.gov.au

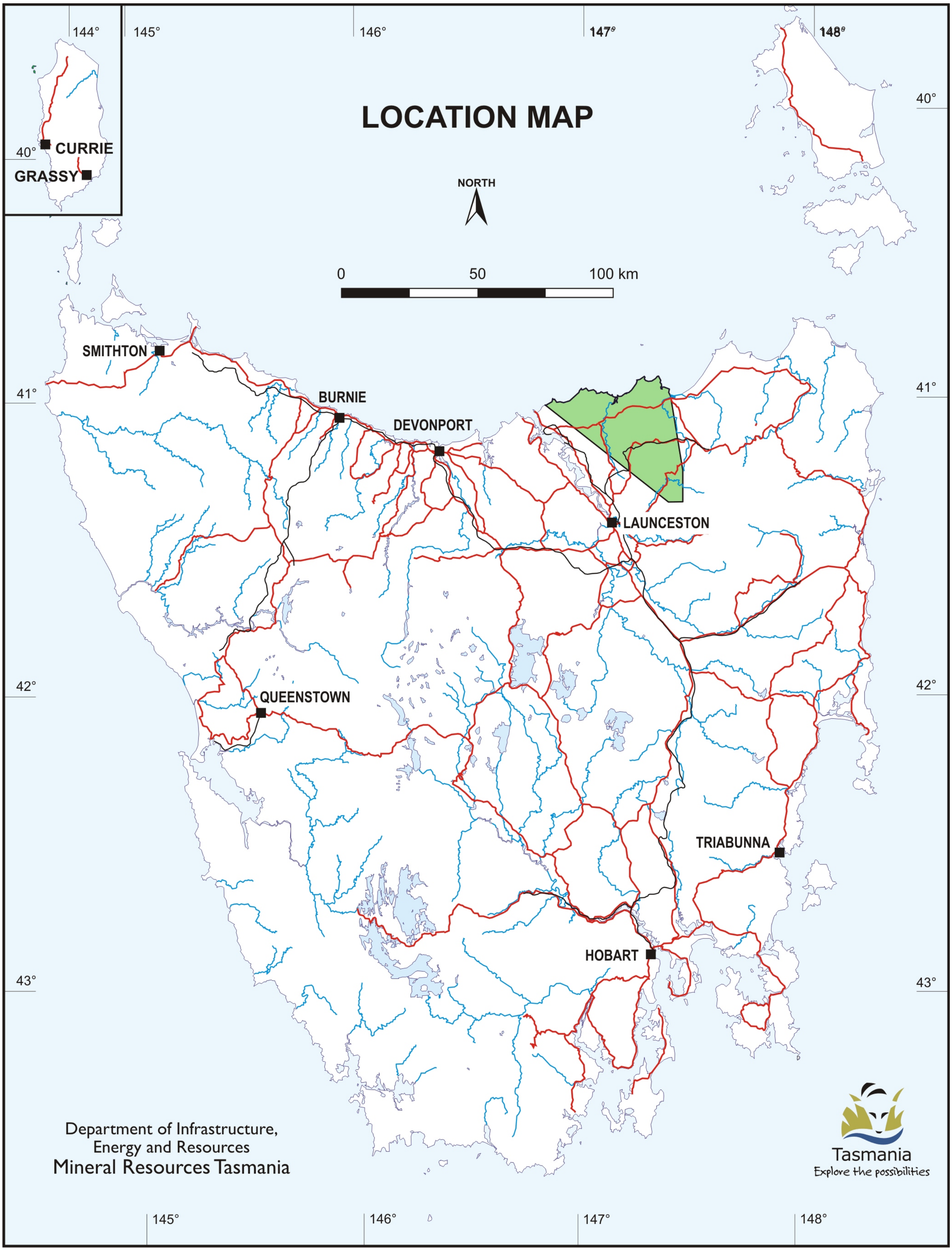


SEYMOUR, D. B.; WOOLWARD, I. R.; MCCLENAGHAN, M. P.; BOTTRILL, R. S. 2011. Stratigraphic revision and re-mapping of the Mathinna Supergroup between the River Tamar and the Scottsdale Batholith, northeast Tasmania. Explanatory report for parts of the 1:25 000 scale Low Head, Tam O'Shanter, Weymouth, Retreat, Lilydale, Bridport, Bowood, Nabowla, Lisle and Patersonia map sheets. *Explanatory Report 1:25 000 Scale Digital Geological Map Series Mineral Resources Tasmania* 4.

# CONTENTS

**INTRODUCTION** … 5
Previous work … 7
**STRATIGRAPHY** … 11
Stratigraphic revision of the Mathinna Supergroup … 11
Tippogoree Group … 11
*Stony Head Sandstone* … 11
Age control … 11
Field relationships and characteristics … 11
*Turquoise Bluff Slate* … 14
Age control … 14
Field relationships and characteristics … 14
*Industry Road Member* … 14
*Main body* … 14
Panama Group … 15
*Yarrow Creek Mudstone* … 15
Age control … 15
Field relationships and characteristics … 15
*Retreat Formation* … 16
Age control … 16
Previous work … 16
Field relationships and characteristics … 17
*Lone Star Siltstone* … 17
Age control … 17
Field relationships and characteristics … 17
*Sideling Sandstone* … 20
Age control … 20
Previous work … 20
Field relationships and characteristics … 20
**STRUCTURAL GEOLOGY** … 22
Introduction … 22
Structural relationship between the Tippogoree and Panama groups … 22
Structural analysis … 28
*Tippogoree Group structure* … 28
*Be*$D_1$ structures … 28
?*Ta*$D_1$ structures … 31
*Ta*$D_3$ structures … 31
*Panama Group structure* … 32
Yarrow Creek Mudstone … 32
*Ta*$D_1$ *structures* … 32
*Ta*$D_2$ *structures* … 32
*Ta*$D_3$ *structures* … 32
Retreat Formation … 32
*Ta*$D_1$ *structures* … 33
*Ta*$D_2$ *structures* … 33
*Ta*$D_3$ *structures* … 33
Lone Star Siltstone … 36
*Domain analysis* … 36
Sideling Sandstone … 45
Structural effects of granitoid intrusion … 50
**METAMORPHISM** … 51
Granitoid-related contact metamorphism … 51
**GEOPHYSICS** … 51
Introduction … 51
Gravity … 51
*Anomalies and features* … 51
*Worms* … 52
Magnetics … 52

*Anomalies and features* … 52
*Worms* … 55
Radiometrics … 56
*Anomalies and features* … 56
**GOLD MINERALISATION** … 57
Orogenic gold: Lefroy–Back Creek goldfields … 57
Intrusion-related gold … 59
*Lisle goldfield* … 60
*Golconda, Panama and Cradle Creek goldfields* … 60
*Denison goldfield: hybrid deposits?* … 60
*Other deposits of note* … 61
**SUMMARY AND DIRECTIONS FOR FURTHER WORK** … 62
Acknowledgements … 63
**REFERENCES** … 64
**APPENDIX 1:** ASUD stratigraphic definitions … 66
**APPENDIX 2:** Palaeontology and biostratigraphy … 78
**APPENDIX 3:** Major and trace element analyses, Lone Star Siltstone and Sideling Sandstone … 80

## TABLES

1. Revised stratigraphy for Mathinna Supergroup … 11

## FIGURES

1. Evolution of geological mapping of Ordovician–Devonian sedimentary successions between the River Tamar and the Scottsdale Batholith … 6
2. Evolution of structural models for Ordovician–Devonian sedimentary successions in NE Tasmania … 8
3. Revised stratigraphic model for Ordovician–Devonian sedimentary successions in NE Tasmania … 10
4. Summary map of MRT *TasExplore* project remapping and stratigraphic revision of the Mathinna Supergroup … 12
5. Representative outcrop photographs of the Stony Head Sandstone … 13
6. K-Th-U RGB image of merged WTRMP and *TasExplore* project airborne radiometric data … 16
7. Representative outcrop photographs of the Retreat Formation … 18
8. Outcrop characteristics of the Lone Star Siltstone … 19
9. Geochemical discrimination diagrams showing analyses of samples of siltstone from the Lone Star Siltstone and Sideling Sandstone, and sandstone from the Sideling Sandstone … 21
10. Structural profiles and cross sections through the Mathinna Supergroup west of the Scottsdale Batholith … 23
11. Representative clips from revised MRT 1:25 000 scale digital geology coverage showing structural relationships across the inferred fault contact between the Tippogoree and Panama groups … 26
12. 3-D oblique orthographic view towards about SSE showing Mathinna Supergroup remapping west of the Scottsdale Batholith in relation to interpretation of offshore reflection seismic line 148/04 … 27
13. Lower hemisphere equal-area stereograms of structural data from the Stony Head Sandstone … 28
14. Lower hemisphere equal-area stereograms of structural data from the Turquoise Bluff Slate … 29
15. $BeS_1$ fabrics in the Turquoise Bluff Slate … 30
16. Lower hemisphere equal-area stereograms of structural data from the Yarrow Creek Mudstone … 33
17. Summary geological map of the outcrop area of the Panama Group west of the Scottsdale Batholith, showing domain boundaries used for structural analysis … 34
18. Lower hemisphere equal-area stereograms of structural data from the Retreat Formation … 35
19. Lower hemisphere equal-area stereograms of structural data from the Lone Star Siltstone … 38
20. Lower hemisphere equal-area stereograms of structural data from the Sideling Sandstone … 46
21. Summary map showing statistically preferred orientations of axes to folds in bedding and of penetrative cleavage in all structural domains in the Panama Group … 48
22. Map showing the result of spatial averaging of 738 measurements of penetrative cleavage in the Panama Group, presented as strikes of resultant average orientations … 49
23. Images of new or updated geophysical coverages following *TasExplore* project data acquisition for the area west of the Scottsdale Batholith, masked to show only responses within outcropping Mathinna Supergroup rocks, and with Middle Devonian granodiorite outcrop, revised faults and geological boundaries overlain … 53
24. 3-D potential field edge data, colour-contoured for upward continuation height, for new or revised geophysical datasets covering the area between the River Tamar and the Scottsdale Batholith … 54
25. Contrasting styles of gold mineralisation in the Lefroy and Lisle areas … 58

# INTRODUCTION

The folded Early Ordovician to Early Devonian clastic sedimentary successions of northeast Tasmania have been referred to as the Mathinna Beds (Banks, 1962; Williams, 1978; Baillie *et al*., 1989), the Mathinna Group (Powell and Baillie, 1992; Powell *et al*., 1993) and the Mathinna Supergroup (Reed, 2001). A full stratigraphic subdivision of the sequence has only been attempted in the area between the western margin of the Scottsdale Batholith and the River Tamar. This is effectively the type area of the Mathinna Supergroup and is also the main subject of this report.

The public-domain geological knowledge base of the Mathinna Supergroup prior to the work reported here was the net result of several overlapping programs of investigation: the regional geological mapping program of the Geological Survey of Tasmania (under its then parent organisation, the Tasmania Department of Mines); a variety of specific thematic project studies carried out by the Department of Mines and its successor Mineral Resources Tasmania; and a number of University Honours thesis and published research studies. The Geological Survey's regional mapping program (at publication scales of 1:63 360 and 1:50 000) in northeast Tasmania spanned the 30-year period from 1963 to 1993, by which time all of the rock sequences now known as Mathinna Supergroup were covered by first-edition geological maps at one of the two scales. Most of the area west of the Scottsdale Batholith was covered by maps published very early in this program (principally Launceston in 1964 and Pipers River in 1965, with minor contributions from Noland Bay in 1967 and Beaconsfield in 1971). Post-1993 program reorganisations meant that the planned second-edition updating of these older maps did not initially proceed. Thus, by the time of commencement of MRT *TasExplore* project work in northeast Tasmania in 2008, and despite several studies focussed on revising the stratigraphy and structural history of the Mathinna Supergroup (and the nature of the Devonian intrusive bodies), the government geological map coverage of its type area had not been updated for some 40 years. During planning of *TasExplore* work in northeast Tasmania this issue particularly stood out as a priority, to validate and extend recent advances in the stratigraphic and structural knowledge of the district and to provide an enhanced understanding of controls on the location of gold deposits.

The *TasExplore* planning phase also identified that northeast Tasmania was the only remaining Strategic Prospectivity Zone (SPZ) not yet completely covered by public-domain airborne geophysical data coverages (particularly TMI and three-channel K-Th-U radiometric data) of quality equal to the 200 m line-spacing coverage previously acquired for all of the western Tasmanian SPZs during the previous Western Tasmanian Regional Minerals Program. This data, when collected under *TasExplore* for northeast Tasmania prior to commencement of ground follow-up, showed strong indications, particularly in the radiometric coverage, that the Mathinna Supergroup west of the Scottsdale Batholith may indeed be subdividable into a number of formation-scale lithological units (probably sandstone-rich and mudstone-rich units, based on the radiometric signatures). Such subdivision had previously been initiated by Powell and Baillie (1992) and Powell *et al*. (1993) based on structural and section-logging studies. In the early stages of *TasExplore* geological fieldwork in northeast Tasmania, reconnaissance of some of the more obvious signature boundaries in the radiometric data confirmed that they reflect real large-scale lithological differences in the Mathinna sequences. The substantial extent of the signature boundaries in the radiometric data, and the implied significant differences from existing geological mapping, to a large degree reduced the ground follow-up program in the Mathinna Supergroup type area to a re-mapping exercise, rather than refining an already near-correct geological map coverage or commencing higher-level studies based on the existing coverage. This also highlighted the need to carefully record the lithological composition of sequences at individual outcrops, in particular to at least qualitatively record proportions of sandstone (and its grain size), siltstone, mudstone and shale — a step which had probably not always been taken in the earlier regional mapping due to a common perception that the Mathinna succession comprised a "monotonous succession of turbidites" in which attempts at subdivision would prove futile. A major advance of the *TasExplore* fieldwork has been to subdivide the Mathinna Supergroup in its type area into six formations (three of them newly defined), including the addition of one newly defined member (fig. 1*d*).

As well as the stratigraphic issues, it was clear at the start of the *TasExplore* work that there were also significant questions to be addressed about previous structural interpretations. The eastern limit of the 'Pipers River recumbent zone' needed to be more precisely mapped, and there was also the question of whether the strongly east-vergent $D_1$ structures were confined to the Ordovician sequences (as concluded by Reed, 2001) or were an expression of an early phase of Devonian deformation which affected the entire Mathinna Supergroup terrane (as proposed by Patison *et al*., 2001).

The *TasExplore* geophysical data acquisition included a significant upgrade of the ground gravity station coverage in northeast Tasmania, and while it has been possible to make some fresh observations from the new data, at the time of completion of this report a revised 3-D model of the Devonian granitoids based on interpretation of the updated coverage was still incomplete. Consequently references herein to gravity-based interpretation of the granitoids refer to the model of Leaman and Richardson (2003).

The re-mapping in this part of the *TasExplore* project covered an area in excess of about 950 km$^2$ (equivalent to nearly five full 1:25 000 scale map sheet areas but spread over parts of eleven sheets), and was by necessity of a standard varying between detailed examination of critical areas to reconnaissance-level in others, in order to meet project deadlines. The fieldwork took place intermittently over two years, assisted by the new geophysical coverages. Project time constraints did not allow inclusion of more time-consuming local data collection such as detailed section

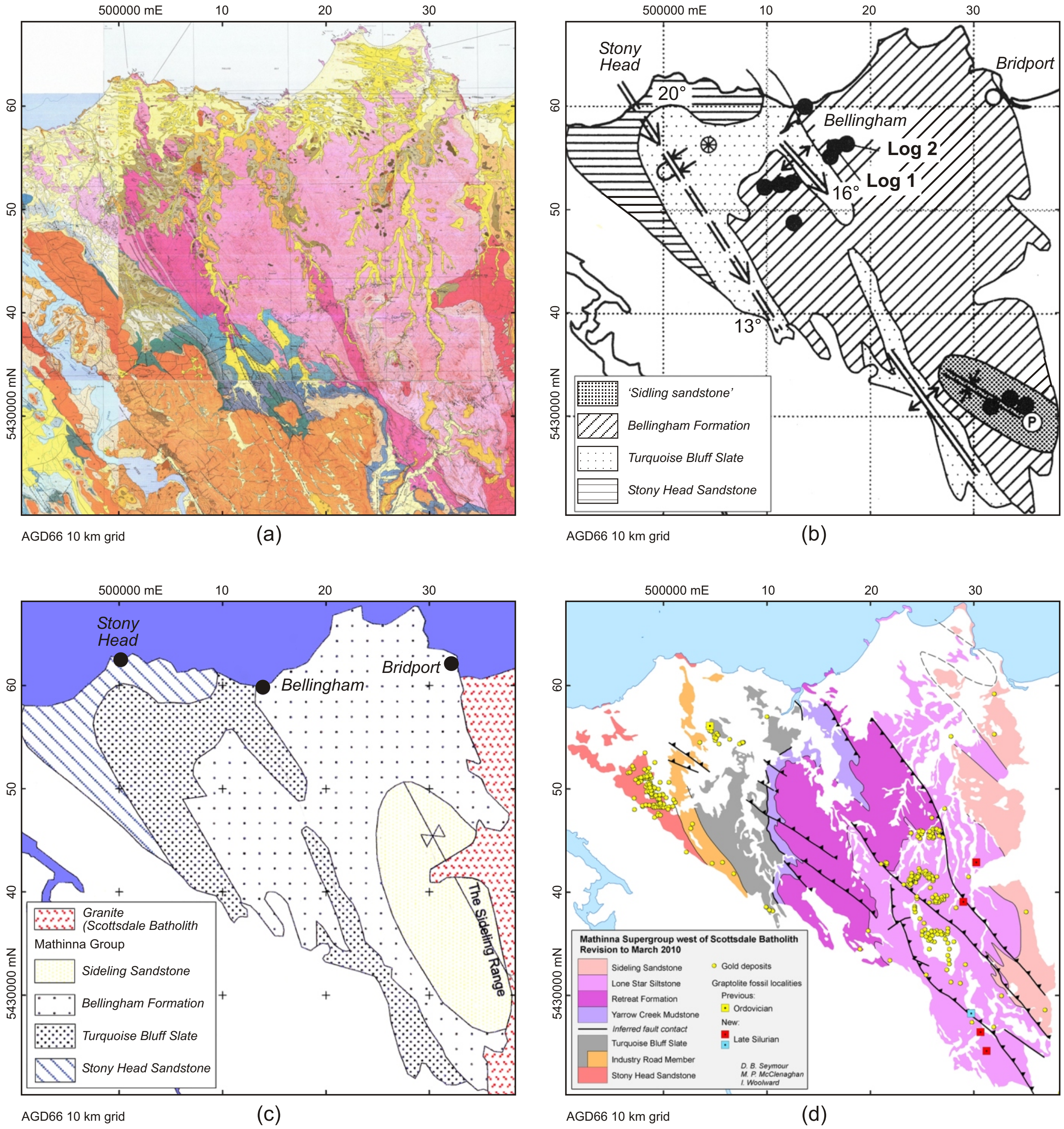


**Figure 1**

*Evolution of geological mapping of Ordovician–Devonian sedimentary successions between the River Tamar and the Scottsdale Batholith: (a) Geological Survey 1:63,360 scale mapping 1964–1971; (b) Powell et al. (1993); (c) Thompson (2000); (d) MRT TasExplore Project 2008–2010.*

logging and statistical analysis of palaeocurrents at individual outcrops. However the main outcomes, of upgraded geological mapping, a revised stratigraphic framework for the Mathinna Supergroup, and improved knowledge of the structural architecture, were achieved and will provide a better framework for mineral exploration and further stratigraphic-sedimentological studies of the type pioneered by Powell *et al*. (1993).

For consistency with the revised 1:25 000 scale maps, all grid references in the text are GDA94 datum and are MGA co-ordinates in Zone 55, quoted in the form xxxxxx/yyyyyyy, where the first six numbers are metres east and the last seven numbers are metres north; all azimuths quoted in the text are relative to grid north in the same datum. Grids on some GIS-generated regional-scale map figures are in the superseded AGD66 datum (and annotated accordingly), due to datum migration in MRT's map production system being in progress during the course of the project; the legacy datum should not be an issue at the reproduction scale of these figures. As the revised 3-D geological model of northeast Tasmania is initially being built in AGD66 datum, georeferencing coordinates on all of the structural profiles and cross sections in Figure 10 (which are part of the control for the new model) are also in the legacy AGD66 datum.

## Previous work

Banks (1962) divided the 'Mathinna Beds' into two lithological associations: a lutite association consisting dominantly of lutite with a subordinate arenite component; and an arenite-lutite association consisting of sandstone or coarse siltstone grading up into fine siltstone or claystone in most places, the latter being equal or subordinate in thickness to the former. This is also essentially the subdivision that was used in the first-generation 1:63,360 scale geological survey maps (published between 1963 and 1971) covering the region between the River Tamar and the Scottsdale Batholith (fig. 1*a*). Structural analysis associated with the production of the Pipers River map sheet (Marshall *et al*., 1965; Marshall, 1969) yielded the first published evidence that the 'Mathinna Beds' had been affected by two phases of folding and associated cleavage formation. Marshall (1969) also recognised a significant $D_1$ structural domain boundary within the Pipers River map sheet area, whereby the $S_1$ penetrative cleavage is dominantly recumbent in an area in the western part of the sheet largely occupied by the lutite association, and dominantly upright further to the east. This appears to be the first recognition of the 'Pipers River recumbent zone', now believed to be confined to the Ordovician components of the Mathinna Supergroup, and which was to feature prominently in later structural interpretations.

The establishment of a formal stratigraphic subdivision of the 'Mathinna Beds' did not begin until the work of Powell and Baillie (1992), who introduced the name Mathinna Group and used the terms Stony Head Sandstone, Turquoise Bluff Slate and Bellingham Formation for its three lowermost outcropping formations (the base of the sequence is not exposed). The principal age control was an Early Ordovician graptolite which had previously been recovered from the Turquoise Bluff Slate (Banks and Smith, 1968). Powell and Baillie (1992) also constructed a composite structural profile along the line of Bridport Road, which delineated the 'Pipers River recumbent zone' and showed that it is largely, if not completely, confined to the Ordovician successions (Stony Head Sandstone and Turquoise Bluff Slate). Their interpretation correlated these east-vergent recumbent local $D_1$ structures with the more upright (but still east vergent) local $D_1$ structures in the Bellingham Formation, and attributed all of these $D_1$ structures, and the later west-vergent semi-upright $D_2$ structures, to Early Devonian orogenesis (but $D_1$ pre-dating emplacement of the St Marys Porphyrite at 388 1 Ma; Turner *et al*., 1986). The zone of recumbent structures was attributed to body rotation of originally more upright $D_1$ structures above an east-dipping ramp in a $D_2$ sole thrust at a depth of about 10 km below the 'recumbent fold zone' (fig. 2*a*). As noted by Reed (2001) and by E. Williams (pers. comm., 1993), the Powell and Baillie (1992) structural model generates the recumbent fold zone by body rotation only without internal deformation in the rotated block, which creates accommodation problems at the margins of the recumbent zone. If the internal simple shear necessary to avoid the geometric problems is introduced within the rotated block, the rotation of pre-existing structures generated is insufficient to produce the observed shallowly-dipping axial surfaces, unless the model is re-generated with an unrealistically steep ramp angle on the sole thrust (Reed, 2004).

The stratigraphic terminology introduced by Powell and Baillie (1992) was fully formalised in the stratigraphic-sedimentological study by Powell *et al*. (1993), which included definitions of the new units. Also included was an informal unit, the 'Sidling sandstone' (note that the name of the reference topographic feature, either the highway section known as The Sideling or the Sideling Range, was inadvertently mis-spelt), overlying the Bellingham Formation and containing Early Devonian plant fossils.

This publication included a somewhat generalised regional-scale geological map showing the inferred extent of the new units in the area west of the Scottsdale Batholith (fig. 1*b*), although data collection was largely confined to a traverse across the north of the area and centred on Bridport Road, together with some localities on The Sideling in the south. Detailed section logging and palaeocurrent measurements were focussed on turbiditic sandstone-rich sections, in the lower part of the Bellingham Formation, and in correlates of the 'Sidling sandstone' (and possibly the upper Bellingham Formation) in the Scamander area in the eastern part of the then-termed Mathinna Group terrane. Reconnaissance palaeocurrent data were collected from the 'Sidling sandstone' type area. The Bellingham Formation data indicated deposition of quartzose sublitharenite in a submarine fan system prograding to the ENE, consistent with derivation from stable platform areas to the southwest. The 'Sidling sandstone' type area data indicated southeast-directed currents, implying a source from the northwest.

Data from the 'Sidling sandstone'/upper Bellingham Formation correlates at Scamander indicate deposition in two large fan systems with mutually opposed palaeocurrent

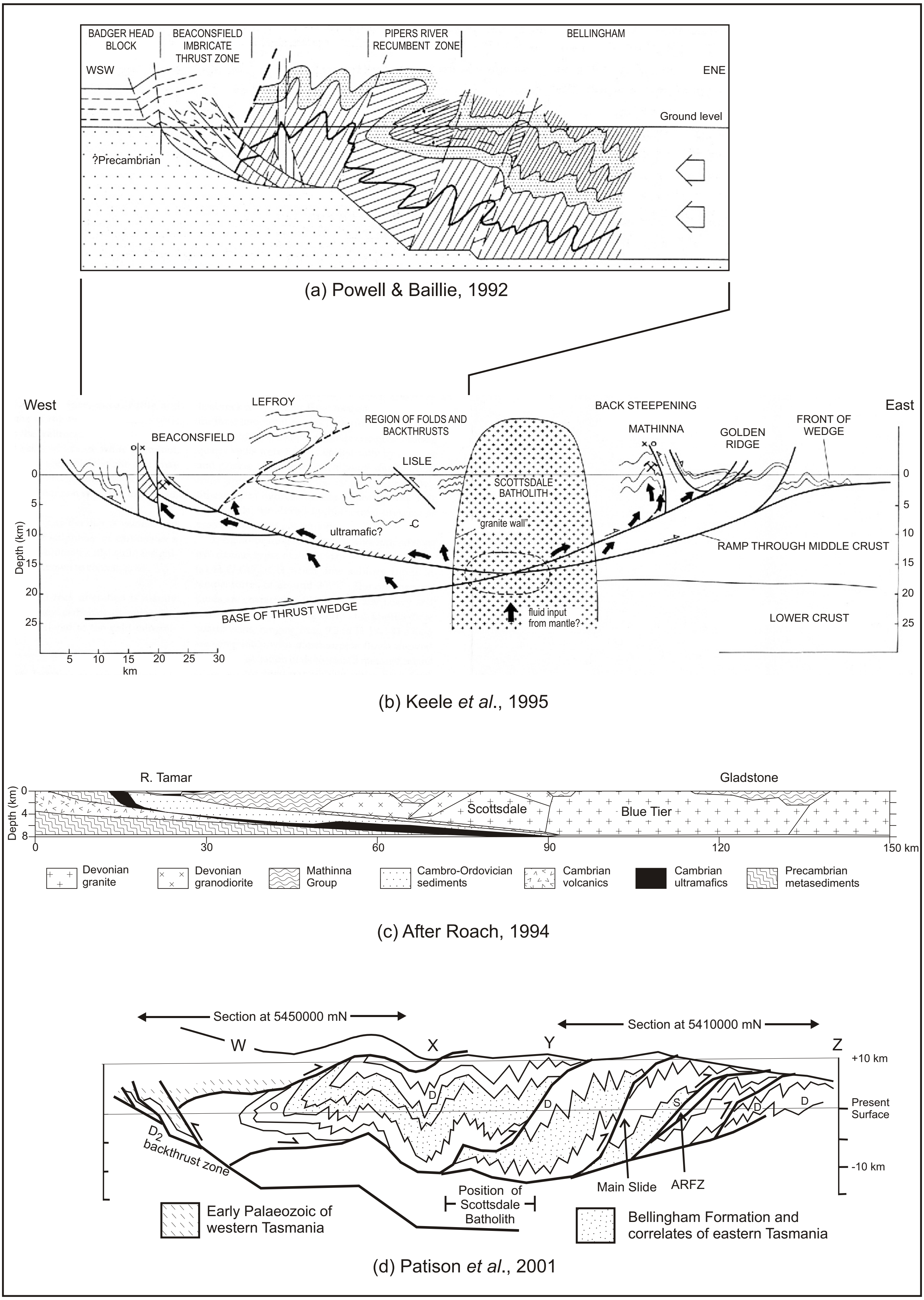


**Figure 2**

*Evolution of structural models for Ordovician–Devonian sedimentary successions in northeast Tasmania. Sources as shown.*

directions parallel to a NNW elongate basin. Sandstone compositions of sublitharenite to litharenite with a minor but significant proportion of feldspar, particularly in the SSE prograding fan system, were interpreted as due to derivation of the latter from Late Silurian–lowermost Devonian silicic igneous rocks in southeastern Australia. It is noteworthy that detrital zircons from a sandstone sampled near a Late Silurian graptolite locality stratigraphically below the Scamander sections (Black *et al*., 2004; Rickards *et al*., 1993) show no age peaks younger than 455   12 Ma (Late Ordovician–Early Silurian) but further detrital zircon sampling from the Scamander area would be needed to investigate this further.

In a structural interpretation for MRT's NetGold project, Keele *et al.* (1995) modelled the Eastern Tasmanian terrane as a gently west-dipping thrust wedge, composed of mid-Palaeozoic strata which experienced crustal thickening during mid-Devonian orogenesis (fig. 2*b*). West of the Scottsdale Batholith, the model shows upright to recumbent folds above a region of major back-thrusting lying some 10 km below the 'Pipers River recumbent zone' and surfacing at Beaconsfield, and which originated from a point where the main $D_1$ thrust wedge ramped up through the strong middle crust (fig. 2*b*). The 'Pipers River recumbent zone' is interpreted to be the lower side of a shallowly dipping east-directed thrust, or a 'pop-up' zone, which may be linked at depth to the west-directed back-thrust system (fig. 2*b*). Maximum crustal thickening and tectonic uplift of the wedge is inferred at the Tamar Valley, where Devonian strata are elevated by up to 10 km compared to strata of the same age in the front part of the wedge. The model suggests overall eastward tectonic transport in the Eastern Tasmanian terrane, consistent with eastward structural vergence within the Melbourne Zone of central Victoria.

Publication of the NetGold work coincided with completion of a geophysics doctoral thesis by Roach (1994), who produced regional cross sections through northeast Tasmania based on simultaneous modelling of magnetic and gravity data. Compared with previous models, a lower angle on the west-directed thrusts west of the Scottsdale Batholith was required, with the main west-directed thrust penetrating to less than six kilometres depth below the 'Pipers River recumbent zone' (fig. 2*c*). The model includes a substantial slab of (presumably Early Cambrian) ultramafic rock above this thrust at depth (to explain a large deep-sourced magnetic anomaly in the Noland Bay–Anderson Bay area), a feature which was also included in the Keele *et al.* (1995) model. While this major thrust by implication has significant Devonian movement (because of the age of the rocks it displaces at Beaconsfield), its representation as the structural contact between a slab of presumed Early Cambrian ultramafic rocks and underlying pre-Mathinna Supergroup ?Proterozoic basement implies that it is likely to be a reactivated Cambrian structure.

A university honours thesis study by Thompson (2000) used the formal name Sideling Sandstone (correcting the previous mis-spelling, although a formal definition and nomination of a type section were not provided) and produced a detailed structural, stratigraphic and sedimentological analysis of this unit. Several sandstone facies were recognised within the sequence. An included revision of the Powell *et al.* (1993) map showed a considerably greater areal extent for the Sideling Sandstone (fig. 1*c*).

A combined structural and metamorphic study by Patison *et al.* (2001) envisaged an eastward-tapering tectonic wedge subsequently exhumed by westward back-thrusting, yielding a total crustal thickening of approximately 10 km (fig. 2*d*), essentially a refinement of the model of Keele *et al.* (1995). In an essentially two-phase structural history, an Early Devonian $D_1$ event involved east-directed thrusting and tectonic thickening, and a foreland-propagating thrust wedge. $D_1$ pre-dated the extrusive phase of the St Marys Porphyrite (388   1 Ma; Turner *et al*., 1986) and probably all of the large Early to Middle Devonian granodiorite plutons. Peak metamorphism occurred after the east-directed thrusting as a result of crustal thickening. During $D_2$, which post-dated the St Marys Porphyrite but pre-dated the Middle to Late Devonian adamellite and granite plutons, $D_1$ structures were refolded about an upright $S_2$ cleavage, linked to back-thrusting in the Beaconsfield area (as suggested by Powell and Baillie, 1992). In this model, the 'Pipers River recumbent zone' is largely a product of $D_1$, while the more upright structures to the east of it, and overprinting it, would be assigned to $D_2$. What is not adequately explained is why the recumbent structures are apparently confined to the Ordovician successions, and why the locally-earliest upright folds in the successions immediately to the east have penetrative axial planar cleavage (when axial planar crenulation cleavage might be expected if these folds are younger than the recumbent foliation).

Reed (2001) proposed an alternative structural model for northeastern Tasmania, in which east-vergent recumbent folds and thrusts were generated during a $D_1$ event correlated with the early Silurian Benambran Orogeny (Gray and Foster, 1997) of mainland Australia, and which affected only the Ordovician units (the Stony Head Sandstone and Turquoise Bluff Slate). This was followed by two Devonian deformation events: $D_2$, which pre-dated Devonian granitoid intrusion, and produced generally upright folds with NE vergence and some reactivation of earlier recumbent folds (recognised by a second, disjunctive cleavage at an acute angle to and overprinting the slaty axial-plane cleavage in some recumbent folds, both these cleavages pre-dating upright $S_3$ crenulation cleavage); and $D_3$, which post-dated dominantly I-type but pre-dated dominantly S-type granitoids, reversed the tectonic vergence and thrust eastern Tasmania against the western Tasmanian Proterozoic basement, producing generally upright folds with SW vergence and SW-directed thrusts (including the Beaconsfield imbricate thrust zone). The prospect of a major deformation event separating the upper and lower parts of what was previously known as the Mathinna Group led Reed (2001) to propose its elevation to supergroup status, encompassing two new groups separated by an inferred unconformity: the Tippogoree Group comprising the Stony Head Sandstone and Turquoise Bluff Slate; and the Panama Group encompassing the remaining, younger units including the Bellingham Formation and the 'Sidling sandstone' (fig. 3).

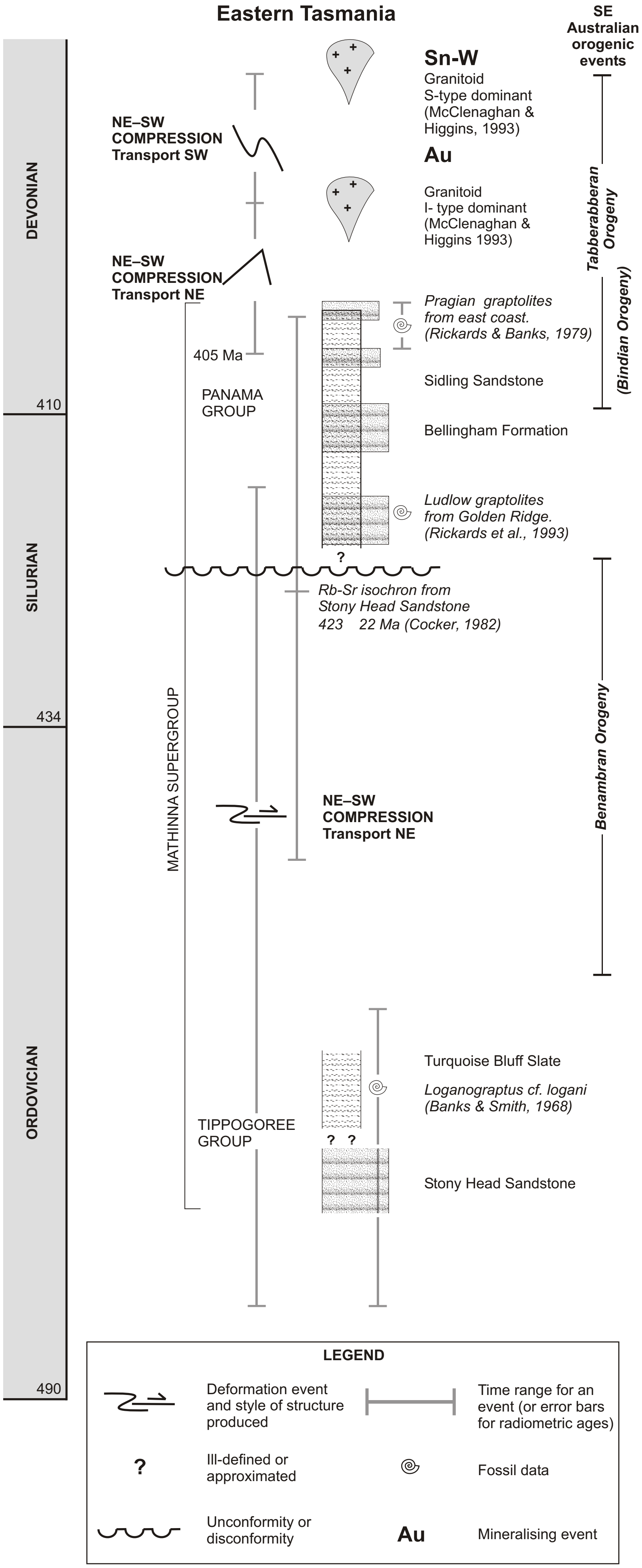


**Figure 3**

*Revised stratigraphic model for Ordovician–Devonian sedimentary successions in northeast Tasmania, according to Reed (2001).*

## Stratigraphic revision of the Mathinna Supergroup

Remapping of the Mathinna Supergroup type area during the *TasExplore* project, assisted by the new airborne geophysical coverages, has enabled the establishment of a revised stratigraphy with the addition of four new formal units (fig. 4, Table 1). The most prominent change is the replacement of the previous Bellingham Formation with three new formations below the Sideling Sandstone (now fully formalised with corrected spelling) in the Panama Group. In the Tippogoree Group, the new Industry Road Member is distinguished as a basal transitional facies within the Turquoise Bluff Slate. The subdivision by Reed (2001) into the Tippogoree and Panama groups is retained, and the new mapping has revealed indications of a fault boundary between the two groups (as first suggested by Turner, 1980).

In map view, a narrow strip of pelite interpreted on previous maps as a structural inlier of Turquoise Bluff Slate in the central southern part of the area (fig. 1*b,c*) is now recognised as part of an extensive late Silurian pelitic unit defined as the Lone Star Siltstone, which contains several new graptolite fossil localities discovered by Ian Woolward during the *TasExplore* fieldwork (fig. 4; Appendix 2). A further significant change to the map is the much larger extent of the Sideling Sandstone, now recognised in a series of linked synclinal cores spanning a 43 km north–south distance along the eastern margin of the area (fig. 4).

## Tippogoree Group

### *Stony Head Sandstone*

#### Age control

The Stony Head Sandstone is the oldest exposed unit of the Mathinna Supergroup. At the time of the work of Powell and Baillie (1992) and Powell *et al.* (1993), the main constraint on the age of the formation was an Early Ordovician graptolite (*Loganograptus* sp.) previously recovered from the overlying Turquoise Bluff Slate (Banks and Smith, 1968) — although on the latest (2008) ICS timescale the age range of this fossil may be early to middle Ordovician. A further constraint now exists in that the deposition of the Stony Head Sandstone must post-date the age of the youngest detrital zircon grains within it. Black *et al.* (2004) found that the youngest zircons are likely to comprise three separate populations: 584 11 Ma (18 analyses), 525 8 Ma (27 analyses) and 455 30 Ma (4 analyses). With all constraints taken into account, the age of deposition of the Stony Head Sandstone is most probably Early Ordovician.

#### Field relationships and characteristics

While not the main focus of their work, Powell *et al.* (1993) described the Stony Head Sandstone as comprising thick (>1 m), graded beds of medium to fine-grained sandstone with minor amounts of pelite, the sandstone being characterised by a distinctive stripy cleavage spaced at centimetre intervals in the coarser bases of sandstone beds

**Table 1**

*Revised stratigraphy for Mathinna Supergroup*

| | Group | Formation | Member | Age | Brief description | ASUD status |
|---|---|---|---|---|---|---|
| Mathinna Supergroup | Panama Group | Sideling Sandstone | | Early Devonian (plant fossils) | Dominantly fine-grained sandstone, some interbedded siltstone | Spelling correction & formalisation of existing unit |
| | | Lone Star Siltstone | | Late Silurian (graptolites) | Dominantly thin-bedded siltstone, with interbedded fine-grained sandstone increasing towards top | New formal unit |
| | | Retreat Formation | | Silurian? | Interbedded turbiditic medium to very fine grained sandstone and subordinate siltstone-mudstone | New formal unit |
| | | Yarrow Creek Mudstone | | Silurian? | Dominantly thin-bedded mudstone, with subordinate cross-laminated siltstone | New formal unit |
| | *Inferred fault contact* | | | | | |
| | Tippogoree Group | Turquoise Bluff Slate | | Early–Middle Ordovician (graptolites) | Phyllitic dark grey-black slate; recumbent folds and cleavage | Existing formal unit |
| | | | Industry Road Member | Early–Middle Ordovician? | Interbedded phyllitic slate and foliated very fine-grained sandstone; ridge-forming; recumbent folds and cleavage | New formal unit |
| | | Stony Head Sandstone | | Early Ordovician? | Graded thick-bedded fine-grained turbiditic sandstone with minor interbedded pelite; large-scale recumbent folds and cleavage | Existing formal unit |

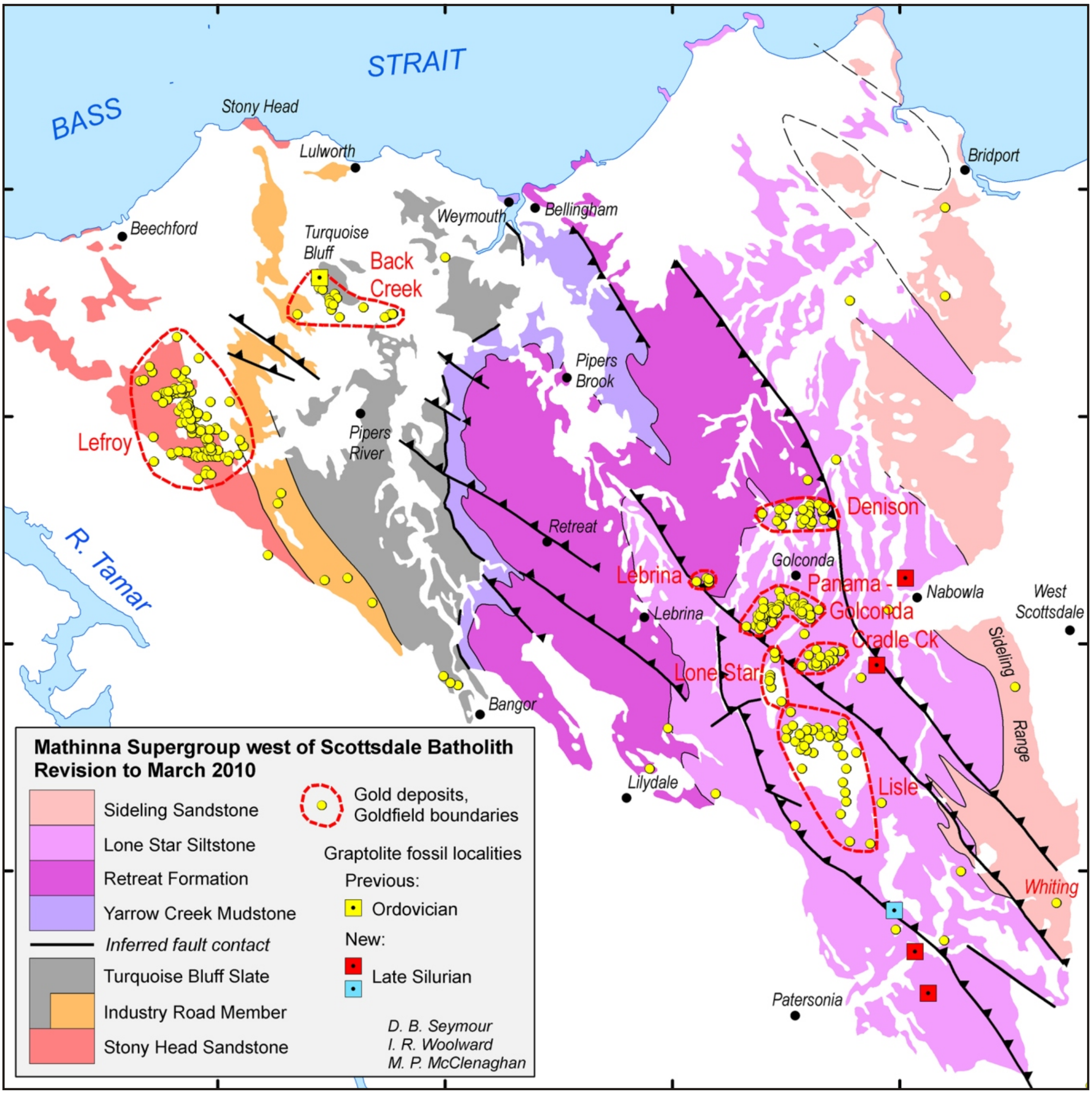


**Figure 4**

*Summary map of MRT TasExplore Project revision of the Mathinna Supergroup between the River Tamar and the Scottsdale Batholith. Gold deposits and previous and new fossil localities indicated (new locality attribution: red points — Ian Woolward, MRT; blue point — Launceston Field Naturalists Club and Queen Victoria Museum and Art Gallery, Launceston).*

(fig. 5*a*). The latter feature was noted to be in common with Early Ordovician turbidites exposed near Bermagui on the New South Wales south coast. The facies was correlated with Facies C of Walker and Mutti (1973), i.e. medium to fine-grained sandstones representing classical proximal turbidites beginning with Bouma's division A. Formation thickness was estimated as >1 km, with no exposed base and a fairly sharp transition at the top into overlying massive cleaved mudstone of the Turquoise Bluff Slate.

The Stony Head Sandstone is well exposed in weathered road cuts on Bridport Road between 498430/5448245 and 500895/5448745, and in somewhat fresher outcrops on the Bass Strait coast one to three kilometres west of Beechford. Probably the best single exposure is in a large abandoned quarry at 496700/5449735 on the eastern shore of the Curries River reservoir (fig. 5*b*). All of these exposures were re-examined in the fieldwork for this report, but the work did not extend to detailed section logging. Unfortunately the coastal section at Stony Head now lies within an active artillery range administered by the Australian Army, and cannot be accessed for other than brief accompanied visits.

The Bridport Road and Beechford sections, and other isolated exposures in between, all lie on the overturned limb of a major northeast-vergent semi-recumbent fold (Powell and Baillie, 1992; fig. 10*a*). While some second-order folding is present, it is not as prominent as in the other units in the Mathinna Supergroup, and typical outcrops show overturned sandstone beds with minor interbedded slaty

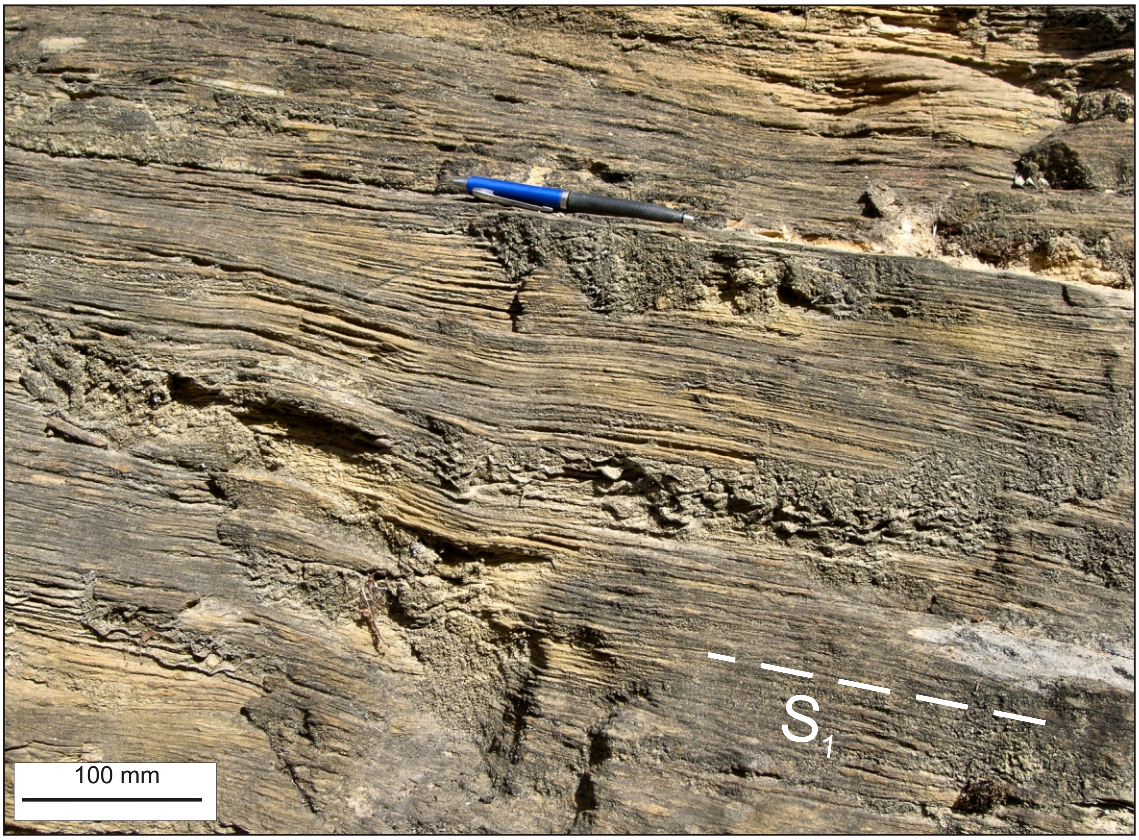


(a)

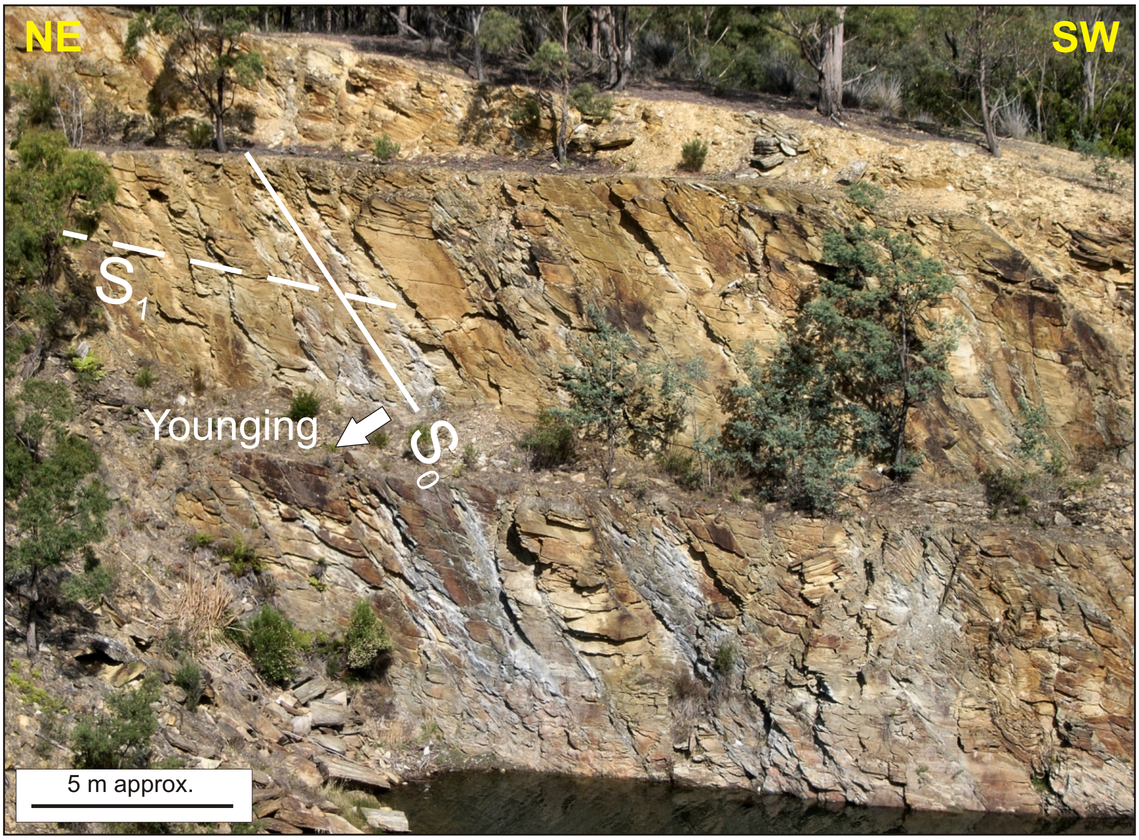


(b)

**Figure 5**

*Representative outcrop photographs of the Stony Head Sandstone: (a) BeS$_1$ stripy cleavage in a weathered road cutting at 499385/5448505 on Bridport Road; (b) overturned thick-bedded sandstone sequence of the Stony Head Sandstone in a disused quarry at 496700 / 5449715 on the eastern shore of Curries River Reservoir.*

pelite, dipping southwest at 30–65° with a prominent gently dipping $S_1$ foliation which is commonly expressed as a stripy cleavage in the sandstone beds (fig. 5*a*). The sandstone is quartz rich and occurs in graded beds, which are up to two metres in thickness in some exposures. Grain size calibration at re-examined outcrops indicates that most of the sandstone is very fine grained, with fine and rarely medium grades occurring in the lower to basal parts of some graded beds. Structural profiles suggest a revision of the minimum formation thickness to perhaps 1.5 km (fig. 10).

It is notable that the detrital zircon age spectrum of the Stony Head Sandstone shows little or no evidence of provenance in either the Cambrian Mt Read Volcanics or the Proterozoic inliers of western Tasmania, which has been taken as an indication that western and northeastern Tasmania were not joined or in close proximity at the time of deposition (Black *et al*., 2004).

## Turquoise Bluff Slate

### Age control

The age of the Turquoise Bluff Slate is based on two specimens of the graptolite *Loganograptus* sp. recovered from the Australasian Slate Quarries (504570/5456375), and assigned an Arenigian to Llanvernian age (possibly upper Castlemanian stage) by Banks and Smith (1968). A later assignment to the stage range Bendigonian Be1 to Darriwilian Da3 (pers. comm. Fons VandenBerg in Reed, 2001) would translate to Early to Middle Ordovician on the most recent (2008) ICS stratigraphic chart. Despite regular examination of the slate quarry exposures by a number of later workers, no further graptolite specimens have yet turned up and the original discovery has proven fortuitous for age control of the Tippogoree Group.

### Field relationships and characteristics

*Industry Road Member*

While the top of the thick-bedded sandstone-dominant succession which typifies the Stony Head Sandstone is fairly abrupt, as noted in the definition by Powell *et al*. (1993), it has become evident during the *TasExplore* remapping that the lower 1200–1300 m of the overlying Turquoise Bluff Slate is different in overall character to the remainder of the latter formation. This has led to the definition of a basal member of the Turquoise Bluff Slate, the Industry Road Member (see Appendix 1), which consists of interbedded phyllitic slate and foliated, very fine-grained quartz-rich sandstone, and appears to represent a transition package between the dominant facies in the underlying Stony Head Sandstone and in the rest of the Turquoise Bluff Slate.

The mix of resistant quartz-rich lithologies and more easily weathered slate gives the unit a distinctive topographic pattern of parallel strike ridges which distinguish it from the underlying and overlying units. This pattern is particularly visible in high-resolution DEM or LiDAR data and to a lesser extent in aerial photography. The unit shows a subdued striped light-dark pattern on K-Th-U RGB images of airborne radiometric data, presumably due to the interlayered slate and quartz-rich lithologies.

The unit is generally not well exposed despite its ridge-forming tendency. The best exposures may occur within the Australian Army Stony Head Artillery Range (e.g. on Ryans Hill), but because of severe access restrictions this is not considered suitable as a type area. Intermittent representative exposures of the unit occur in road cuttings on Industry Road between 502525/5445380 and 503405/5447600, and this has been nominated as the type area.

The slate component is similar to the lithology dominating the remainder of the Turquoise Bluff Slate. It is typically dark grey and indistinctly bedded internally, probably partly due to the high strain associated with the intense penetrative cleavage, which commonly shows a phyllitic sheen on the foliation surfaces. The other component interbedded with the slate typically comprises quartzose siltstone to fine-grained quartz-rich sandstone with a somewhat less intense but still high-strain penetrative cleavage commonly at a low angle to bedding. Sedimentary structures indicating facing are typically scant, perhaps partly due to the high strain state.

*Main body*

Above the Industry Road Member, the remainder of the Turquoise Bluff Slate typically consists of dark grey-black (weathering to pale grey or white) slate with an intensely developed penetrative cleavage of shallow to intermediate dip which dominates in outcrop, to the extent that bedding is either indistinct or not discernible. The penetrative cleavage commonly shows a distinct phyllitic sheen on foliation surfaces (a characteristic rarely seen in pelites of the overlying Panama Group in the region west of the Scottsdale Batholith). Less commonly, bedding in the slate may be defined by minor, widely-spaced thin beds of quartz-rich siltstone. Rarely, outcrops show distinct thin bedding, or thin layers of pyrite on bedding planes (e.g. in a slate quarry at 510580/5438305 near Bangor). The succession also includes rare sections up to several metres thick dominated by fine-grained quartz-rich sandstone, in which the sandstone:slate ratio may locally reach 2:1 or more (e.g. in road cuts near 510465/5456200). Quartz veins parallel to $S_1$ are common, probably a consequence of the high strain state, and have resulted in the formation of a high proportion of vein quartz float and lag in soil overlying the unit. This is thought to be the cause of a less bright signature on K-Th-U RGB radiometric imagery than would otherwise have been expected, given the very pelitic composition of the unit. The penetrative cleavage is commonly overprinted by a later steep-spaced crenulation cleavage and associated open folds. Profile sections suggest there could be up to one kilometre of preserved section of the Turquoise Bluff Slate above the Industry Road Member, but this is uncertain due to common mesoscopic semi-recumbent folding.

Powell *et al*. (1993) equated the Turquoise Bluff Slate with Facies G of Walker and Mutti (1973), i.e. pelagic and hemipelagic shale and marl — deposits of very dilute suspensions. Except for the rare beds and intervals of quartz-rich sandstone or siltstone, most of the unit essentially represents background sedimentation in which the Bouma sequence is not applicable.

## Panama Group

### *Yarrow Creek Mudstone*

#### Age control

The Yarrow Creek Mudstone is the lowest unit of the redefined Panama Group, a conformable sequence of four formations in which the third formation from the base, the Lone Star Siltstone, contains Late Silurian (Ludlow) graptolites. It is in fault contact with the underlying Turquoise Bluff Slate which contains Early Ordovician graptolites. The Panama Group is inferred to have an unconformable relationship with the Tippogoree Group (see *Structural Geology* section), but as the unconformity is apparently not exposed it is uncertain whether a basal conglomerate or other units below the Yarrow Creek Siltstone exist but remain concealed. The Yarrow Creek Mudstone is probably Silurian in age, but no fossils have yet been recovered from it.

#### Field relationships and characteristics

One of the more subtle features identified in K-Th-U RGB imagery of the *TasExplore* radiometric data is a narrow, distinct band of relatively bright signature running north–south east of the Pipers River (between points 1 and 2 on fig. 6), then at its northern end curving around to the east to occupy what appears to be the core of a southeast-plunging anticline SSE of Bellingham (point 3, fig. 6). Subsequent fieldwork has shown that this pattern corresponds to a pelitic unit which is distinct in character from the Turquoise Bluff Slate, and occupies the interval between that unit and the newly defined, sandstone-rich Retreat Formation (see below). The unit has been defined as the Yarrow Creek Mudstone, a new basal formation to the Panama Group (see Appendix 1). Its full thickness is uncertain due to the faulted base, but profile sections indicate a minimum thickness of about 900 metres. It appears to have been partially included in the Turquoise Bluff Slate by Powell *et al.* (1993).

The most obvious distinction between the Turquoise Bluff Slate and the Yarrow Creek Mudstone is a structural one. The Turquoise Bluff Slate is characterised by high strain states, recumbent folds with intensely developed shallowly-dipping axial plane cleavage, and substantial associated quartz veining. Reed (2001) argued that these structures are an expression of an early Silurian deformation event (Benambran Orogeny) which pre-dated the deposition of the Panama Group, but others disagree (Patison *et al.*, 2001). At the mapped contact with the Yarrow Creek Mudstone there is an abrupt and major change in structural style, the latter unit being characterised by upright to steeply inclined, close to less commonly tight folds with a substantially less intensely developed penetrative axial plane cleavage, structures which are inferred to be Devonian in age as they affect a conformable sequence (Panama Group) which includes Late Silurian and Early Devonian fossils. The abrupt change in structural style at the contact has contributed to the mapping of an inferred fault in this position (see further discussion, *Structural Geology* section). In retrospect, the same abrupt structural style boundary appears to be evident about half way along the composite profile published in Powell and Baillie (1992; their fig. 4).

As well as the structural style differences, and more importantly for stratigraphic definition, there are less obvious lithological differences between the Turquoise Bluff Slate and the Yarrow Creek Mudstone. The latter is typically a thin-bedded sequence (bed thickness <300 mm) of cleaved grey mudstone, with subordinate to minor pale-weathering beds of quartz-rich siltstone to very fine-grained sandstone, commonly cross laminated, and occasional beds of fine-grained quartz-rich sandstone. The overall ratio of mudstone : quartz-rich siltstone + sandstone is about 2.7:1, lower than the Turquoise Bluff Slate which probably averages more than three times that figure above the Industry Road Member. The unit is more well bedded, and the mean bed thickness is probably also less, than typical Turquoise Bluff Slate. The unit is reasonably well exposed in low road cuttings on a 1350 m long traverse of Lewis Road between 511320/5444235 and 511990/5444945, which has been nominated as the type locality (see Appendix 1). A 260 m road cut on Bridport Road between 509825/5452195 and 510085/5452170 enables a traverse from typical Turquoise Bluff Slate with dominant intensely developed shallowly-dipping slaty foliation at the western end, through a poorly exposed contact zone which appears to be yielding substantial amounts of vein quartz float, to upright-folded thin-bedded mudstone-siltstone of the Yarrow Creek Mudstone at the eastern end.

One of the two sections that Powell *et al.* (1993) logged in detail within the Bellingham Formation (their Log 1 on Bridport Road) now falls within an area of Yarrow Creek Mudstone on the revised map (fig. 6). However outcrops of the Yarrow Creek Mudstone in the vicinity of Log 1 seem to contain a higher proportion of quartz siltstone to fine quartz-rich sandstone than is typical of most of the formation, and so assignment of the sequence here is somewhat equivocal. Log 1 may represent an upper transitional facies of the Yarrow Creek Mudstone close to the contact with the overlying Retreat Formation. Powell *et al.* (1993) characterised this section as of distal aspect with ENE palaeoflow (after correction for horizontal rotation due to later megakinking, Goscombe *et al.*, 1994). The log showed thin to thick-bedded classical distal turbidites (facies D of Walker and Mutti, 1973) with a relatively low coarse to fine-division ratio (1.3) and ABC index (27%), and two substages that are similar to lobe-fringe or basin-plain (substage 1) and lobe (substage 2) settings. Deposition was envisaged as due to ENE progradation and vertical accretion of the distal part of a turbidite lobe over its fringe and/or adjacent basin plain.

There remains a possibility, that probably cannot be discounted at this stage, that the Yarrow Creek Mudstone represents an uppermost facies or subdivision of the Turquoise Bluff Slate (although the bounding fault makes it impossible to judge whether the latter formation fines upward overall). Even if this were the case, the substantial contrast in strain state and structural style across their mutual contact would suggest that two different levels in the orogenic pile have been juxtaposed on a fault at the contact. On balance, the view is held here that there are sufficient

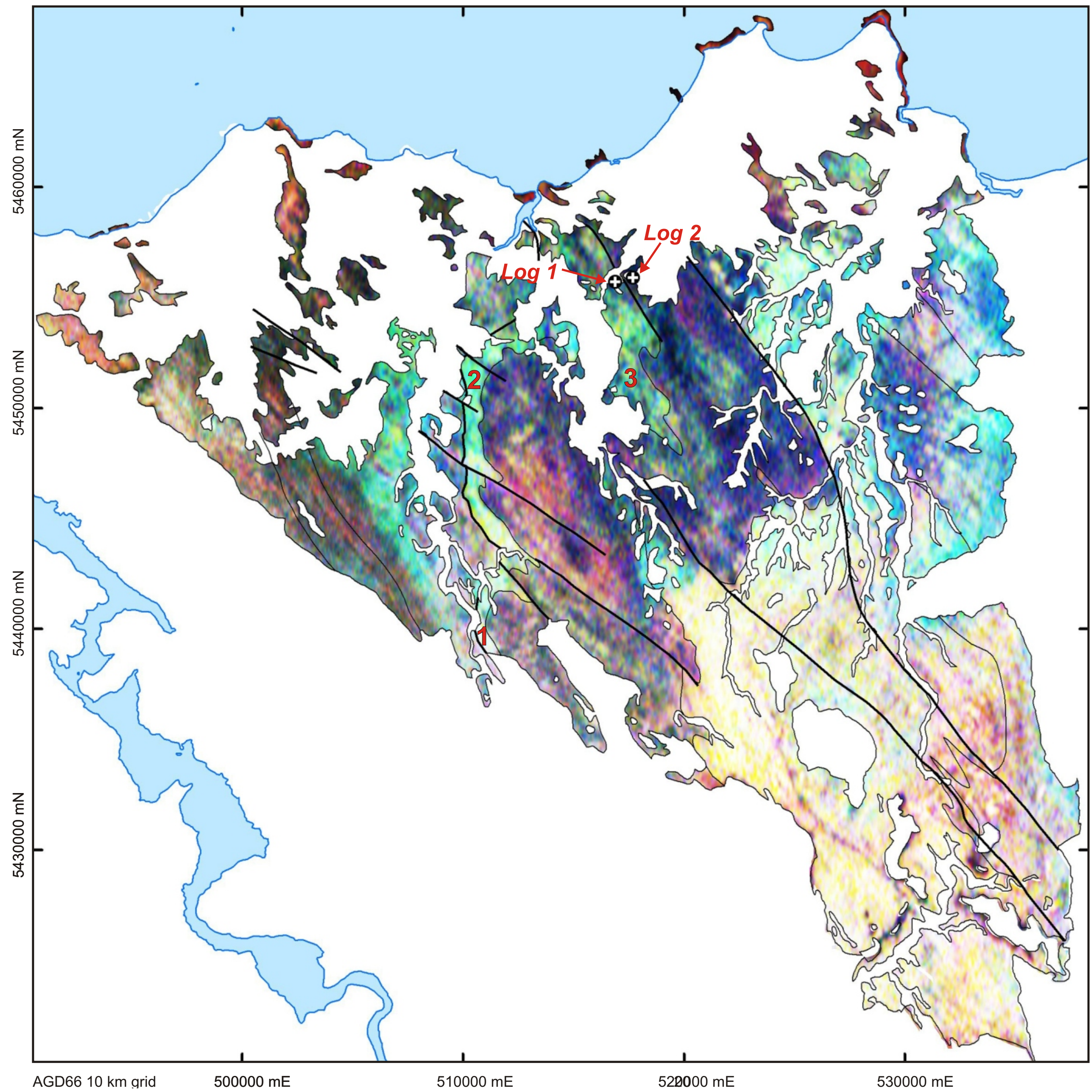


**Figure 6**

*K-Th-U RGB image of merged WTRMP and TasExplore Project airborne radiometric data for the area between the River Tamar and the Scottsdale Batholith, masked to show only responses from areas mapped as Mathinna Supergroup. Overlain boundaries and faults are from Figure 4. Numbered localities shown in red are referred to in text; locations of Logs 1 and 2 of Powell et al. (1993) indicated.*

differences in lithological character for the Yarrow Creek Mudstone to be defined as a separate unit, at the current state of knowledge.

## Retreat Formation

### Age control

Field evidence indicates that the Retreat Formation conformably overlies the Yarrow Creek Mudstone and is conformably overlain by the Lone Star Siltstone. Its age controls are similar to those of the Yarrow Creek Mudstone, i.e. it is older than Late Silurian graptolites in the Lone Star Siltstone and younger than Early Ordovician graptolites in the Turquoise Bluff Slate of the Tippogoree Group. It is probably Silurian in age, but no fossils have yet been discovered within it.

### Previous work

The second of the two sections logged by Powell *et al*. (1993) in the Bellingham Formation, Log 2, falls within an area now assigned to the Retreat Formation and represents a sandstone-rich part of the latter unit (see below). The section was characterised as of proximal aspect with the same ENE palaeoflow as recorded in the nearby Log 1. Using the terminology of Walker and Mutti (1973), the section was classified as facies D, C and ?B2 turbidites, typically thick to very thick bedded (increasingly so up section), intercalated with facies ?G mudrock and thin-bedded facies D turbidites. The coarse to fine-division ratio (2.1) and ABC index (48%) were higher than in Log 1. These facies associations were interpreted, respectively, as channel fill, and interbedded channel-related overbank and hemipelagic deposits. Deposition was envisaged as due to episodic aggradation and ENE progradation of a depositional channel-fill complex and associated overbank deposits ongoing with hemipelagic accumulation.

### Field relationships and characteristics

A prominent feature in the K-Th-U radiometric imagery is a distinctive dark signature (low response in all three channels) forming a Z-shaped pattern in the centre of the area, immediately southeast of the Yarrow Creek Mudstone signature, and which suggests the presence of a set of large plunging folds crossed by northwest-trending faults in several places (fig. 6). Initial field inspection showed that this signature corresponds to a relatively sandstone-rich succession contrasting with the more pelitic units below (Yarrow Creek Mudstone) and above it (Lone Star Siltstone), and subsequent fieldwork has led to its definition as a new formal unit, the Retreat Formation (see Appendix 1).

The Retreat Formation comprises interbedded turbiditic medium to fine-grained quartz-rich sandstone with subordinate to minor interbedded siltstone-mudstone. The percentage of sandstone varies vertically and possibly also laterally within the unit, and this is reflected in variation in the radiometric signature, with darker areas corresponding to the more sandstone-rich sections (fig. 6). Representative folded sections through the more sandstone-rich parts of the formation are exposed on Bare Hill Road and its spur roads, between the intersection with Golconda Road (520700/5443170) and a point some 5.6 km to the north (521565/5448730), and this has been nominated as the type area. Folded reference sections exposing parts of the formation with more interbedded siltstone-mudstone are intermittently exposed on Retreat Road between 513860/5445420 (about 1.5 km north of Retreat), to the intersection with Bridport Road some seven kilometres to the north (512780/5452270). The formation intersects the Bass Strait coast between Pipers Head (near Bellingham) and Fordington, an area in which sandstone-rich sections have been previously noted (e.g. Williams, 1989).

Sandstone-rich parts of the formation (e.g. in the type area) contain graded beds up to two metres thick of quartz-rich medium to fine-grained sandstone commonly showing Bouma A-B or A-B-C bed subdivisions (fig. 7*a,b*), with interbedded combinations of typically thinner-bedded quartzose siltstone (commonly cross laminated), laminated mudstone and shale. These sections typically have ratios 2:1 of sandstone : siltstone-mudstone-shale. Less sandstone-rich sections (e.g. in the reference area) are generally thinner bedded ( 0.5 m) and typically comprise interbedded fine to very fine-grained quartz-rich sandstone, siltstone, grey mudstone and shale with ratios of sandstone : siltstone-mudstone-shale of about 1:1, although some outcrops may show a paucity or absence of sandstone (fig. 7*c–f*). Some sandstone beds and bed sequences in these sections are massive or plane laminated only, and lack grading or other classical Bouma turbidite bed structures (fig. 7*c,e*).

The sandstone-rich parts of the Retreat Formation are partially classifiable as Facies C of Walker and Mutti (1973), i.e. medium to fine sandstones — classical proximal turbidites beginning with Bouma's division A. The less sandstone-rich sequences may in part fall into Facies D (fine and very fine sandstones, siltstones — classical distal turbidites beginning with Bouma's division B or C), but the finer-grained structureless and/or ungraded sandstones and quartzose siltstones may be equivalent to Facies B of Walker and Mutti (1973), in which the Bouma sequence is not applicable. The Retreat Formation was probably deposited in a series of overlapping, laterally migrating and partially coalescing submarine fan complexes, with some of the finer grained and less sandstone-rich sequences deposited in interfan areas of the depositional basin. This would explain the compositional variation which has resulted in the observed variations in radiometric signature (fig. 6).

## *Lone Star Siltstone*

### Age control

Field evidence indicates that the Lone Star Siltstone conformably overlies the Retreat Formation, and is conformably and transitionally overlain by the Sideling Sandstone. Direct age evidence comes from four new graptolite fossil localities discovered during the *TasExplore* fieldwork, together with a previous discovery by the Launceston Field Naturalists Club, a collection from which is housed at Launceston's Queen Victoria Museum and Art Gallery (fig. 4). Formal identification of the fauna at one of the new localities (at 529115/5439235 on Lisle Road) has indicated a Ludlow (mid-Ludfordian) age (Appendix 2). The faunas at all five new localities show strong similarities to an assemblage previously discovered in a correlate of the Lone Star Siltstone at Boags Ridge (542240/5411665; Appendix 2) southeast of the area covered by this report, and to a previously documented fauna at Golden Ridge further east in the terrane (Rickards *et al.*, 1993). Formal identification of both latter faunas has yielded the same biostratigraphic age as the Lisle Road fauna. There is an emerging suspicion that all of these localities may be outcrops of the same horizon, which if so could represent the first terrane-wide marker horizon in the Mathinna Supergroup, currently traceable over a point-to-point distance of 80 km across northeast Tasmania.

### Field relationships and characteristics

Traverses across the upper contact of the sandstone-rich Retreat Formation SSE of Lebrina and west and north of Golconda (fig. 4) reveal it to be a relatively abrupt transition over several metres into an overlying sequence of thin bedded, typically plane-laminated siltstone, mudstone and shale, which is generally lacking in sandstone beds for a substantial interval above the contact. This facies, which has a distinctive bright yellow signature on K-Th-U RGB radiometric imagery (fig. 6), dominates the lower part of a folded, cleaved and faulted siltstone-dominant succession up to about 1.5 km thick, in which beds of quartz-rich sandstone progressively become more common upwards until a transitional contact with the overlying Sideling Sandstone is

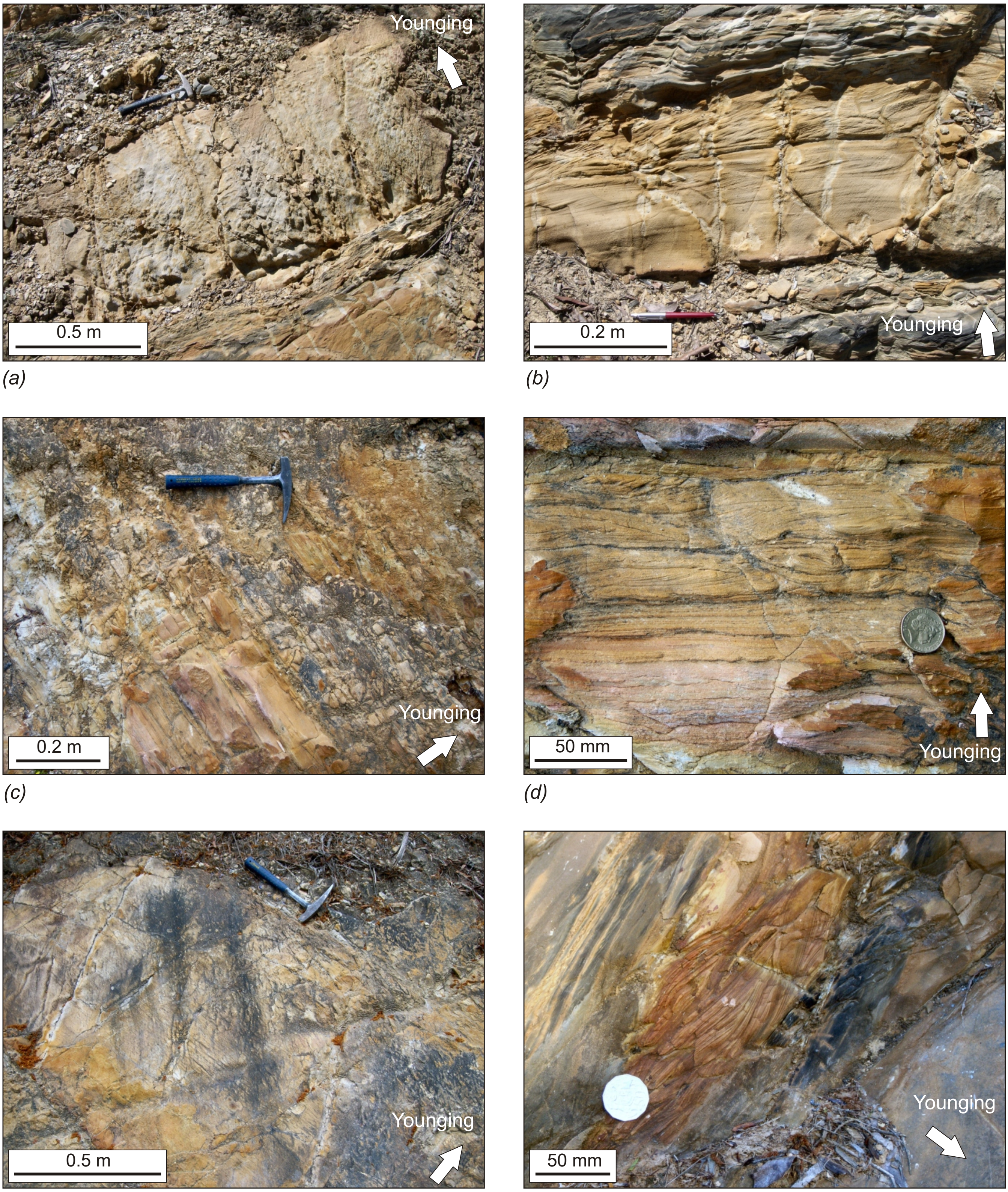


**Figure 7**

*Representative outcrop photographs of the Retreat Formation:*
*(a) 0.75 m thick turbidite bed of graded medium to fine-grained sandstone showing uneven erosive base and Bouma bed subdivision sequence A-B, at 511415/5450270 on a forestry road west of Retreat Road; (b) same outcrop as (a), showing 0.28 m thick turbidite bed of graded sandstone with Bouma bed subdivision sequence A-B-C; (c) thin-bedded dominantly plane-laminated fine-grained quartz-rich sandstone, quartzose siltstone and minor pelite, at 513460/5445235 near the intersection of South Retreat Road and Security Road; (d) same outcrop as (c) showing detail of cross-laminated fine-grained sandstone bed; (e) One metre thick ungraded bed of fine-grained quartz-rich sandstone, internally almost structureless apart from indistinct plane lamination in the middle of the bed, at 513445/5445215 near the intersection of South Retreat Road and Security Road; (f) thin individual bed of cross-laminated quartzose siltstone within locally pelite-dominant succession, at 513070/5439880 on South Retreat Road.*

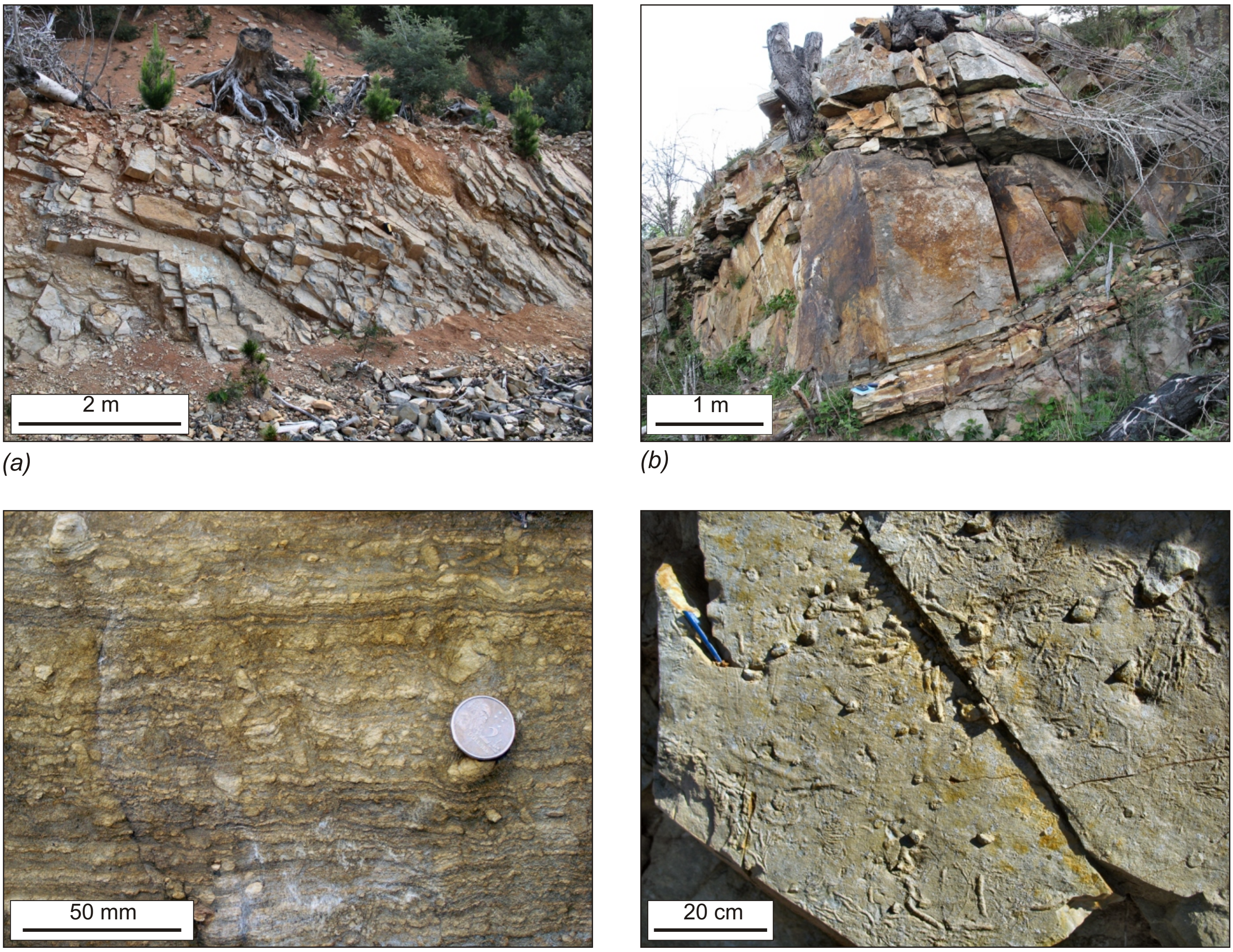


(a) (b) (c) (d)

**Figure 8**

*Outcrop characteristics of the Lone Star Siltstone: (a) thinly interbedded shale and laminated siltstone showing slabby bedding typical of the contact metamorphic aureoles, 529940/5433330 southeast of Lisle; (b) two metre thick lens of fine-grained sandstone with minor normal and reverse grading, within medium-bedded fine-grained sandstone and minor very thin-bedded laminated siltstone, 530970/5426855 near Targa Hill Road bridge; (c) probable bioturbation structures in laminated siltstone in the lower part of the Lone Star Siltstone, 525875/5444265 near Golconda; (d) bioturbation structures on a bedding plane, same outcrop as (a).*

reached (mapped as the point where sandstone dominates over siltstone and finer-grained lithologies). The upper part of the succession is less distinctive in radiometric signature relative to that of the Sideling Sandstone (fig. 6), perhaps due to the upward-increasing sandstone component. An alternative explanation, that the signature change is due to contact metamorphic overprint as the western margin of the Scottsdale Batholith is approached, seems unlikely due to a lack of reported evidence for broad scale metasomatism associated with the granitoids; also, an artefact due to better exposure of more resistant metamorphosed rocks does not seem to be supported by DEM data. The stratigraphic interval between the top of the Retreat Formation and the transitional base of the Sideling Sandstone has been defined as a new formation, the Lone Star Siltstone, of the Panama Group (Appendix 1). The name is adopted from Lone Star Ridge (524512/5435393) over which it is the dominant bedrock. Together with the Yarrow Creek Mudstone and the Retreat Formation, the Lone Star Siltstone replaces the previous Bellingham Formation (Powell *et al*., 1993). The type area has been nominated as a series of road cut exposures between points 528962/5423313 and 532302/5431363 on the Tasman Highway, and including south Targa Hill Road and Myrtle Bank Road.

Where distinguished, the basal unit comprises cleaved, upright folded, variably bioturbated marine siltstone with significant shale and mudstone. Thin planar laminations are typical, but may be obscured by deformation, bioturbation or weathering. The thinly laminated siltstone is typically thin bedded and fine to medium-grained, although it may form slabby medium beds approaching and within hornfelsed zones (fig. 8*a*). Fine-grained lithologies are micaceous, and although locally weakly deformed on long fold limbs, elsewhere they assume a slaty cleavage with a phyllitic sheen. Significant black shale is rare, typically pyritic and locally graptolite bearing. Where well exposed, the richest graptolitic shale intervals are typically less than five metres thick. Furthermore, as noted above, the localities which have yielded Late Silurian (Ludlow) grapotolites to date, including Boags Ridge and Golden Ridge outside the area covered by this report, may all represent the same horizon; if so a widespread mass mortality event may have occurred at this timeline.

Soft sediment deformation, rare isolated cross beds and mud drapes have been observed in the basal unit. Significant but variable trace fossils and bioturbation are also present in fine-grained siltstone in the basal unit (fig. 8*c,d*). Examples of burrows, faecal pellets and bedding obscured by bioturbation occur at 529095/5423824 on the Tasman Highway. The interpreted, but yet to be confirmed presence of *Chondrites* of the *Nereites* ichnofacies indicates a deep marine environment for the lower part of the formation.

Units of massive, medium to thick-bedded quartz-rich sandstone, rarely lenticular, become more common eastwards and up-section towards the overlying Sideling Sandstone (fig. 8*b*). The sandstone is mostly fine-grained with a significant matrix. Sorting is typically poor. Sedimentary structures associated with sandstone deposition are uncommon but increase in frequency up sequence.

A number of siltstone samples from both the Lone Star Siltstone and the Sideling Sandstone were analysed for major and trace elements as part of the *TasExplore* work (Appendix 3), and the data plotted on standard discrimination diagrams from the published literature (fig. 9). The geochemical signatures of the siltstones show a clear indication of a passive margin depositional environment with derivation from a quartzose sedimentary provenance (fig. 9*c,e*).

The Lone Star Siltstone was deposited in a marine sedimentary environment, based on the presence of graptolites, bioturbation and local turbidites, within a passive margin setting. The basal siltstone and shale of the formation is distal, and forms a relatively passive environment between the sandy submarine fan complexes of the underlying Retreat Sandstone and the increasing sandy sheet flows up-section to the east, which lead up to further sandy submarine fan complexes of the overlying Sideling Sandstone.

## *Sideling Sandstone*

### Age control

The Sideling Sandstone has an imprecise age of Early Devonian as it conformably overlies the Lone Star Siltstone which contains Late Silurian graptolites, it has yielded fragments of the Early Devonian plant fossil *Hostimella* (Cookson, 1937; Banks, 1962), and it has been intruded by Middle Devonian granodiorite of the Scottsdale Batholith (Black *et al*., 2005).

### Previous work

Powell *et al.* (1993) described the 'Sidling sandstone' as a relatively thick-bedded arenite-rich succession of turbidites without cleavage in the sandstone beds. Palaeocurrent measurements of flutes, grooves and tool marks on the Sideling section of the Tasman Highway from 534613/5429383 to 531613/5431183 showed a vector mean of currents to the southeast almost parallel to the local fold axis. The geographic distribution of the 'Sidling sandstone' in the Sideling Range was only very approximately delineated (fig. 1*b*).

As noted above, Thompson (2000) introduced the formal name Sideling Sandstone but did not formally define the unit, fully determine its extent or establish type sections. Several sandstone facies were recognised within an estimated 1500 m thick sequence. Facies 1 is the coarsest overall and is characterised by ungraded, thick-bedded massive and structureless medium to fine-grained sandstone. Facies 2 comprises classical Bouma turbidites with the bed-structure sequences A-C-D-E (A: graded medium to fine-grained sandstone; C and D: fine-grained sandstone; E siltstone) or C-D-E (C and D: fine-grained sandstone; E: siltstone). Facies 3 is the finest grained and consists of Bouma D-E (fine-grained sandstone–siltstone) alternations.

### Field relationships and characteristics

The Sideling Sandstone has a transitional conformable boundary with the Lone Star Siltstone which underlies it to the west. To the east it is intruded by granodiorite of the Middle Devonian Scottsdale Batholith. The formation extends north from the Tasman Highway, forming the Sideling Range, and along the western margin of the Scottsdale Batholith to the coast north of Bridport (fig. 4). It also extends southeast of the highway for about five kilometres. A formal definition for the unit has now been submitted to the Australian Stratigraphic Units Database (Appendix 1), and the type area has been nominated as a traverse along the Tasman Highway between points 535610/5431680 and 536310/5434683, where the highway crosses the Sideling Range about 15 km southwest of Scottsdale.

The dominant rock type of the formation is pale grey quartz-rich, fine to medium-grained sandstone with minor interbeds of siltstone. The sandstone beds range in thickness from 0.1–3 m but are generally 1–2 m thick. Some beds show grading from fine-grained sandstone to siltstone, with the siltstone horizon showing horizontal lamination and/or cross lamination (Bouma A-B-C or A-C-D turbidites). Sole marks and load casts may occur. A penetrative cleavage is strongly developed in the finer grained silty tops of turbidite depositional units and in siltstone interbeds but is poorly developed or absent in sandstone. In thin section the sandstones show poorly-sorted subangular grains and a high proportion of groundmass. The dominant detrital grain type is monocrystalline quartz with undulose extinction. There is also a minor component of polycrystalline quartz grains. Grain size may range up to 0.5 mm but is generally about 0.15 mm. Minor components include <5% of plagioclase grains generally <0.1 mm in size and rare detrital muscovite clasts up to 0.15 mm in size. The groundmass includes sericitic mica <0.03 mm in length, fine-grained quartz and minor chlorite. Other minor components are opaques, tourmaline, zircon, apatite and rutile. The poor sorting and high proportion of groundmass are typical of turbidite deposits.

The siltstones are medium to dark grey when fresh (weathering to pale brown/buff), massive to laminated, and generally have a strongly developed cleavage which in some cases obscures bedding. They are present as thin intervals between sandstone beds or in some cases as thicker units up to several metres thick. In thin section the siltstones consist dominantly of sericite, quartz, chlorite and minor plagioclase and ilmenite with a grain size generally about 0.01 mm. They are poorly sorted with some quartz grains up 0.05 mm. The sericitic mica may have a strong planar orientation parallel to cleavage. Compositional layering in some samples is due to

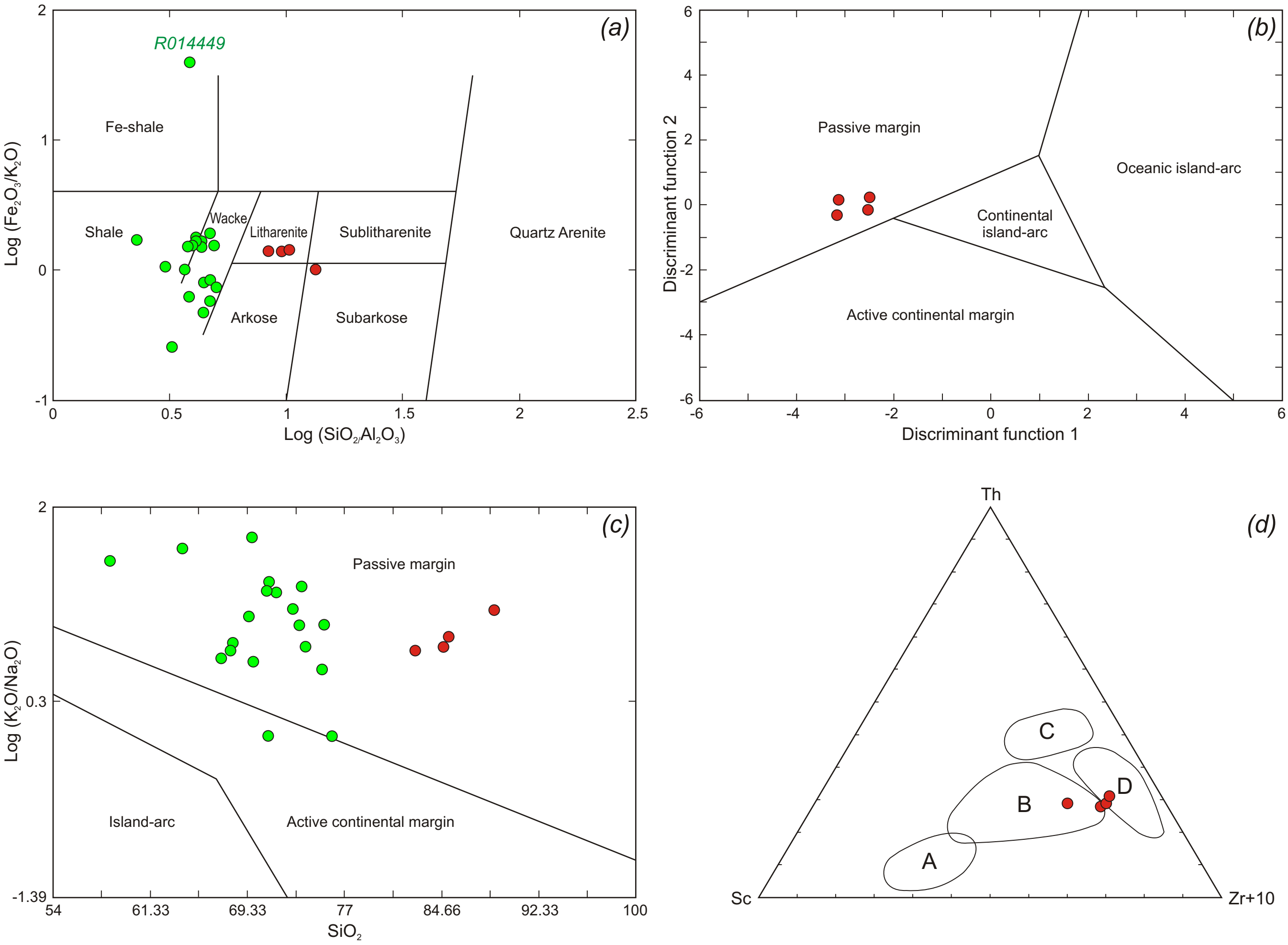


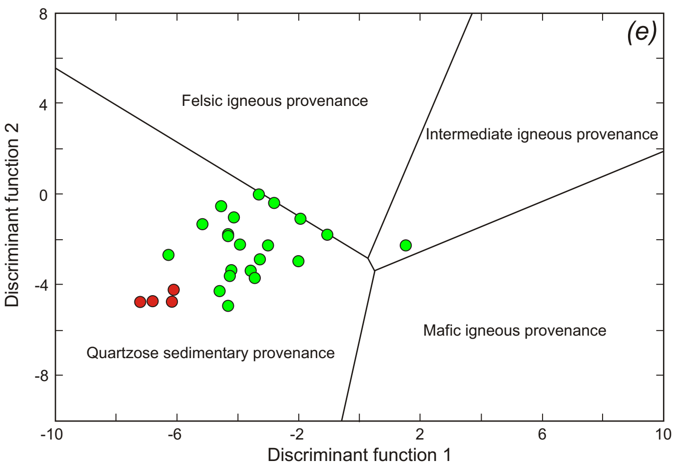


**Figure 9**

*Geochemical discrimination diagrams showing analyses of samples of siltstone from the Lone Star Siltstone and Sideling Sandstone (green circles), and sandstone from the Sideling Sandstone (red circles): (a) classification diagram of Herron (1988); note R014449 is an unusual iron-rich, probably mineralised sample from the Lone Star Siltstone and may not represent a primary composition; (b) discriminant function diagram for sandstones (Bhatia, 1983); (c) discrimination diagram of Roser and Korsch (1986) for sandstone-mudstone suites; (d) discrimination diagram for greywackes (Bhatia and Crook, 1986); the fields are A = oceanic island-arc, B = continental island-arc, C = active continental margin, D = passive margin; (e) discriminant function diagram for provenance signatures of sandstone-mudstone suites using major elements (Roser and Korsch, 1988).*

the presence of lenses with a higher proportion of coarser grained quartz.

On standard discrimination diagrams, the geochemical signatures of analysed siltstone and sandstone samples from the Sideling Sandstone (Appendix 3) show clear indications of a dominantly passive margin sedimentary environment with a quartzose sedimentary provenance (fig. 9). This is consistent with the detrital mineralogy of these rocks which is dominated by quartz in monomineralic clasts with only very minor amounts of plagioclase and rare muscovite clasts. The strained character of the detrital quartz and the rare muscovite clasts suggest a metamorphic source terrain. Palaeocurrent measurements from the Sideling Sandstone on the Tasman Highway by Powell *et al.* (1993) indicate a southeasterly flow, suggesting that the source terrain lay to the northwest.

The Sideling Sandstone was deposited in a marine passive margin tectonic setting, and like the Retreat Formation sedimentation probably occurred in one or more sandy submarine fan complexes. In contrast with the Retreat Formation, the Sideling Sandstone appears to show a higher proportion of massive sandstone beds to which the Bouma sequence is not applicable (*cf.* facies B of Walker and Mutti, 1973), and the sandstone content may be somewhat finer grained overall than in the Retreat Formation.

# STRUCTURAL GEOLOGY

## Introduction

The Mathinna Supergroup is a complexly folded and faulted suite of rocks, and the *TasExplore* project work in its 'type area' west of the Scottsdale Batholith would inevitably include a re-examination of issues to do with the structural architecture and interpretation. Even prior to acquisition of the new geophysical data, it was obvious that the 'Pipers River recumbent zone', and particularly the contact between the rocks affected by it and the younger sequences, was worthy of further focus. The recognition of a more complex stratigraphy in the sequence enhanced the opportunity to re-examine the structural architecture and the structural relationships between the units, a task assisted by construction of a series of structural profiles and cross-sections covering the area (fig. 10). The latter were also a necessary input for another fundamental requirement of the overall project, the construction of a revised 3-D geological model for the Mathinna Supergroup.

## Structural relationship between the Tippogoree and Panama groups

A significant outcome of the *TasExplore* work is the inference of a fault contact between the Tippogoree and Panama groups, a return to an interpretation close to that of Turner (1980). This is an early fault, as it appears to have been affected by later folds and faults which affect formation contacts in the Panama Group, but it may have a steeper overall easterly dip than the latter contacts (see further detail below).

The contact is not well exposed in any of the outcrop areas examined during *TasExplore* fieldwork, but relatively good exposures of the adjacent rock sequences to within short distances of the contact have enabled evaluation of the degree and abruptness of changes in structural geometry and character across the contact. Two key areas for this comparison are shown in Figure 11. The southernmost area (covering about 6.5 km$^2$) has regular bedrock exposures in road cuttings, and illustrates the marked and abrupt contrast in orientation of '$S_1$' penetrative cleavage across the inferred fault contact between the Turquoise Bluff Slate (Ott) and the Yarrow Creek Mudstone (SDpy) (fig. 11*a*), an observation which is also well reflected in broader-scale domain analysis described below.

A slightly less obvious feature, but more so when outcrop lithology data from this area are viewed spatially, is the markedly higher frequency of observations of vein quartz in the Turquoise Bluff Slate compared with the Yarrow Creek Mudstone. These observations were mostly at sites where copious vein quartz float or lag is present in the relatively thin soil profile, but also include sites where noticeably high frequencies of quartz veins occur in outcrop (fig. 11*a*). There is an obvious concentration of vein quartz observations in that part of the area underlain by the Turquoise Bluff Slate (and also along or close to the contact in several places). The penetrative foliation in the Turquoise Bluff Slate is also very intense, with common development of a noticeable sheen on the foliation surfaces, a feature generally absent from the less intense penetrative cleavage in the Yarrow Creek Mudstone. This indicates significantly higher strain in the Turquoise Bluff Slate, which is probably also the reason for the observed greater frequency of quartz veining in the unit. The latter, as noted in the *Stratigraphy* section, may help explain the surprisingly 'non-pelitic' radiometric signature of the Turquoise Bluff Slate.

The contact can also be traversed in an intermittent series of road cuttings on the south side of Bridport Road between 509825/5452195 and 510350/5452140 (fig. 11*b*). The inferred fault contact is placed in a zone of substantial vein quartz development at 509950/5452185. West of this zone, typical pale-weathered quartz-veined cleavage-dominant Turquoise Bluff Slate shows an intense penetrative foliation dipping at 20° to 32° to between east and east-southeast. East of the zone of vein quartz, thin-bedded grey mudstone with minor beds of quartzose siltstone, typical of the Yarrow Creek Mudstone, shows a structural style of NE-vergent open folds plunging gently to 125–130° with axial surfaces inclined steeply to the southwest, and associated steep axial plane penetrative cleavage which is markedly less intense than that in the Turquoise Bluff Slate. The abrupt contrast in orientation of structural elements across the contact is similar to that in the area shown in Figure 11*a*.

The evidence presented above provides strong support for the existence of a fault contact between the Tippogoree and Panama groups. The fault is not a late one, as the geometry of its surface trace suggests it has been affected by subsequent folding and faulting events (fig. 4).

The question of the relationship between '$D_1$' structures in the two sequences is more complex, and has been the subject of conflicting interpretations in the previous literature. Patison *et al.* (2001) assigned the same (Devonian) age to '$D_1$' structures in both the Tippogoree and Panama groups, but a possible extension to their model would have the high-strain recumbent early structures in the Tippogoree Group forming at a deeper structural level than the more upright early structures in the Panama Group, the two structural levels being juxtaposed on a later (possibly late-$D_1$) fault. This modification begs the expectation of a drop in metamorphic grade from the Tippogoree Group to the younger rocks, a difference which is not apparent in the illite crystallinity data of Patison *et al.* (2001), although a larger number of samples closer to the contact may be needed to be sure either way. Alternatively, Reed (2001) favoured an interpretation in which the recumbent folds and associated intense penetrative slaty cleavage in the Turquoise Bluff Slate were a product of the Benambran Orogeny (early Silurian on the 2008 ICS timescale), prior to deposition of the Panama Group. In this scenario the Tippogoree and Panama groups are separated by an inferred unconformity. The Reed (2001) model has gained support from $^{40}Ar/^{39}Ar$ dating of white mica from a pelite within the Stony Head Sandstone at Lefroy, which yielded a plateau age of 426.7 2.4 Ma for metamorphism and penetrative cleavage formation (Bierlein *et al.*, 2005) — an age which

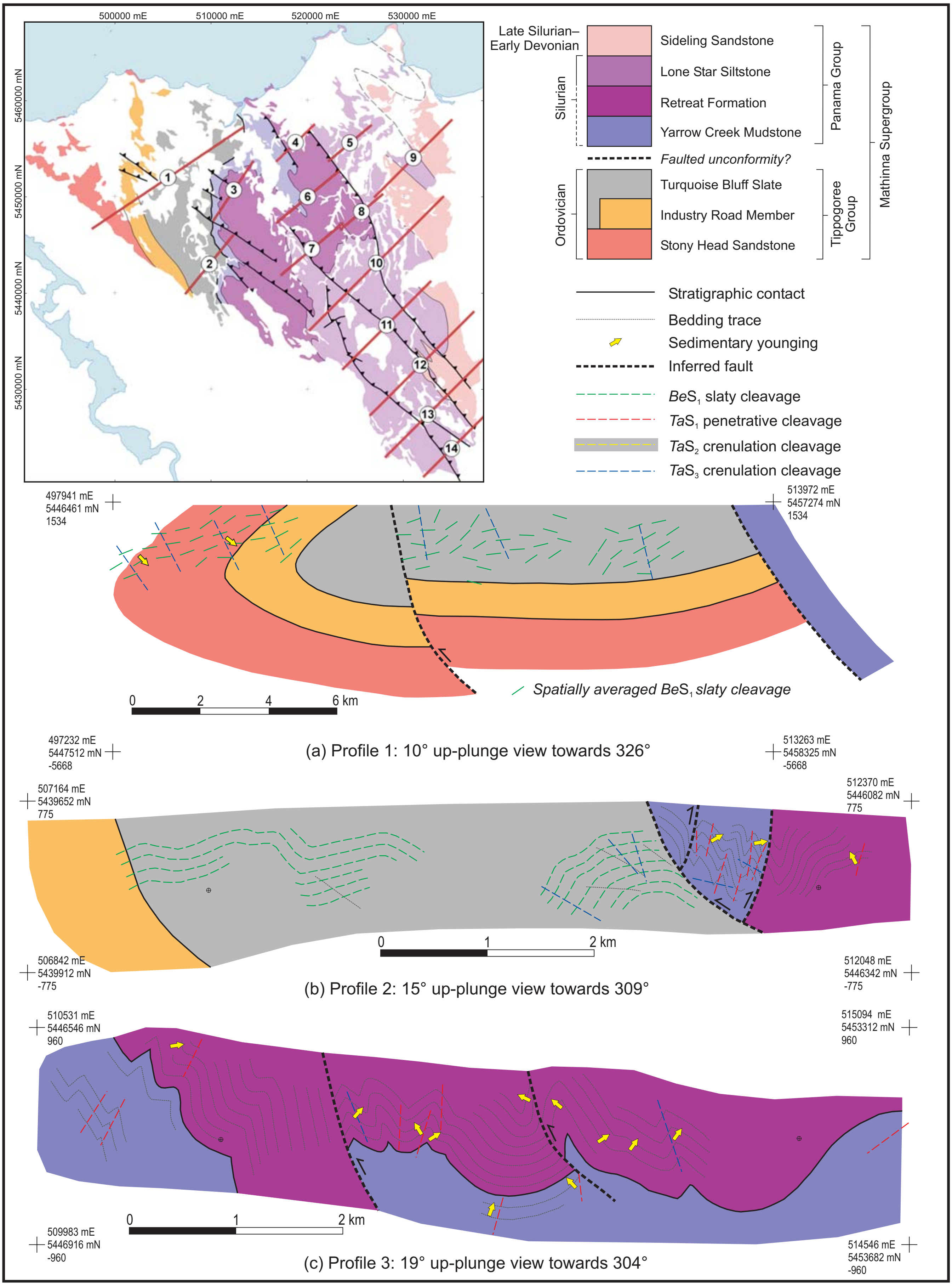


**Figure 10 (a–c)**

*Structural profiles and cross sections through the Mathinna Supergroup west of the Scottsdale Batholith. Profiles 1 to 8 are projected true structural profiles normal to mean local fold axis orientation (which varies for each profile) and do not show topography; Sections 9 to 14 are vertical cross sections normal to average regional fold axis trend and are clipped to topographic traces along the sections. All grid coordinates on this figure are in AGD66 datum, AMG Zone 55.*

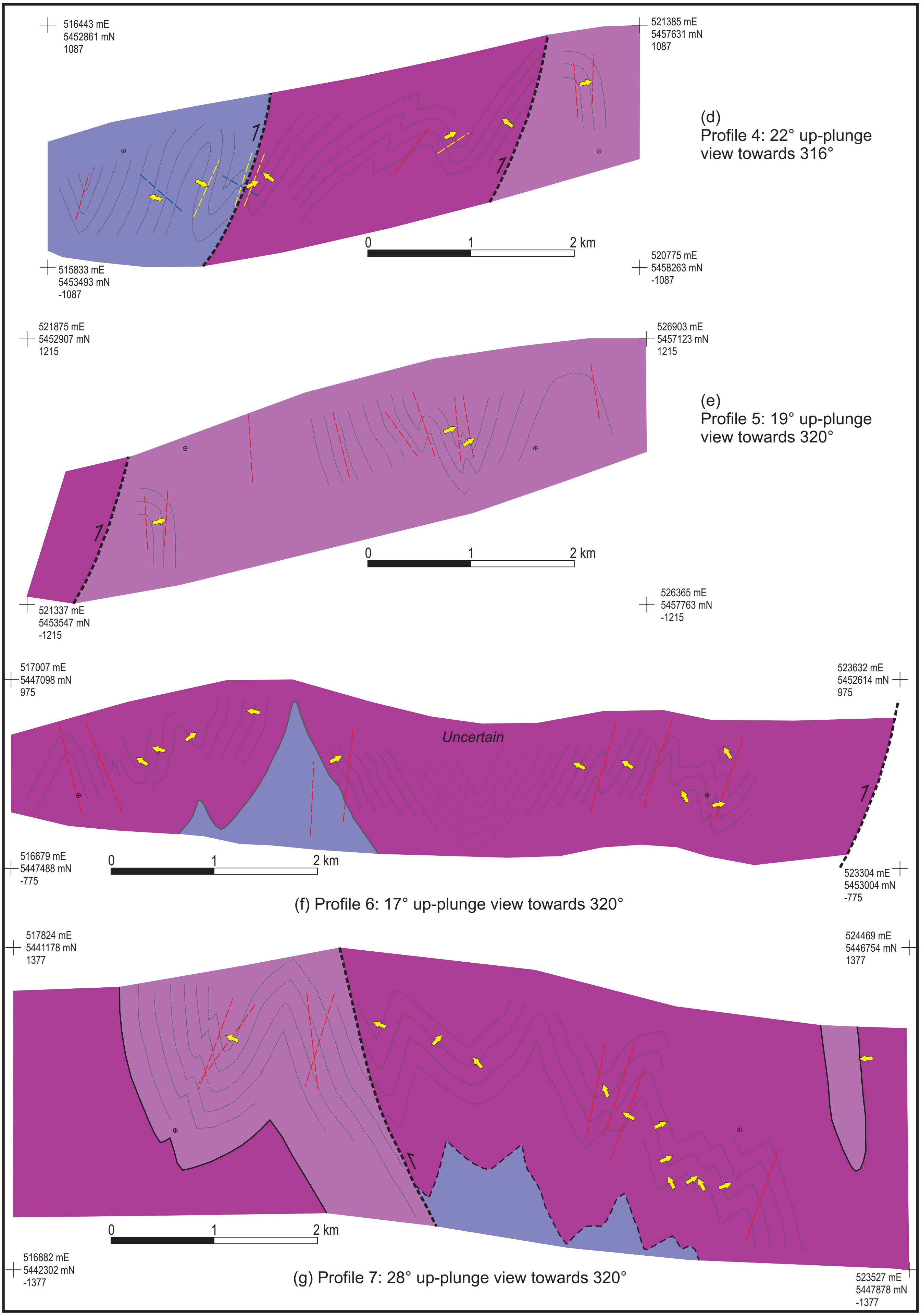
516443 mE
5452861 mN
1087
521385 mE
5457631 mN
1087
(d)
Profile 4: 22° up-plunge
view towards 316°
0
1
2 km
515833 mE
5453493 mN
-1087
520775 mE
5458263 mN
-1087
521875 mE
5452907 mN
1215
526903 mE
5457123 mN
1215
(e)
Profile 5: 19° up-plunge
view towards 320°
0
1
2 km
521337 mE
5453547 mN
-1215
526365 mE
5457763 mN
-1215
517007 mE
5447098 mN
975
523632 mE
5452614 mN
975
Uncertain
516679 mE
5447488 mN
-775
0
1
2 km
523304 mE
5453004 mN
-775
(f) Profile 6: 17° up-plunge view towards 320°
517824 mE
5441178 mN
1377
524469 mE
5446754 mN
1377
0
1
2 km
516882 mE
5442302 mN
-1377
(g) Profile 7: 28° up-plunge view towards 320°
523527 mE
5447878 mN
-1377

**Figure 10 (d–g)**

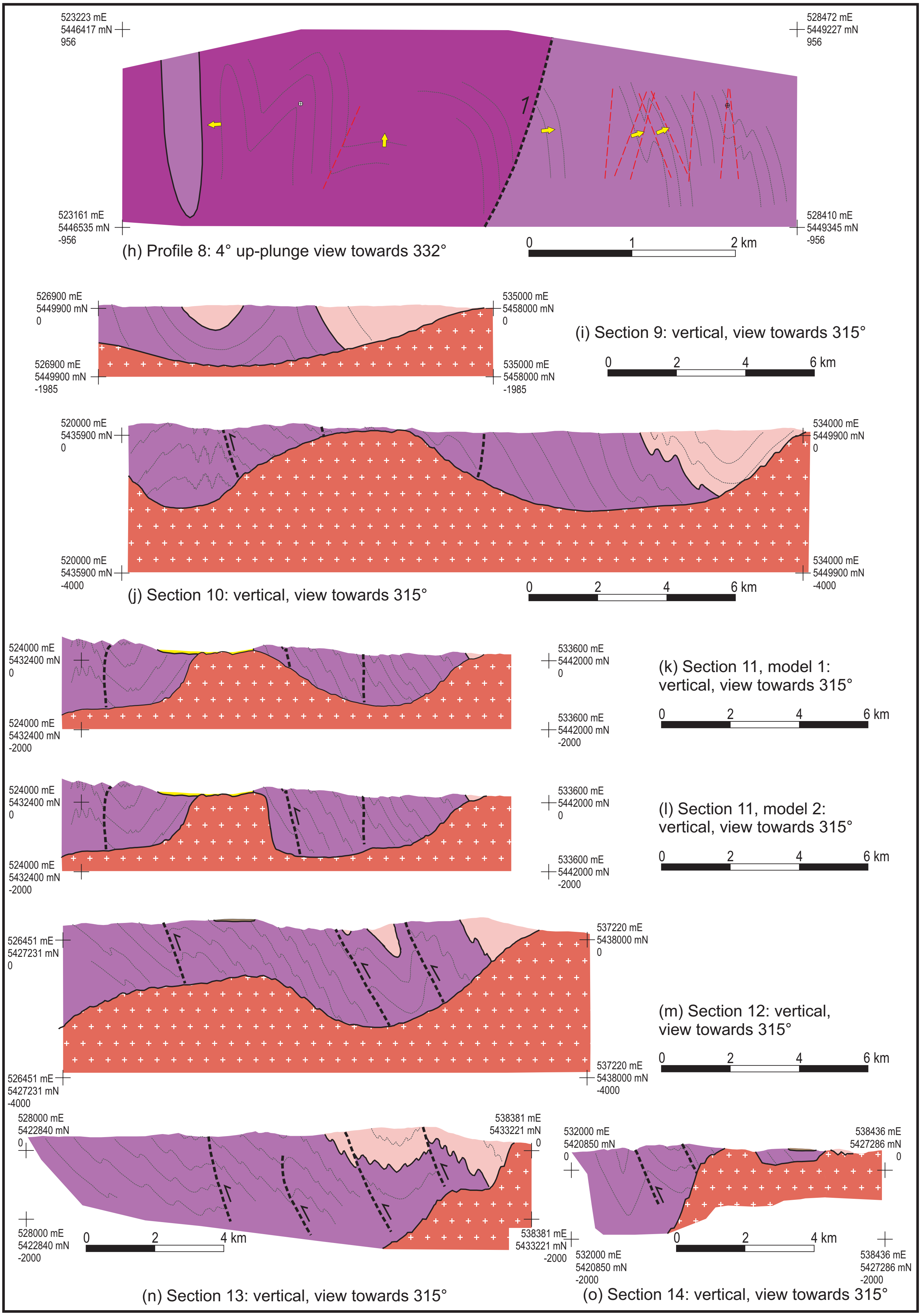

523223 mE
5446417 mN
956
528472 mE
5449227 mN
956
523161 mE
5446535 mN
-956
528410 mE
5449345 mN
-956
0
1
2 km
(h) Profile 8: 4° up-plunge view towards 332°
526900 mE
5449900 mN
0
535000 mE
5458000 mN
0
526900 mE
5449900 mN
-1985
535000 mE
5458000 mN
-1985
(i) Section 9: vertical, view towards 315°
0
2
4
6 km
520000 mE
5435900 mN
0
534000 mE
5449900 mN
0
520000 mE
5435900 mN
-4000
534000 mE
5449900 mN
-4000
(j) Section 10: vertical, view towards 315°
0
2
4
6 km
524000 mE
5432400 mN
0
533600 mE
5442000 mN
0
524000 mE
5432400 mN
-2000
533600 mE
5442000 mN
-2000
(k) Section 11, model 1:
vertical, view towards 315°
0
2
4
6 km
524000 mE
5432400 mN
0
533600 mE
5442000 mN
0
524000 mE
5432400 mN
-2000
533600 mE
5442000 mN
-2000
(l) Section 11, model 2:
vertical, view towards 315°
0
2
4
6 km
526451 mE
5427231 mN
0
537220 mE
5438000 mN
0
526451 mE
5427231 mN
-4000
537220 mE
5438000 mN
-4000
(m) Section 12: vertical,
view towards 315°
0
2
4
6 km
528000 mE
5422840 mN
0
538381 mE
5433221 mN
0
528000 mE
5422840 mN
-2000
538381 mE
5433221 mN
-2000
0
2
4 km
(n) Section 13: vertical, view towards 315°
532000 mE
5420850 mN
0
538436 mE
5427286 mN
0
532000 mE
5420850 mN
-2000
538436 mE
5427286 mN
-2000
0
2
4 km
(o) Section 14: vertical, view towards 315°


**Figure 10 (h–o)**

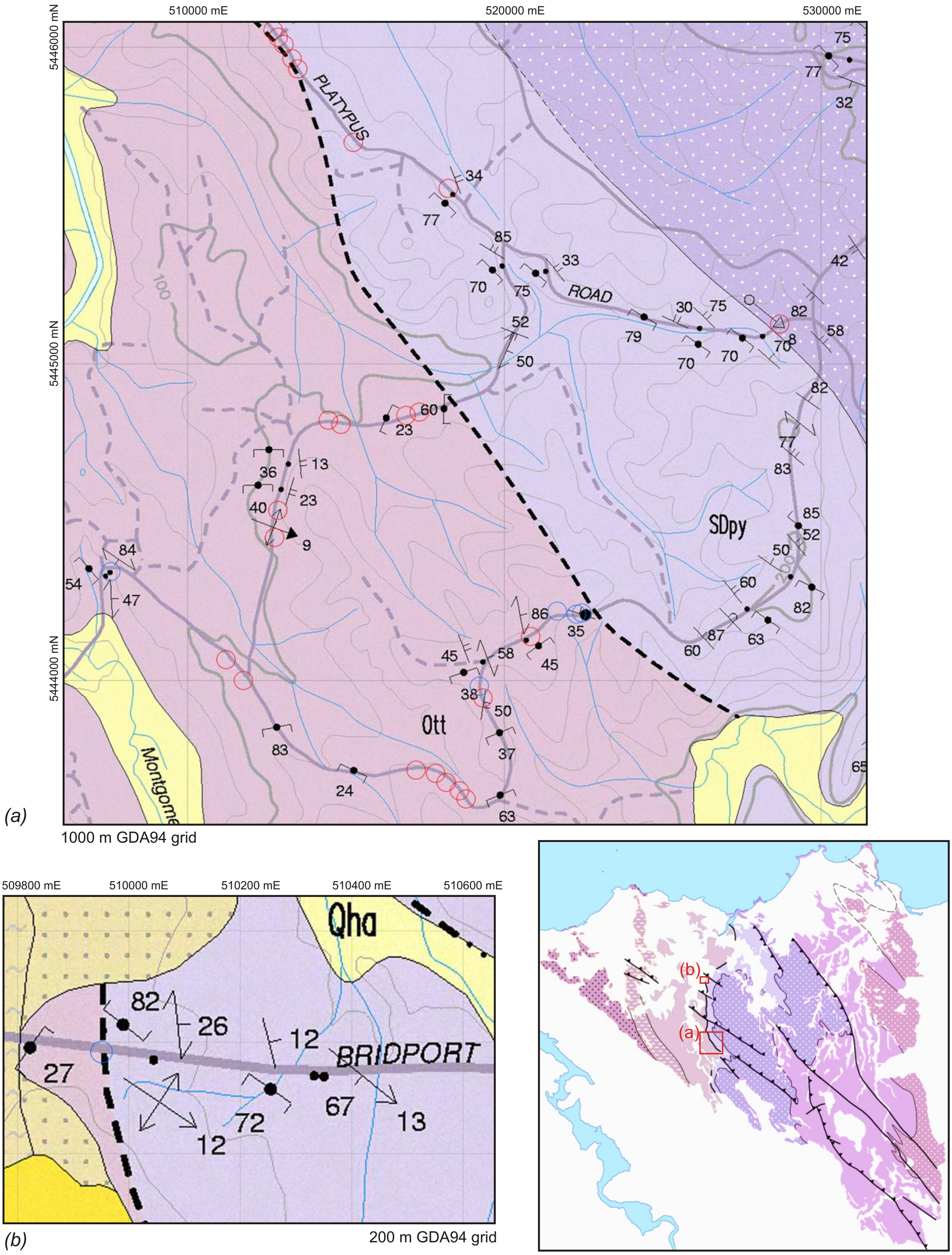


**Figure 11**

*Representative clips from revised MRT 1:25 000 scale digital geology coverage (in final published map colours) showing structural relationships across the inferred fault contact between the Tippogoree and Panama groups: (a) 1:15 000 scale view of an area in the vicinity of the intersection of Security and Platypus roads showing the marked difference in orientation of penetrative cleavage (pronged symbol with central dot) across the contact; rock units — Ott Turquoise Bluff Slate, SDpy Yarrow Creek Mudstone; (b) 1:10 000 scale view of a series of road cuttings showing the marked structural contrast across the contact on Bridport Road. Additional symbology in both maps: red circles — substantial vein quartz float or lag; blue circles — substantial quartz veins in bedrock. Locations are shown on the guide map which has also been adjusted to approximate final published 1:25 000 scale map colours.*

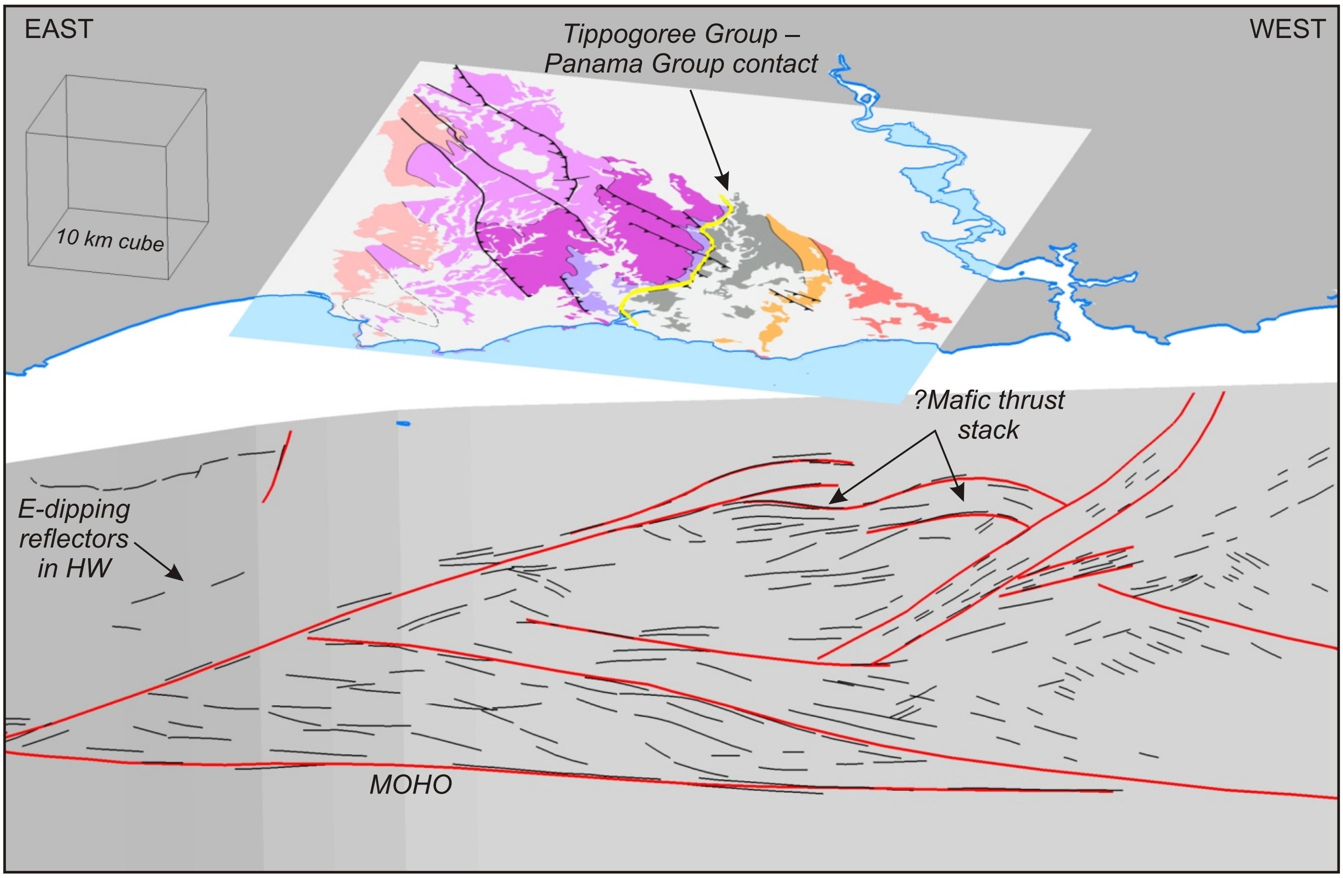


**Figure 12**

*3-D oblique orthographic view towards about SSE showing Mathinna Supergroup remapping west of the Scottsdale Batholith in relation to Geoscience Australia interpretation (Barton, 1999b) of offshore reflection seismic line 148/04 (reflectors — black; interpreted faults — red).*

plots as mid-Silurian on the 2008 ICS timescale but which could still pre-date commencement of deposition of the Panama Group.

As noted by Reed (2001) and further evident in discussion below, one problem with the unconformity model is the lack of widespread clear overprinting of the $D_1$ recumbent structures in the Tippogoree Group by more upright but still northeast-vergent folds and associated cleavages which represent the apparently earliest structures in the Panama Group. Reed (2001) did record east-vergent $D_2$ cleavages obliquely overprinting the shallowly-dipping intense $S_1$ slaty cleavage in the Turquoise Bluff Slate, and partly on this basis appealed to local reactivation of the early (inferred Benambran) recumbent structures during the first (NE-vergent) phase of subsequent Tabberabberan upright folding.

One approach which may be a key to further understanding of this issue is to re-examine what is currently known or implied about the geometry of the contact. Reed (2001) partially supported his unconformity model with the statement that the contact is inferred, from offshore seismic data, to dip east, referring to a conference abstract by Barton (1999*a*) which was based on an M.Sc. research study (Barton, 1999*b*) which reprocessed earlier NGMA Project seismic data. However comparison of the seismic interpretation and the *TasExplore* revised mapping in 3-D projection shows that the east-dipping reflector referred to is displaced further west from a position which would be down-dip from the surface trace of the Tippogoree–Panama contact (fig. 12). The reflector forms the eastern boundary of, and extends downward into the lower crust from, a set of strong reflectors interpreted as a ?mafic thrust stack (with west-vergent geometry) about six kilometres thick lying at a depth of four kilometres beneath the western part of the Mathinna Supergroup. The upper crust above this feature is relatively bland seismically and few major structures were interpreted within it. In the middle crust a few east-dipping reflectors are present in the hanging wall above and to the east of the main reflector (fig. 12), and these are closer to a position down-dip of the Tippogoree–Panama contact.

Further insight into the contact geometry can be attained by analysis of the surface trace established in the new mapping (fig. 4). At the scale presented in Figure 4 the position of this trace can be considered to be mostly accurate (the only uncertainty being its exact position under Tertiary and younger cover between Pipers Brook and Weymouth). Two observations stand out: that the trace shows a quite high degree of parallelism with the traces of formation boundaries within the Panama Group (noting positional uncertainties under cover); and that it appears to have been affected by the same set or sets of SE-plunging upright folds that affect the Panama Group. Within these constraints it is quite difficult to model a west-dipping 3-D geometry for the Tippogoree–Panama contact, and simpler to interpret the contact as a folded, generally east or southeast-dipping fault. The lower overall amplitude of fold-related deflections in the

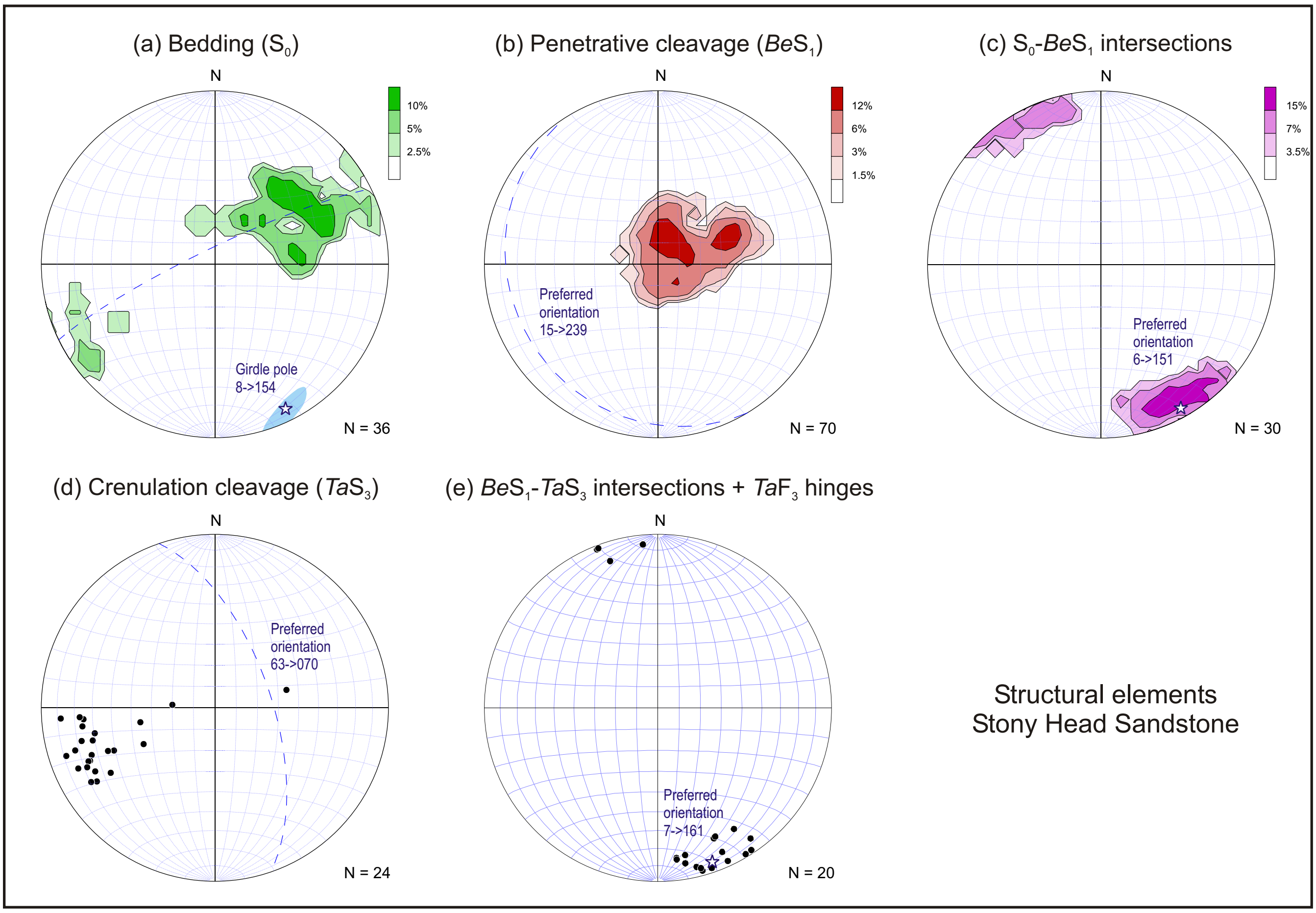


**Figure 13**

*Lower hemisphere equal-area stereograms of structural data from the Stony Head Sandstone. Statistical uncertainties on girdle poles are shown by blue fields.*

surface trace of this fault, compared with formation boundaries in the Panama Group, suggests it has a steeper overall dip than the latter.

A further possible interpretation, consistent with all of the evidence, is that the Tippogoree–Panama contact initiated as an extensional, basin-margin fault at the commencement of Panama Group deposition, and that it was active as a growth fault during the depositional history of the sequence. Such a fault would likely have been partially inverted, but also folded and faulted, during subsequent Devonian compressional events. This model would also explain the lack of exposed basal conglomerate in the Panama Group, as such a unit may still be concealed at depth where the true stratigraphic base of the Panama Group intersects the growth fault surface somewhere down-dip of the present erosion level.

## Structural analysis

While there remain uncertainties which are discussed below, for the purpose of this discussion the Reed (2001) model, which attributes $D_1$ structures in the 'Pipers River recumbent zone' to the Benambran Orogeny, is provisionally accepted. For convenience, inferred Benambran structures are tagged with the prefix '*Be*' (e.g. $BeS_1$), while structures attributed to the Devonian Tabberabberan Orogeny are prefixed '*Ta*' (e.g. $TaS_1$, $TaS_2$ etc.). Some sets of structures may be considered to be the product of two events and may be tagged e.g. $TaS_{1\text{-}2}$.

Considerable use was made of commercial structural analysis software for generating projected 2-D profile views of planar data needed to construct down-plunge or up-plunge structural profiles, for domain analysis, and for generating stereographic plots of planar and linear structural elements. Statistical subroutines enabled objective identification of preferred orientations, generation of confidence limits around girdle-generated statistical fold axes on the stereographic plots, and spatial averaging of orientation data where required in both map and profile views.

## Tippogoree Group structure

### $BeD_1$ structures

The first-generation structural architecture in the Tippogoree Group is dominated by a large-scale NE-vergent near-recumbent syncline with a shallowly SW-dipping axial surface and a shallow southeasterly axial plunge (fig. 10*a*). Comparable second-order and third-order folds in bedding are commonly observed at outcrop scale. These folds have an associated well-developed to intense axial plane cleavage which generally dips at shallow to moderate angles to the southwest, but varies considerably in orientation due to one or more phases of later, more upright folding (fig. 10*a*,*b*). These early near-recumbent structures together comprise the 'Pipers River recumbent zone' of previous workers.

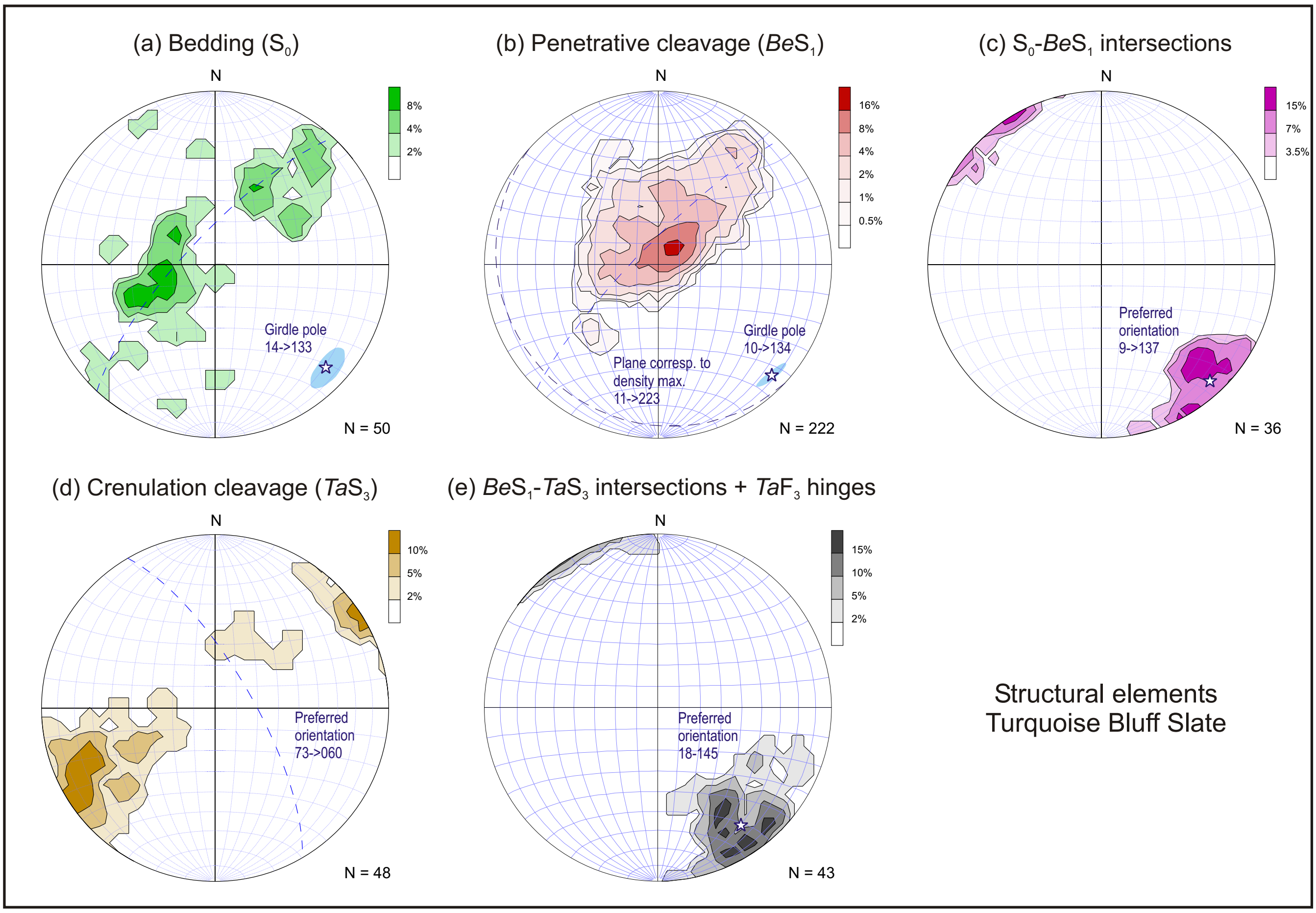


**Figure 14**

*Lower hemisphere equal-area stereograms of structural data from the Turquoise Bluff Slate. Statistical uncertainties on girdle poles are shown by blue fields.*

Outcrops visited in the Stony Head Sandstone during this project are mostly situated on the upper, overturned limb of the large $BeD_1$ syncline (fig. 10*a*). Second order $BeD_1$ folding is not prevalent in this relatively competent unit, and so a plot of bedding polar data shows only weak girdle development (fig. 13*a*), and any apparent girdle could be partially due to overprinting by later upright folding. The pole to the bedding girdle is very close to the preferred orientation of intersections between bedding and $BeS_1$ cleavage (fig. 13*a,c*), both indicating $BeD_1$ fold axes plunging gently (6–8°) to the SSE. Outcrops in the Turquoise Bluff Slate are mostly distributed through the core and towards the lower limb of the first-order $BeD_1$ syncline (fig. 10*a*) and this less competent unit has more common higher-order folding — consequently a bedding polar plot shows better girdle development (fig. 14*a*). The bedding girdle pole is again close to the preferred orientation of bedding–$BeS_1$ intersections (fig. 14*a,c*) but there appears to be evidence of a 17–18° anticlockwise rotation of $BeD_1$ structures from the Stony Head Sandstone to the Turquoise Bluff Slate (in which $BeD_1$ fold axes are inferred to plunge at 9–14° to the SE).

$BeS_1$ cleavage in the Stony Head Sandstone is essentially clustered in orientation, with a preferred dip of 15° to the southwest (fig. 13*b*). Morphologically the cleavage is penetrative to grain scale, but commonly shows a 'stripy' appearance in outcrop (fig. 5*a*), probably due to a varying degree of mineralogical differentiation and/or centimetre-scale strain partitioning associated with cleavage development. This morphological characteristic is absent from all observed sandstone cleavages in the Panama Group, and has been compared with stripy cleavage development in Lower Ordovician turbidites near Bermagui in southeastern NSW (Powell and Baillie, 1992).

$BeS_1$ cleavage in the Turquoise Bluff Slate shows a wider range of orientations with development of a broad girdle on the stereogram (fig. 14*b*), probably largely due to the fact that this less competent unit has responded more to refolding by later $TaD_3$ southwest-vergent upright folds (see below). Nonetheless there remains a concentration of cleavage poles corresponding to a dip comparable to that of $BeS_1$ in the Stony Head Sandstone but rotated 16° anticlockwise in dip direction (fig. 14*b*) — a rotation comparable to that observed in the bedding girdle poles and bedding–$BeS_1$ intersections between the two formations. Estimates of the high strain associated with development of $BeS_1$ cleavage in the slate have been obtained from tightly folded thin beds of cherty siltstone in the Australasian Slate quarry (504575/5456340) near Turquoise Bluff, and range from 70–89% minimum shortening normal to the cleavage (Powell and Baillie, 1992; Reed, 2001; fig. 15*a*).

In thin section the $BeS_1$ fabric shows evidence of variations in strain intensity, but even at the relatively lowest strain states it is still an intensely developed fabric which is penetrative down to grain scale. At these lower strain states scattered original clastic quartz grains are evident in some cases, but

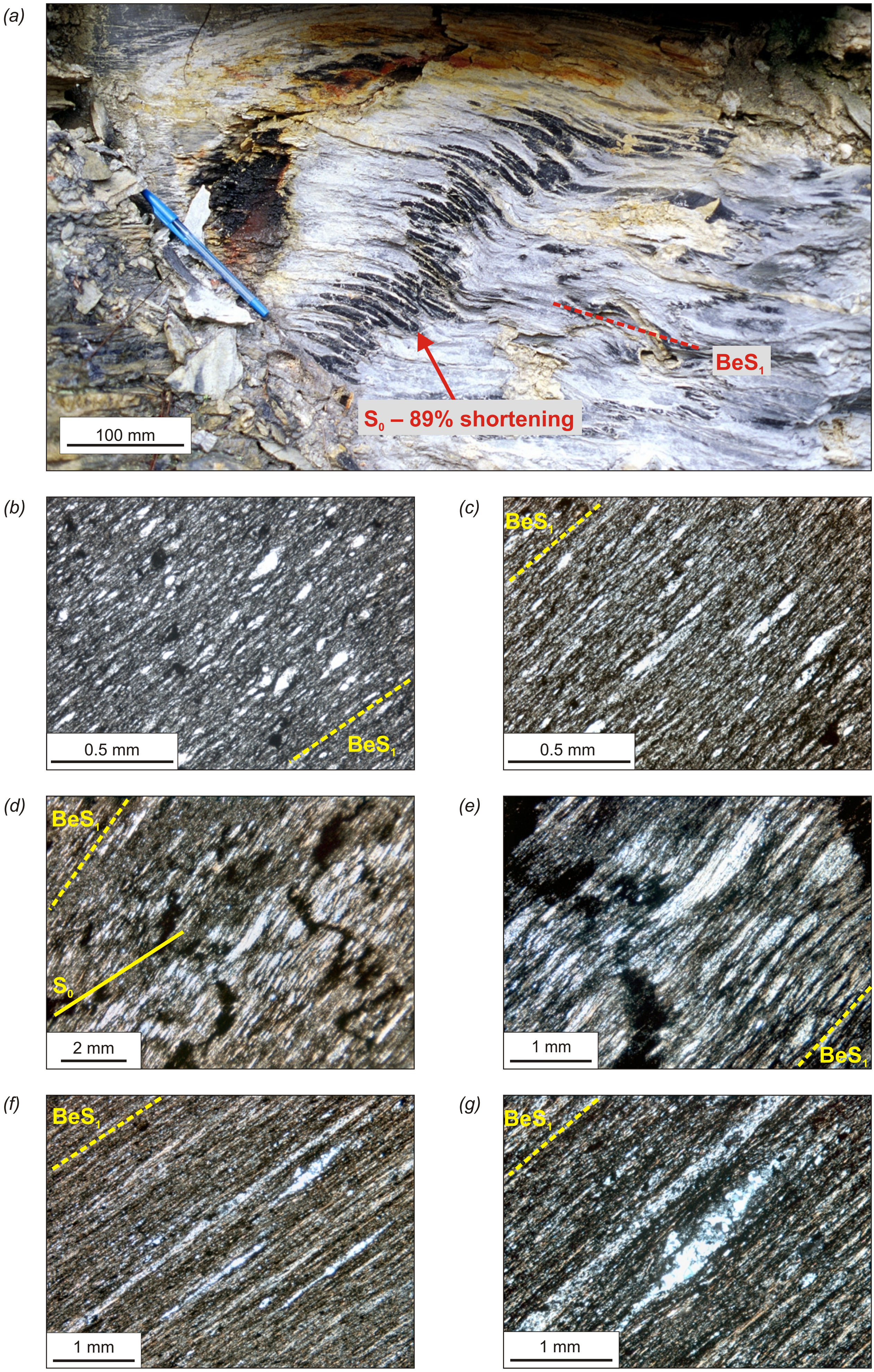
(a)
BeS1
S0 – 89% shortening
100 mm
(b)
0.5 mm
BeS1
(c)
BeS1
0.5 mm
(d)
BeS1
S0
2 mm
(e)
1 mm
BeS1
(f)
BeS1
1 mm
(g)
BeS1
1 mm

typically with substantial pressure solution corrosion on their cleavage-parallel sides (fig. 15*b*). These effects become more evident at higher strain levels (fig. 15*c*). In the relatively few cases where bedding lamination is still discernible in slate outcrops, in thin section this is commonly almost obliterated by development of the intense *Be*$S_1$ fabric (fig. 15*d,e*). At the highest strain states the *Be*$S_1$ fabric is extremely intense, comprising two fabric elements; highly aligned, very fine-grained mica, and sub-parallel to parallel elongate lenses and ribbons either of polycrystalline quartz or of a mixture of aligned mica and very fine-grained quartz (fig. 15*f,g*). The polycrystalline quartz lenses in this fabric may be in part the highly strained and recrystallised equivalents of original clastic quartz grains.

There have been reports (Dr Robert Scott, ARC Centre of Excellence in Ore Deposits, University of Tasmania, pers. comm. February 2006) that thin sections of drill core from Lefroy show that in pelite in the hinge zones of the recumbent folds adjacent to contacts with sandstone layers, the cleavage referred to above as *Be*$S_1$ is a very closely spaced crenulation cleavage overprinting a well developed, very fine-grained continuous mica fabric also suspected to be a tectonic foliation. Scott compares these fabrics to similar Benambran-aged foliations in the Ordovician of central Victoria, reinforcing the interpretation by Reed (2001) that the recumbent early cleavage in the Tippogoree Group is Benambran in age. It has not been possible to confirm Scott's observations in surface samples taken during the *TasExplore* fieldwork, as *Be*$S_1$ is invariably penetrative to grain scale in the thin sections, although thin quartz-rich ribbon veins parallel to *Be*$S_1$ produce a closely spaced general appearance to the fabric in some cases. There are a few examples of later southwest-dipping crenulation cleavages obliquely overprinting *Be*$S_1$, recorded both by Reed (2001) and in the *TasExplore* work, but these are interpreted as Tabberabberan structures (see below). The possibility remains that *Be*$S_1$ is the second of two Benambran-aged tectonic foliations, and that at some localities it may be the net product of both.

### ?*Ta*$D_1$ structures

Reed (2001) reported two cleavages, at an acute angle to one another and both near to axial planar to the *Be*$D_1$ recumbent folds, in the Stony Head Sandstone in the vicinity of 499510/5448580 near the crest of Volunteer Hill on Bridport Road. In detail, he observed a finely spaced disjunctive cleavage overprinting the *Be*$D_1$ slaty cleavage in pelitic beds, and a spaced cleavage locally overprinting a slaty to spaced *Be*$D_1$ cleavage in sandstone strata. Both cleavages pre-dated a late northeast-dipping crenulation cleavage (assigned to *Ta*$D_3$ here, see below). Reed (2001) concluded that there had been at least local reactivation of the early recumbent structures during a subsequent phase of more upright NE-vergent folding which he interpreted as the first phase of Tabberabberan deformation (*Ta*$D_1$ here). In a similar relationship further south at 513175/5439750 on South Retreat Road, Reed's thin sections showed that a slaty cleavage associated with tight recumbent folds is obliquely overprinted by a second, closely spaced, disjunctive cleavage in pelitic units. Sandstone in a quarry nearby at 513685/5438680 shows northeast-directed low-angle thrust faults that may be related. A complication here is that *TasExplore* remapping has now included both of these localities within a larger surrounding area of Panama Group rocks, although the possibility of one or more small structural inliers of Tippogoree Group cannot be discounted and may need further local mapping to investigate. Further supporting the concept of *Ta*$D_1$ reactivation of *Be*$D_1$ structures is the common presence of NE-directed thrusts parallel or sub-parallel to *Be*$S_1$ in the Turquoise Bluff Slate, as illustrated at the Australasian Slate quarry where Reed (2004) reported refolding of the slaty cleavage associated with the thrusting.

The *TasExplore* work has added a few extra pieces of evidence for NE-vergent *Ta*$D_1$ structures overprinting *Be*$D_1$ structures in the Turquoise Bluff Slate. At two localities (511265/5454855 and 511690/5454890 on forestry roads north of Bridport Road) steeply SW-dipping close-spaced crenulation cleavage overprints the penetrative *Be*$S_1$ slaty cleavage, and at the first of these two localities is in turn overprinted by a later, close-spaced crenulation cleavage which dips ENE at 42° and is axial planar to open folds plunging at 18° to 144° (these later structures are attributed to *Ta*$D_3$). Reed (2001) commented that NE-vergent upright chevron refolding of the recumbent structures is not demonstrably evident at outcrop scale in the Tippogoree Group, and that this had contributed to previous interpretations that the recumbent folds are of the same age as upright folds in the Panama Group. However, at a scale larger than individual outcrop, the southwestern half of one of the structural profiles constructed from the new *TasExplore* data (fig. 10*b*) shows a pattern of *Be*$S_1$ form lines in the Turquoise Bluff Slate, suggesting the presence of exactly that type of NE-vergent upright second-generation folds — so there may in some cases be a scale issue in recognising *Ta*$D_1$ structures in the Tippogoree Group.

### *Ta*$D_3$ structures

There is limited evidence, discussed below, that two Devonian northeast-vergent upright folding and cleavage-forming events in the Panama Group preceded the late southwest-vergent upright folds and associated

**Figure 15**

*Be*$S_1$ *fabrics in the Turquoise Bluff Slate: (a) outcrop photograph of tightly folded thin bed of cherty siltstone at 504575/5456340 in the Australasian Slate quarry, indicating 89% minimum shortening normal to* *Be*$S_1$ *slaty cleavage (from Reed, 2004);*
*(b) photomicrograph in plane polarized light of medium–high strain* *Be*$S_1$ *fabric in a sample from the Australasian Slate quarry (504615/5456315; sample R012467); (c) higher-strain equivalent of (b) from just above the top of the Industry Road Member (505080/5445270; sample R012466); (d) photomicrograph with crossed polars showing bedding lamination almost obliterated by development of oblique high-strain* *Be*$S_1$ *penetrative slaty cleavage (511690/5454889; sample R012465);*
*(e) detail of central part of (d); (f) photomicrograph with crossed polars of intense* *Be*$S_1$ *cleavage in slate (510440/5456555; sample R012463); (g) detail of (f) showing elongate quartz-rich ribbons and lenses parallel to* *Be*$S_1$*.*

crenulation cleavages ($D_2$ of Patison *et al.*, 2001; $D_3$ of Reed, 2001) which affect both the Panama and Tippogoree groups. The latter structures are consequently assigned to *Ta*$D_3$ in this report. In the Tippogoree Group area these late structures were documented in the first-generation regional geological mapping (Marshall *et al.*, 1965; Marshall, 1969). *Ta*$D_3$ folds in outcrop are open and WSW-vergent with axial planes dipping at 70–75° to the ENE, and hinge lines plunging shallowly to the SSE. The folds commonly exhibit an axial planar close-spaced crenulation cleavage which is best developed in the most pelitic lithologies. Structural data analysis indicates that *Be*$F_1$ and *Ta*$F_3$ folds are close to coaxial, although comparison of lineation orientations suggests that *Ta*$D_3$ structures are rotated about 8–10° clockwise from *Be*$D_1$ structures in both the Stony Head Sandstone (fig. 13*c*,*e*) and the Turquoise Bluff Slate (fig. 14*c*,*e*). *Ta*$L_3$ lineations (i.e. combined *Be*$S_1$-*Ta*$S_3$ intersection lineations and *Ta*$F_3$ hinge lines) appear to show a 16° clockwise rotation from the Stony Head Sandstone to the Turquoise Bluff Slate, very similar to the observed rotation of *Be*$D_1$ structures between the two formations, and thus indicative of either a post-*Ta*$D_3$ rotation or some other control such as large-scale refraction which has equally influenced each of the successive fold events.

*Ta*$D_3$ folding appears to be largely (but not entirely) responsible for the observed variation in orientation of *Be*$S_1$ cleavage in the Tippogoree Group, but much more so in the relatively less competent Turquoise Bluff Slate, where the pattern of poles to *Be*$S_1$ is spread out into a broad girdle on the stereogram (fig. 14*b*). Poles to *Be*$S_1$ in the more competent Stony Head Sandstone show much less of this effect (fig. 13*b*).

## Panama Group structure

### Yarrow Creek Mudstone

#### *Ta*$D_1$ *structures*

The earliest structures in the Yarrow Creek Mudstone, which are assigned here to *Ta*$D_1$, are a generation of steeply inclined, NE-vergent, open to close folds with hinge lines plunging shallowly to the southeast, and common axial planar penetrative cleavage. The abrupt contrast in style between these structures and *Be*$D_1$ first-generation structures in the Turquoise Bluff Slate is particularly apparent in structural profile (fig. 10*b*). *Ta*$F_1$ fold closures are typically chevron to rounded in style, and poles to bedding form a broad girdle on the stereogram (fig. 16*a*), yielding a tightly constrained statistical fold axis plunging at 13° to 131°; *Ta*$L_1$ lineations calculated from intersections between bedding and the *Ta*$S_1$ penetrative cleavage show a similar orientation (fig. 16*c*). Poles to *Ta*$S_1$ form a well-defined cluster on the stereogram, corresponding to a preferred dip of 72° to the southwest (fig. 16*b*). The penetrative cleavage is moderately to well developed depending on lithology, but it lacks the common phyllitic sheen and intense development of the high-strain *Be*$S_1$ slaty cleavage in the Turquoise Bluff Slate. *Ta*$S_1$ in the Yarrow Creek Siltstone is rarely intense enough to make the typical thin bedding and primary lamination in the unit difficult to discern in outcrop, in contrast to typical cleavage-dominant outcrops in the Turquoise Bluff Slate.

A couple of relatively minor SW-dipping inferred thrust faults are shown within the Yarrow Creek Siltstone and at its contact with the Retreat Formation on Profile 2 (fig. 10*b*), and these are sub-parallel to local *Ta*$F_1$ fold axial surfaces. While these connect at depth with a *Ta*$D_3$ southwest-directed thrust which locally forms the contact between the Turquoise Bluff Slate and the Yarrow Creek Mudstone, and could be backthrusts associated with that structure, they are perhaps more likely to be earlier NE-directed thrusts associated with either *Ta*$D_1$ or *Ta*$D_2$. As will be seen below, this interplay between *Ta*$D_{1-2}$ NE-directed thrusts and *Ta*$D_3$ SW-directed thrusts is a common feature of the structural architecture of the Panama Group.

#### *Ta*$D_2$ *structures*

Evidence for a second Devonian generation of NE-vergent structures in the Yarrow Creek Mudstone is scant, and based mainly on outcrops on Bridport Road between 517080/5455775 and 517380/5455955 close to an inferred NE-directed thrust fault contact with the Retreat Formation (fig. 10*d*). Here, steeply inclined NE-vergent folds have a steep SW-dipping axial plane cleavage which in detail appears to be a very close-spaced crenulation cleavage (interpreted here as *Ta*$S_2$), which in the same area pre-dates a less closely-spaced late crenulation cleavage (*Ta*$S_3$) which dips northeast at 38–40° (fig. 10*d*). The inferred NE-directed thrust fault in this area, and a similar structure further east at the contact of the Retreat Formation and the Lone Star Siltstone (fig. 10*d*), are probably also *Ta*$D_2$ structures. The *Ta*$S_2$ crenulation cleavage is close to parallel with *Ta*$S_1$ penetrative cleavage observed in road cuttings a little over one kilometre further southwest (fig. 10*d*), and it is possible that any NE-vergent folds with axial plane penetrative cleavage observed in the Panama Group may be composite *Ta*$D_{1-2}$ structures.

#### *Ta*$D_3$ *structures*

Observations of late, generally NE-dipping spaced crenulation cleavages are scattered throughout the outcrop belt of the Yarrow Creek Mudstone. These structures are assigned here to *Ta*$D_3$. The cleavages are typically best developed in the most pelitic lithologies, and are generally not associated with obvious mesoscopic refolding, although *Ta*$S_1$–*Ta*$S_3$ intersection lineations suggest that any associated folds would plunge gently to the southeast (fig. 16*f*).

In detail, poles to *Ta*$S_3$ are distributed in a partial girdle pattern on the stereogram (fig. 16*e*), resulting in easterly dips in some cases, and suggesting some refolding of *Ta*$S_3$ in a later event almost coaxial with *Ta*$D_3$. In general, *Ta*$S_3$ dips less steeply (mean 35°) in the Yarrow Creek Mudstone than in the Tippogoree Group (mean 69°). The lack of associated mesoscopic folding, and perhaps also the shallower dips, may suggest a weakening of the intensity of *Ta*$D_3$ strain eastwards from the Tippogoree Group into the Panama Group.

### Retreat Formation

For analysis purposes the outcrop area of the Retreat Formation is divided into two structural domains (fig. 17), largely due to significant differences in the influence of the *Ta*$D_3$ deformation in the two areas, although there are also subtle differences in *Ta*$D_1$. The domain boundary passes

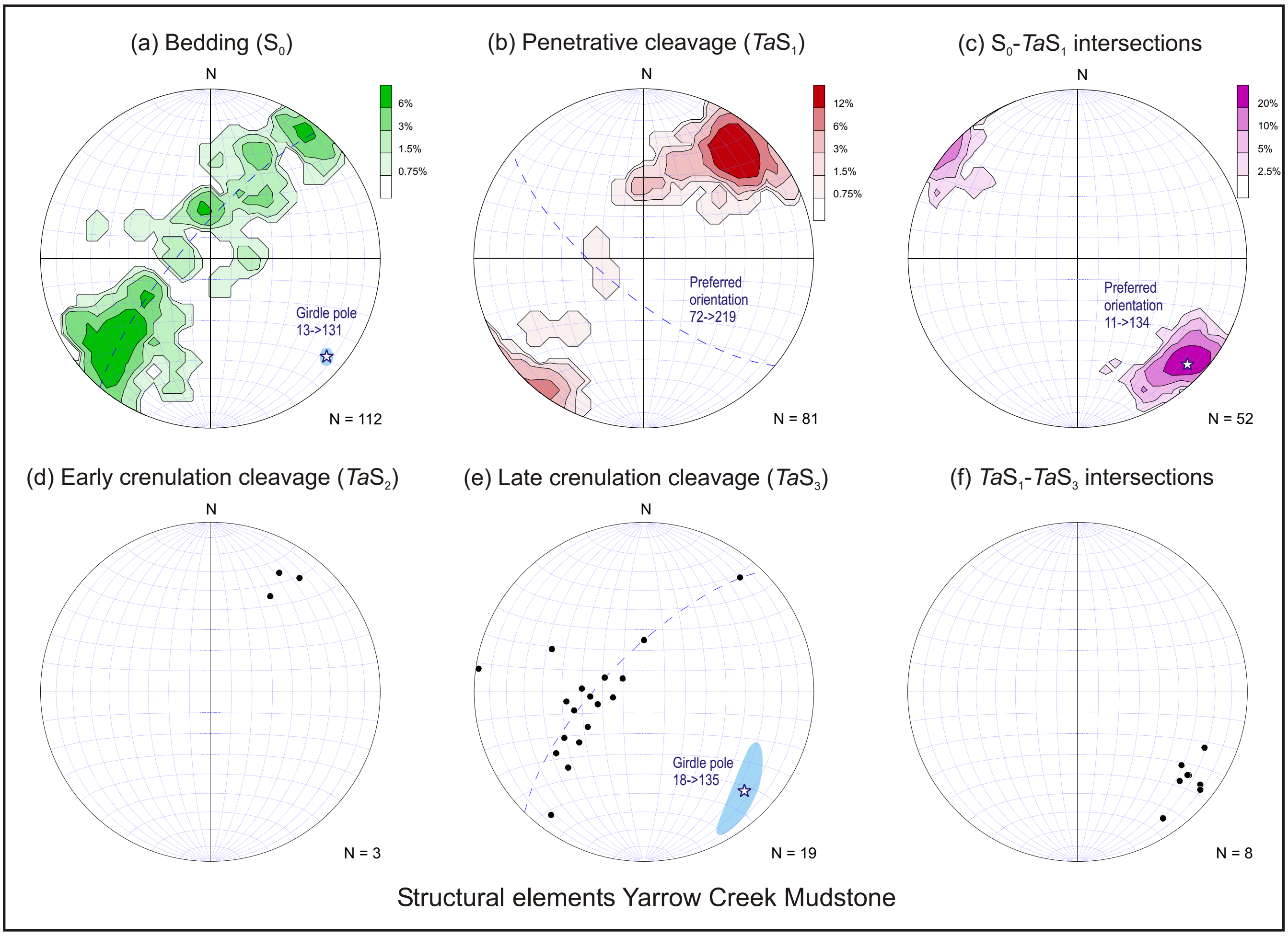


**Figure 16**

*Lower hemisphere equal-area stereograms of structural data from the Yarrow Creek Mudstone. Statistical uncertainties on girdle poles are shown by blue fields.*

close to Pipers Brook, and corresponds to a major *Ta*D$_3$ southwest-directed thrust fault (fig. 17).

### *Ta*D$_1$ structures

Profile 3 through the northern end of domain RF1 (fig. 10*c*) shows a pattern of steeply inclined NE-vergent open to close folds with axial planar penetrative cleavage (all attributed to *Ta*D$_1$), overprinted by later *Ta*D$_3$ SW-vergent folds and thrust faults. The well-defined girdle of domain RF1 bedding poles on the stereogram (fig. 18*a*) is thus probably a net product of coaxial *Ta*D$_1$ and *Ta*D$_3$ folding, around a preferred axial orientation plunging at 16° to the southeast. A similar indication of the preferred *Ta*F$_1$ axis is provided by bedding-*Ta*S$_1$ intersection lineations (fig. 18*c*). *Ta*S$_1$ orientations in domain RF1 show a strong cluster around a preferred dip of 69° to the southwest (fig. 18*b*), although there is a minor spread towards shallower dips which is probably due to *Ta*D$_3$ refolding.

The same pattern of interplay between NE-vergent *Ta*D$_1$ folds and SW-vergent *Ta*D$_3$ folds and thrust faults is repeated in domain RF2, as illustrated in profiles 4, 6, 7 and 8 (fig. 10*d,f, g,h*), although *Ta*D$_3$ is probably less prominent in this area (see below). Both sets of folds are open to close, and chevron to somewhat rounded in style. Stereograms of bedding poles and bedding-*Ta*S$_1$ intersections both suggest a 6° greater plunge of *Ta*F$_1$ folds in this domain compared to RF1 (fig. 18*f,h*).

### *Ta*D$_2$ structures

Evidence of NE-vergent *Ta*D$_2$ structures is rare in the Retreat Formation, but there is a suspicion that the geometry of the dominant NE-vergent *Ta*F$_1$ folds and associated axial plane penetrative cleavage may, to some extent, be a net product of *Ta*D$_1$ and *Ta*D$_2$. Moderately SW-dipping, probable *Ta*S$_2$ close-spaced crenulation cleavage was recorded in minor pelite interbedded with sandstone in one outcrop at 519710/5456500 on Bridport Road in domain RF2 (see profile 4, fig. 10*d*). It is also suspected that inferred NE-directed thrust faults, which form the western and eastern boundaries of the Retreat Formation between Bridport Road and the coast near Bellingham (fig. 10*d*), may be dominantly *Ta*D$_2$ structures.

### *Ta*D$_3$ structures

The structural profiles (fig. 10*c,d,f-h*) indicate that steeply inclined SW-vergent open to close folds with axial plane crenulation cleavages, and associated SW-directed thrust faults, overprint the NE-vergent *Ta*D$_1$ fold train in several relatively narrow (generally 1 km wide) corridors throughout the Retreat Formation outcrop area, but most prominently within domain RF1. These late SW-vergent structures are all attributed to *Ta*D$_3$. Associated lineations based on *Ta*S$_1$–*Ta*S$_3$ intersections (fig. 18*d*) suggest that *Ta*F$_3$ folds are close to coaxial with *Ta*F$_1$, and plunge gently to the southeast.

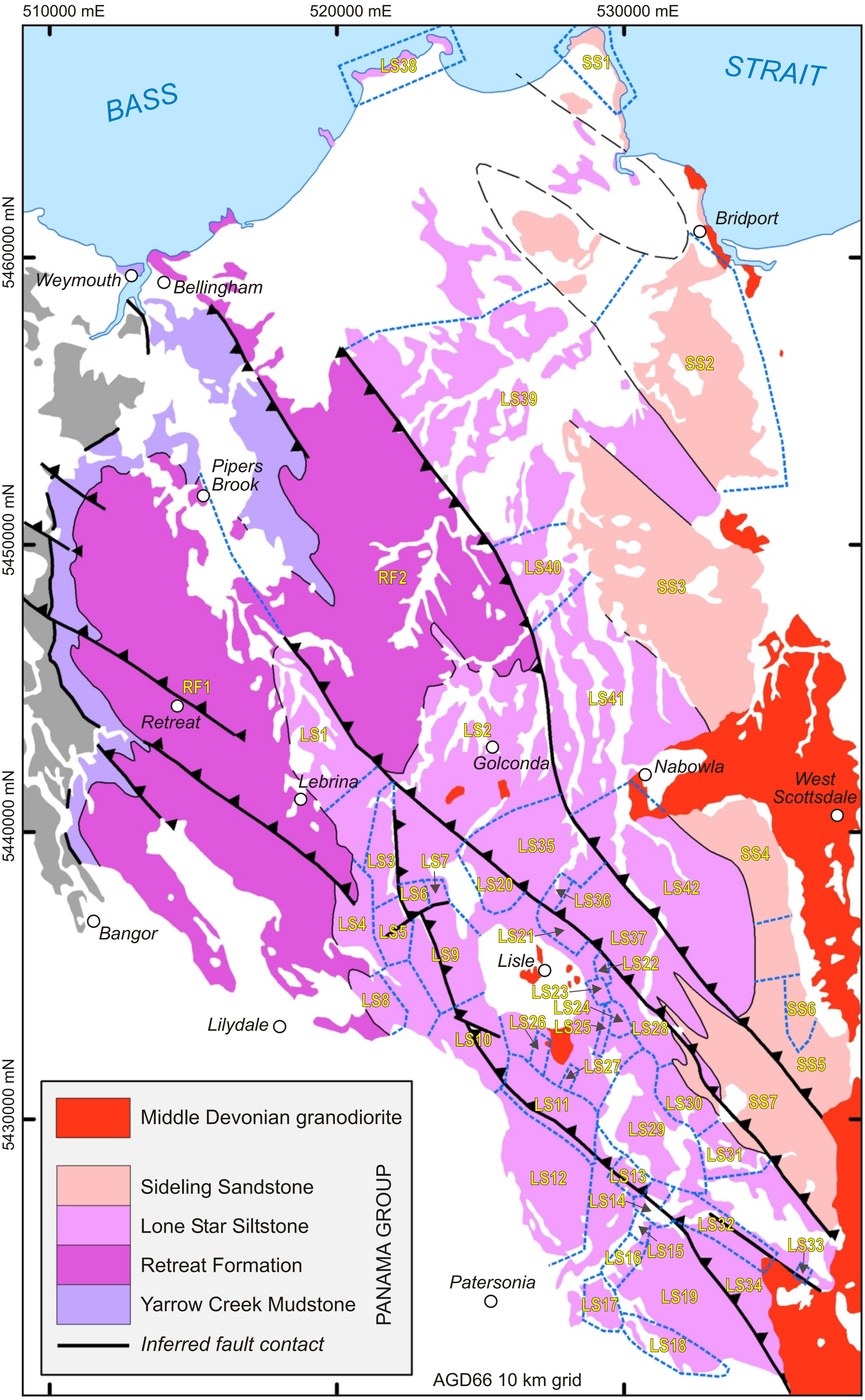


**Figure 17**

*Summary geological map of the outcrop area of the Panama Group west of the Scottsdale Batholith, showing domain boundaries used for structural analysis of the Retreat Formation, Lone Star Siltstone and Sideling Sandstone.*

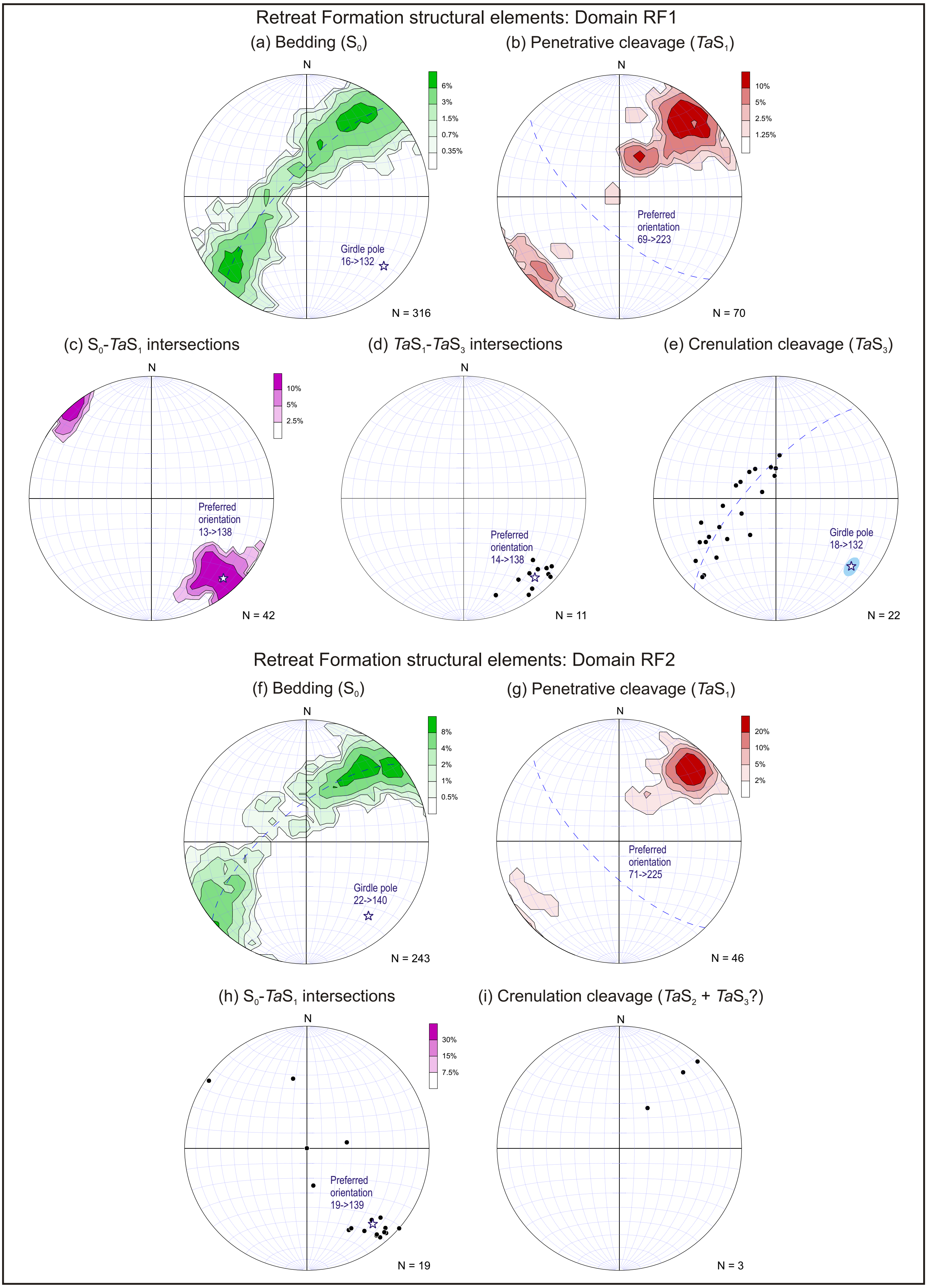


**Figure 18**

*Lower hemisphere equal-area stereograms of structural data from the Retreat Formation. Domains as in Figure 17. Statistical uncertainties on girdle poles and preferred orientations are shown where appropriate by blue fields.*

The *Ta*$S_3$ axial plane foliation is a variably developed close-spaced crenulation cleavage which is commonly best developed in pelite beds, and which in some occurrences shows associated mineralogical differentiation imparting a finely striped mesoscopic appearance to the cleavage. Observations of *Ta*$S_3$ cleavage development are almost totally confined to domain RF1, where the stereogram of *Ta*$S_3$ poles shows a partial girdle pattern (fig. 18e) suggesting some post-*Ta*$D_3$ refolding about axes close to coaxial with the earlier folds — very similar to the late refolding observed in the Yarrow Creek Mudstone (fig. 16e).

## Lone Star Siltstone

The relatively pelitic and ductile Lone Star Siltstone is areally extensive and more tightly folded than the underlying sandstone-rich Retreat Formation. While relatively large domains have sufficed to characterise the structural architecture of the Retreat Formation, it has proven necessary in some areas to subdivide the large volume of mesoscopic structural data collected from the Lone Star Siltstone into a large number of smaller domains, in order to achieve a reasonable approach to geometric consistency within each domain. This is particularly so in the area surrounding the Lisle Granodiorite (fig. 17), where structural orientations change rapidly over relatively short distances.

The new mapping has revealed a surprising aspect of the structural architecture of the Lone Star Siltstone, namely the absence (or rarity) of mesoscopic overprinting relationships, e.g. crenulation cleavage development or refolded folds. This is unexpected, particularly given the relatively easy recognition of late *Ta*$D_3$ structures overprinting earlier structures in Retreat Formation domain RF1 (fig. 18). Typical exposures of the Lone Star Siltstone show a single generation of commonly tight folds (or consistently dipping beds on a limb of such folds) with an associated single generation of axial planar penetrative cleavage. Associated outcrop-scale thrust faults are moderately common, and more major associated thrust faults have been inferred from structural profile relationships in a number of places (fig. 4).

An examination of structural cross sections through the Lone Star Siltstone provides some further insight into this issue (fig. 10). What is immediately evident is that a dominantly upright structural geometry in the northern part of the Lone Star Siltstone outcrop belt (profile 5 and sections 9 and 10, fig. 10) progressively merges into a markedly SW-vergent fold geometry with associated SW-directed thrust faults in the southern part of the belt (sections 11–14, fig. 10). Comparing profile 5 in the northern area with the adjacent profiles 4 and 6 through the Retreat Sandstone (fig. 10*d–f*) suggests that symmetrical upright folds with axial planar penetrative cleavage in the Lone Star Siltstone in this area are dominantly *Ta*$D_1$ structures. In the southern area, sections 12 to 14 show a volume of Lone Star Siltstone dominated by markedly SW-vergent folds (with dominantly NE-dipping axial plane penetrative cleavage, although not depicted on the sections) and a number of NE-dipping, SW-directed thrust faults (fig. 10*m–o*). Section 11 is intermediate in structural geometry but still shows a tendency to southwest vergence (fig. 10*k,l*). Another key point is that one of the major faults in this southern area, when followed northwest onto profile 7 (fig. 10*g*), is seen to be a SW-directed thrust associated with a narrow corridor of SW-vergent folds in the hanging wall, together comprising a set of structures of a different (and probably later) generation than the steeply inclined NE-vergent *Ta*$D_1$ folds with axial planar *Ta*$S_1$ penetrative cleavage which otherwise dominate this profile. Comparable folds and faults further northwest on profile 3 are clearly associated with *Ta*$S_3$ axial planar crenulation cleavage (fig. 10*c*), and so all of these SW-vergent structures on these two profiles are assigned to *Ta*$D_3$.

By implication, the SW-vergent folds in the southern area of the Lone Star Siltstone are also largely a product of *Ta*$D_3$, but the axial plane cleavages associated with them are reported as being of penetrative nature. In this southern area, these observations seem collectively to point to the likelihood of reactivation and re-orientation of pre-existing *Ta*$D_{1-2}$ folds and penetrative cleavage during the later SW-directed compression associated with *Ta*$D_3$, without widespread development of new crenulation-style foliations but perhaps with the development of new SW-directed thrust faults in some cases. A further illustration of this re-activation concept is the *Ta*$D_1$ NE-directed thrust fault at the western end of profile 5 in the northern area (fig. 10*e*), which when traced to the southeast gradually merges into a fault mapped as a SW-directed thrust in the southern area, and which based on the argument above would be identified as a dominantly *Ta*$D_3$ structure. The possibility that reactivation and re-orientation of earlier structures has been the norm in the Lone Star Siltstone (rather than refolding and development of overprinting cleavages) may be a consequence of two factors: its greater ductility compared to the enclosing, substantially more competent sandstone-rich formations; and the fact that *Ta*$D_{1-2}$ and *Ta*$D_3$ folds are close to coaxial and show a typical angular difference in axial plane orientation of less than 40°, and considerably less in some places.

### *Domain analysis*

Structural elements (dominantly poles to bedding and penetrative cleavage, with corresponding bedding-cleavage intersections in some cases) from 42 separate structural domains in the Lone Star Siltstone are presented in stereographic format in Figure 19 *(a–h)*; domain boundaries are shown in Figure 17. For each domain standard statistical routines were allowed to automatically identify the fold axis orientation from the pattern of bedding poles, under the usual assumption of a close approach to cylindrical folding. In those cases where a good approach to a continuous girdle pattern exists in the bedding stereogram (e.g. domain LS2, fig. 19*a*) this assumption is reinforced by the data itself. However this is not so much the case with the more common example of bedding poles forming either two density peaks on the stereogram (e.g. domain LS10, fig. 19*b*), a likely consequence of chevron fold geometry, or when a single density peak is present where a domain is located dominantly on one limb of a chevron fold train (e.g. domain LS34, fig. 19*f*). A substantial process of trial and error data selection was carried out to adjust domain boundaries to achieve reasonable structural consistency within each domain, and valid statistical differences between adjacent domains (or at least a close approach thereto). Statistical uncertainty fields around the calculated fold axes are shown on the bedding stereograms for each domain. Uncertainties around the calculated preferred orientations of cleavage for each domain are more difficult to depict on stereograms, but are probably substantial in some of the common cases where cleavage data is scant. The cleavage preferred orientation data is nonetheless included for a useful comparison with calculated fold axes, particularly as it seems statistically defendable that some domains show folds transected by the penetrative cleavage.

A synoptic view of the results of the domain analysis is provided in Figure 21, in which the statistically derived bedding-fold axis and preferred orientation of penetrative cleavage is plotted at the approximate centre of each domain. Structures in the northern half of the Lone Star Siltstone outcrop belt (approximately north of the Lebrina–Nabowla line) show greater consistency of orientation over larger areas, and the domains are thus larger, than areas further south (fig. 21). Moderate southeastward fold plunge and associated steep axial planar penetrative cleavage are the norm, but some anomalies exist. Amongst these is a reversal in fold plunge direction in domain LS40 (fig. 17, 21) not associated with significant reorientation of cleavage; a similar reversal of fold plunge direction is evident based on legacy data in domain LS38 on the Bass Strait coast. Another anomaly is present in domain LS41 immediately NNW of Nabowla, where a statistically well-established fold axis trend is rotated about 20° anticlockwise from regional, yet relatively scant data suggest that cleavage is close to regional orientation and apparently transects the folds (fig. 19*h*, 21).

Results in the southern half of the Lone Star Siltstone outcrop belt are more complex. One observation which is immediately evident is an apparent substantial clockwise rotation in azimuth of both bedding-fold axes and penetrative cleavage generally across the contact between the Retreat Formation and the Lone Star Siltstone, but excepting domain LS1 immediately north of Lebrina where such relative rotation is not evident (fig. 21). The effect is mostly confined to the set of six domains immediately east of the Lebrina–Lilydale line (fig. 21), and domain LS2 centred on Golconda. Apart from local effects around the Lisle Granodiorite (discussed next), the rotation gradually returns to 'regional' with distance away from the contact with the Retreat Formation. It is possible that this rotation is a result of the substantial competence contrast between the two formations, but there could be other explanations including the influence of reactivated basement structures or deformation due to granitoid intrusion (see below).

The other main complicating effect in the southern area is an apparent bowing of both bedding-fold and cleavage trends around the general form of the Lisle Granodiorite (fig. 21). This could be interpreted in two alternative ways, although a detailed study of the Lisle area by Roach (1994) reported no evidence of tectonic foliation development or other grain-scale deformation effects in the granodiorite, favouring an interpretation that it is a post-tectonic intrusive body. If so, the bowing in structural trends spatially associated with the intrusive body implies that it was at least, to some extent, emplaced forcibly rather than totally passively as has previously been assumed for most of the northeast Tasmanian granitoids (Williams *et al*., 1989).

The domain analysis also shows that the southern part of the Lone Star Siltstone outcrop belt, particularly southeast of a line joining Lilydale and Nabowla, shows penetrative cleavage with dominantly northeasterly dips (fig. 21). The same area includes a number of inferred major SW-directed thrust faults, which together with the NE-dipping cleavage are interpreted to be dominantly the result of the *Ta*$D_3$ phase of deformation (bearing in mind that reactivation of earlier structures has probably taken place, as argued above). It is these *Ta*$D_3$-generation cleavages that are bowed around the Lisle Granodiorite, but an interesting point is that the bedding-folds and penetrative cleavages are bowed to differing degrees in some of the domains closest to the granitoid, particularly on its northeastern, eastern and southeastern flanks (fig. 21), with transected fold relationships appearing again in some cases. If, as suggested, the distortions are due to forceful emplacement of the intrusive body, this can mean that it was emplaced at this structural level at a stage between when folds started forming and when cleavage was completely developed, which may mean the Lisle Granodiorite is to some extent late-*Ta*$D_3$ in relative age rather than completely post-tectonic (or perhaps alternatively that forceful intrusion actually created folds in its own right).

A further illustration of the effects outlined above is provided by a 3-D spatial averaging of all penetrative cleavage orientations in the Panama Group (fig. 22). The results are presented in 2-D only in this figure, but nonetheless the strong clockwise deflection of trends across the Retreat Formation–Lone Star Siltstone contact, and the local bowing effects around the main outcrop area of the Lisle Granodiorite, are well illustrated (fig. 22). Also shown on Figure 22 is the pre-*TasExplore* gravity-derived model for the subsurface forms of the Diddleum and Lisle granodiorites and related bodies, and it is evident that there are some deficiencies in this model (e.g. compare the 1 km isobath with the mapped surface outcrop of the granitoids, also a possible eastward offset of the 1 km isobath around Lisle from the spatially averaged cleavage pattern). Despite these issues, the granitoid model suggests a possibility that the strong clockwise rotation of cleavage trends in the lower part of the Lone Star Siltstone immediately east of the Lilydale–Lebrina line is due to compression between the main cupola of the Lisle Granodiorite and a secondary, non-outcropping cupola immediately north of Lilydale (fig. 22).

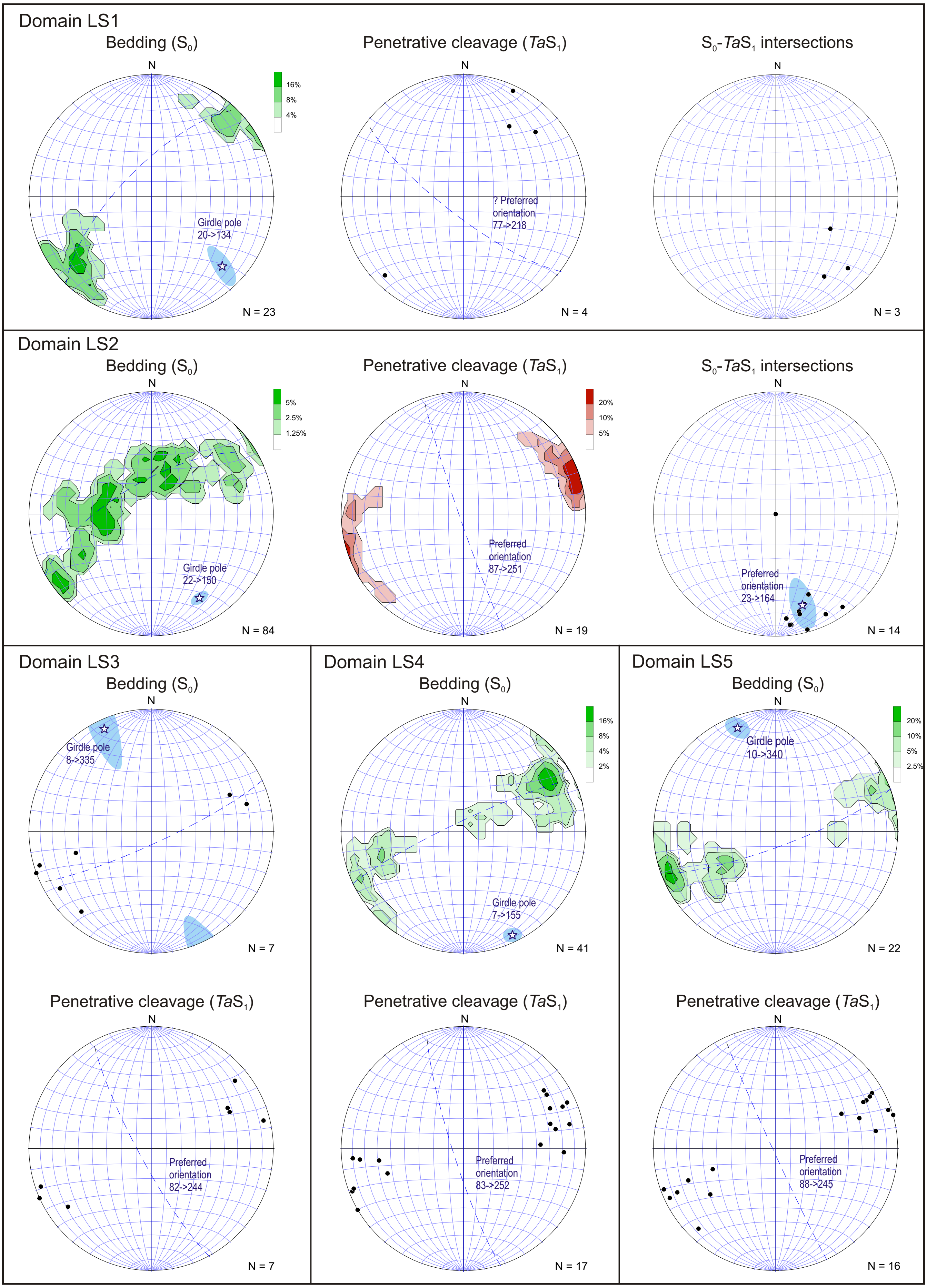


**Figure 19a**

*Lower hemisphere equal-area stereograms of structural data from the Lone Star Siltstone. Domains as in Figure 17. Statistical uncertainties on girdle poles and preferred orientations are shown where appropriate by blue fields.*

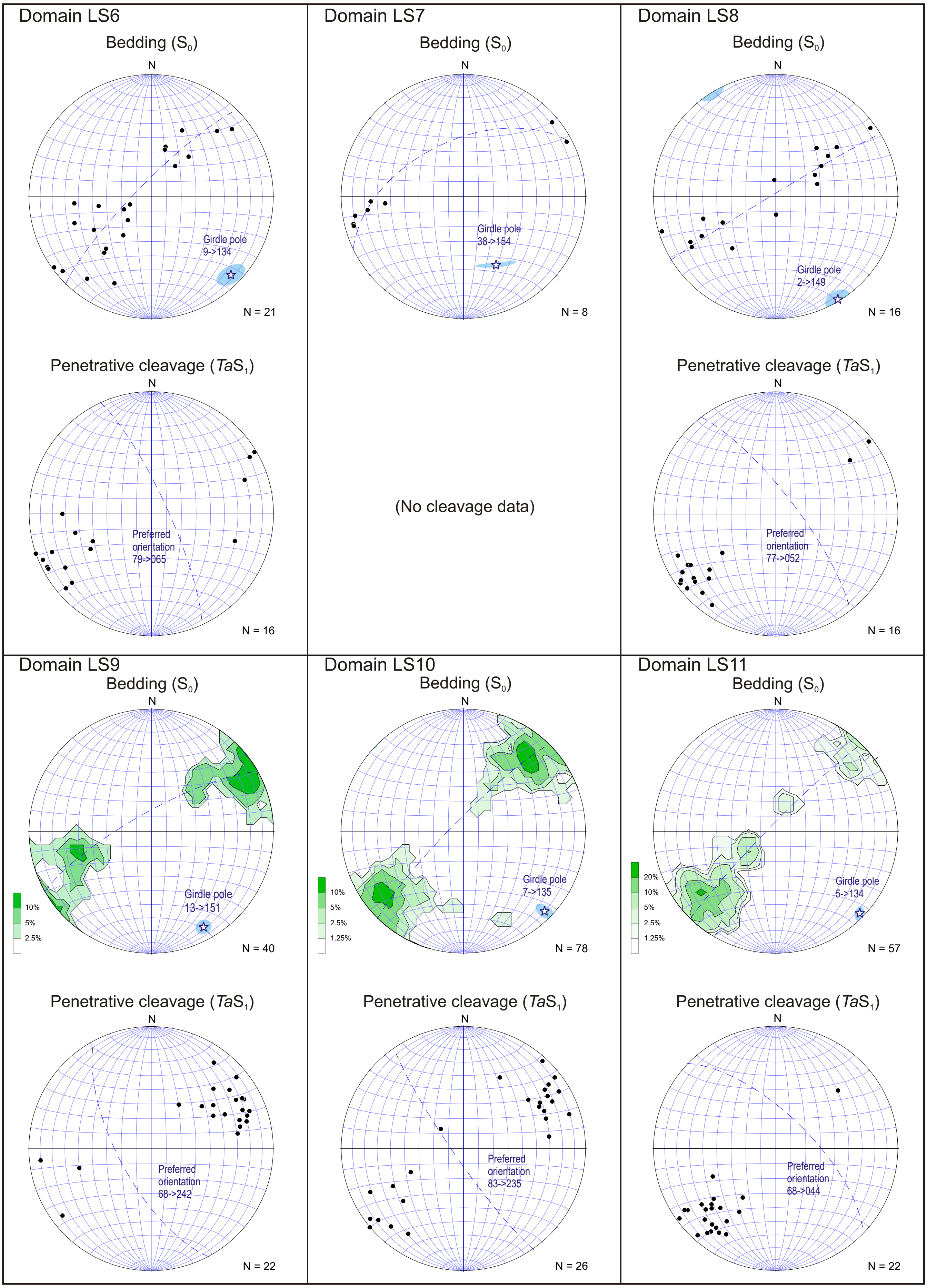


**Figure 19b**

*Lower hemisphere equal-area stereograms of structural data from the Lone Star Siltstone. Domains as in Figure 17. Statistical uncertainties on girdle poles and preferred orientations are shown where appropriate by blue fields.*

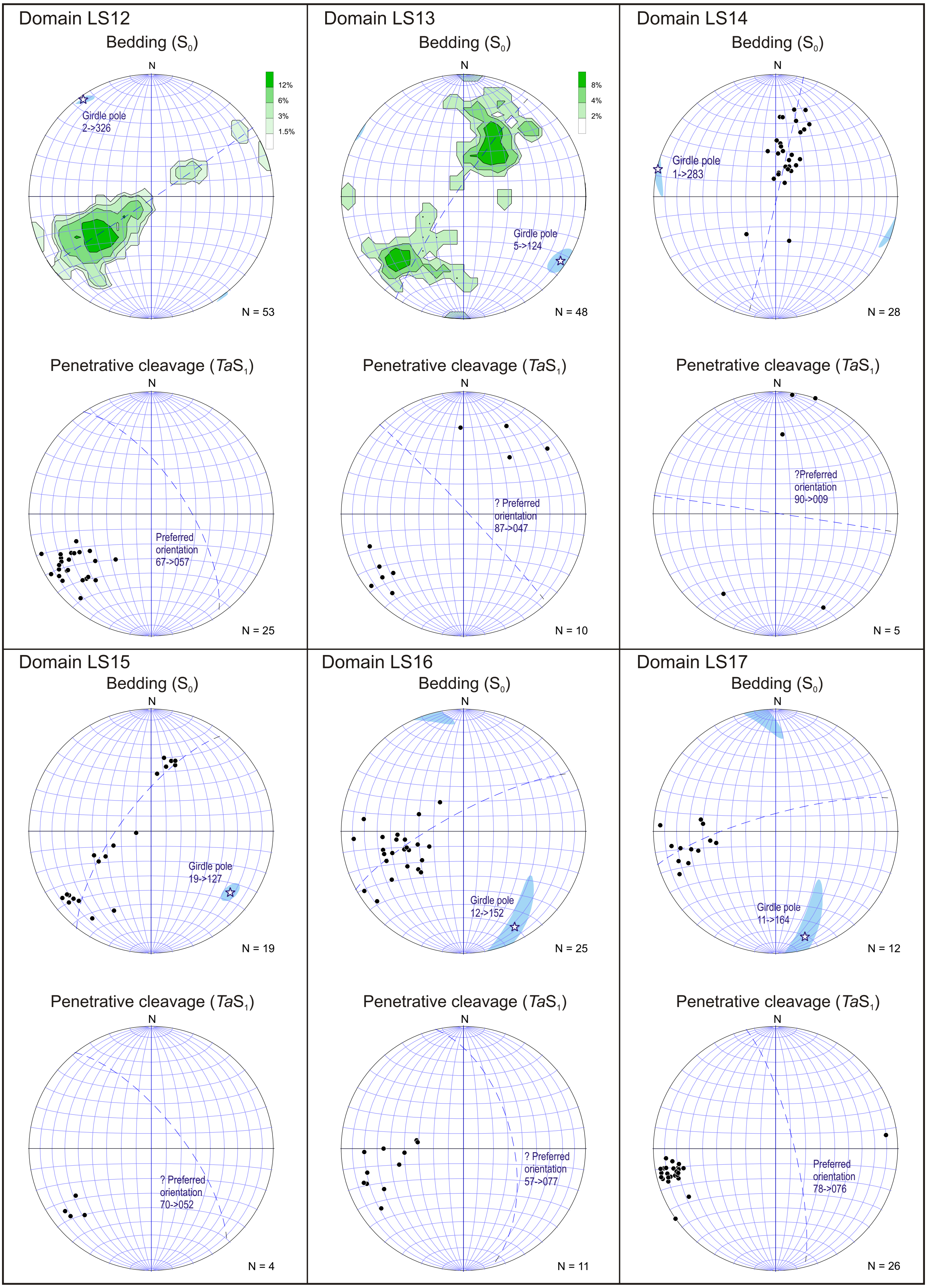


**Figure 19c**

*Lower hemisphere equal-area stereograms of structural data from the Lone Star Siltstone. Domains as in Figure 17. Statistical uncertainties on girdle poles and preferred orientations are shown where appropriate by blue fields.*

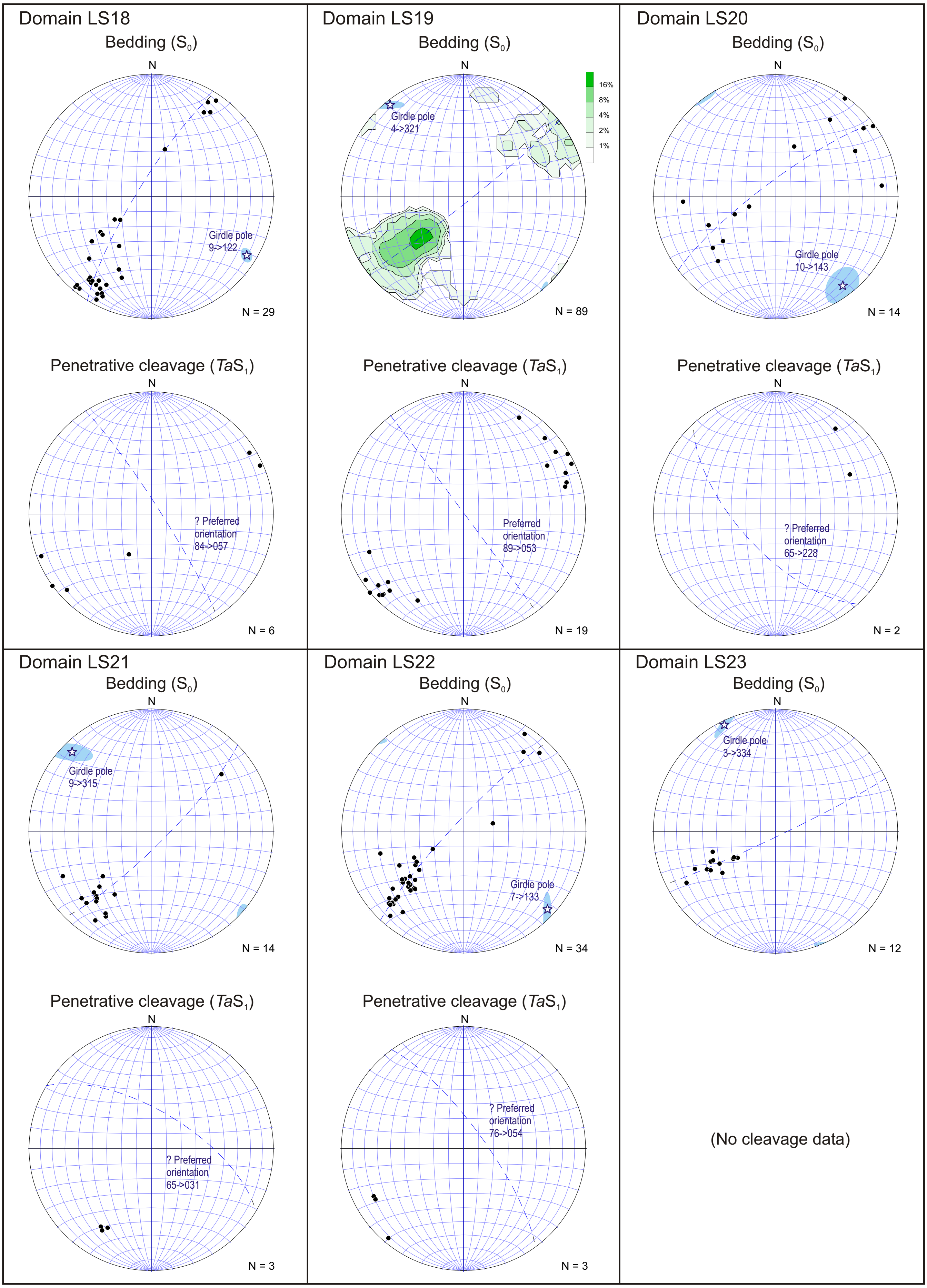


**Figure 19d**

*Lower hemisphere equal-area stereograms of structural data from the Lone Star Siltstone. Domains as in Figure 17. Statistical uncertainties on girdle poles and preferred orientations are shown where appropriate by blue fields.*

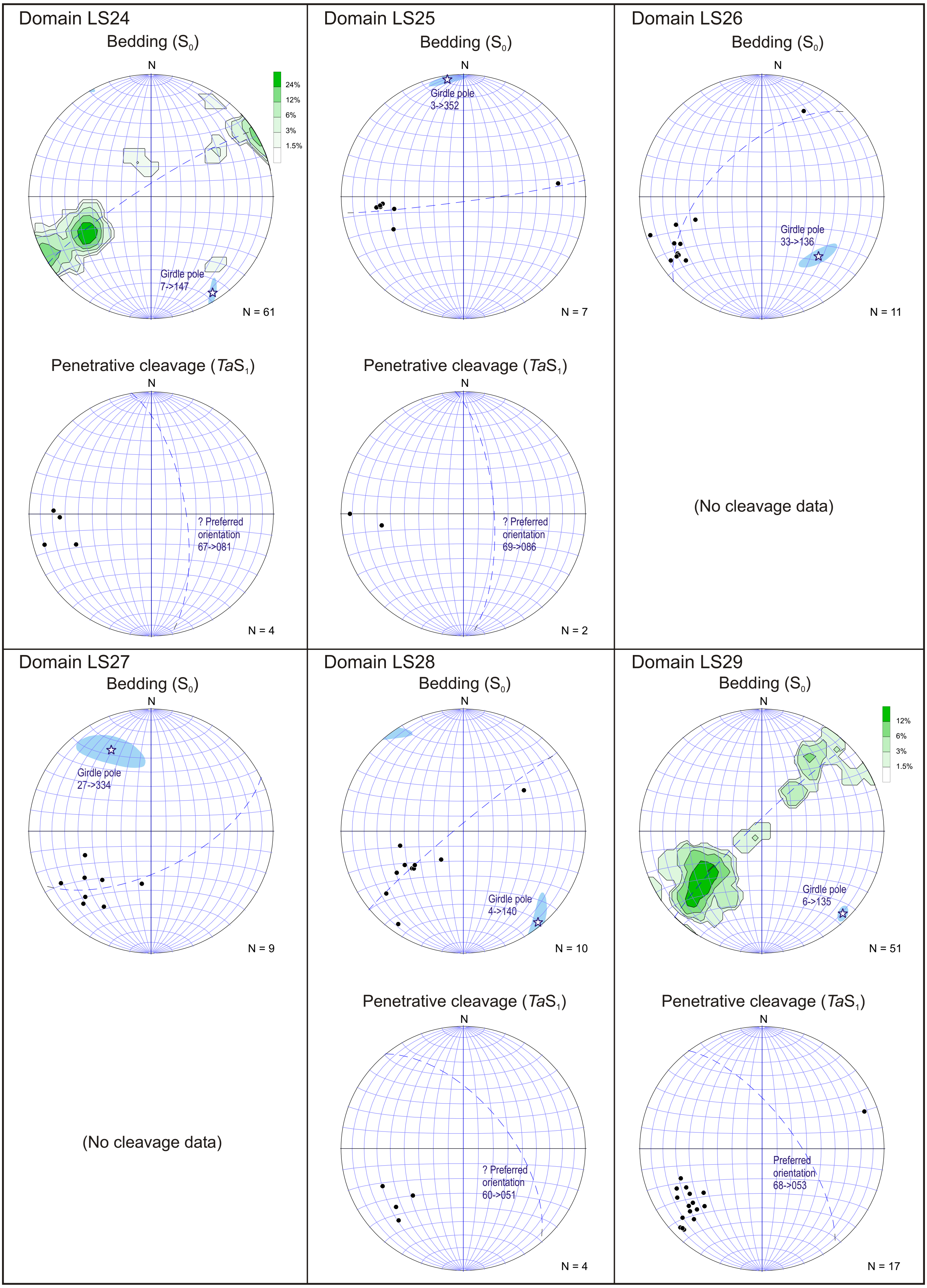


**Figure 19e**

*Lower hemisphere equal-area stereograms of structural data from the Lone Star Siltstone. Domains as in Figure 17. Statistical uncertainties on girdle poles and preferred orientations are shown where appropriate by blue fields.*

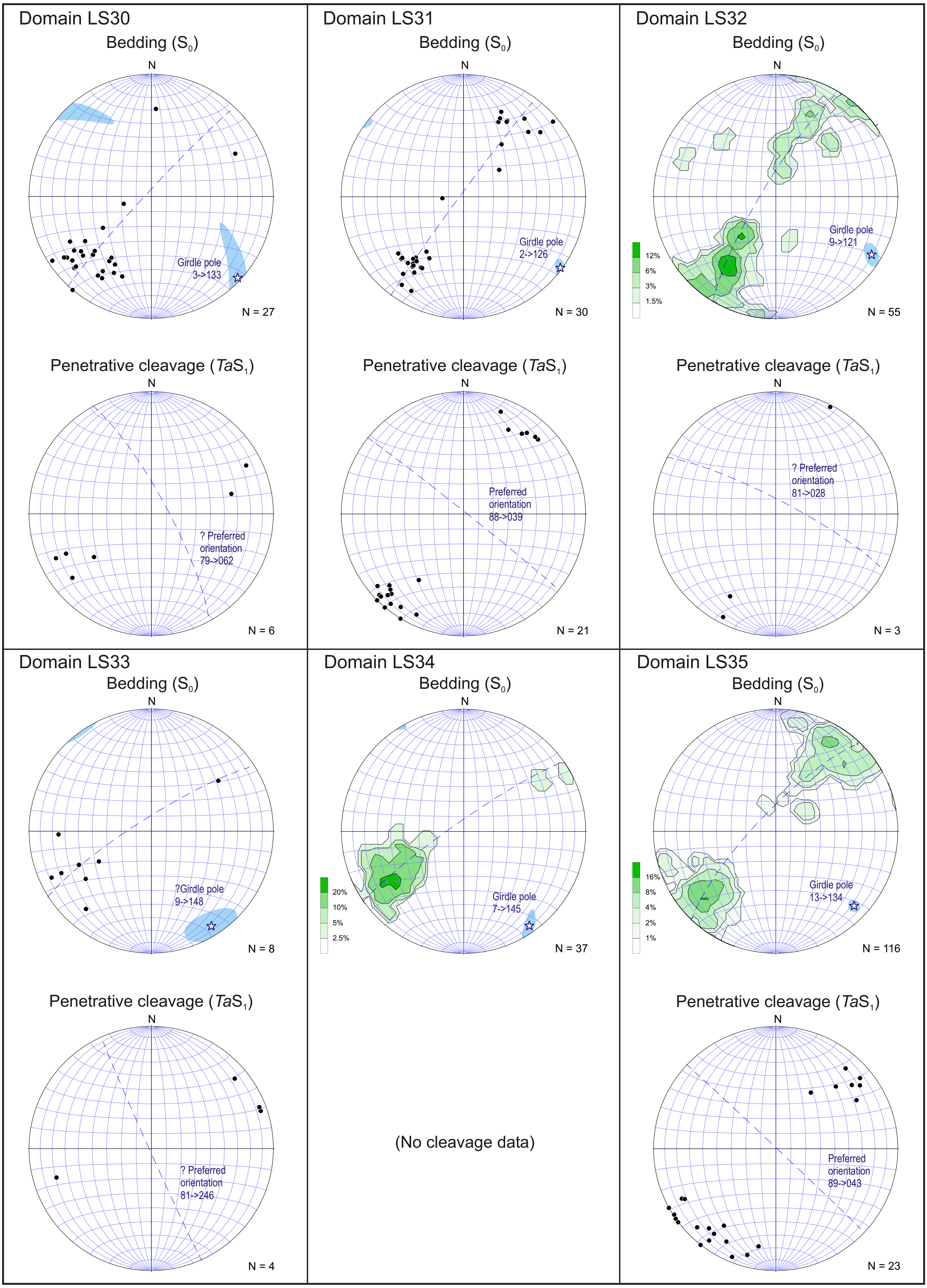


**Figure 19f**

*Lower hemisphere equal-area stereograms of structural data from the Lone Star Siltstone. Domains as in Figure 17. Statistical uncertainties on girdle poles and preferred orientations are shown where appropriate by blue fields.*

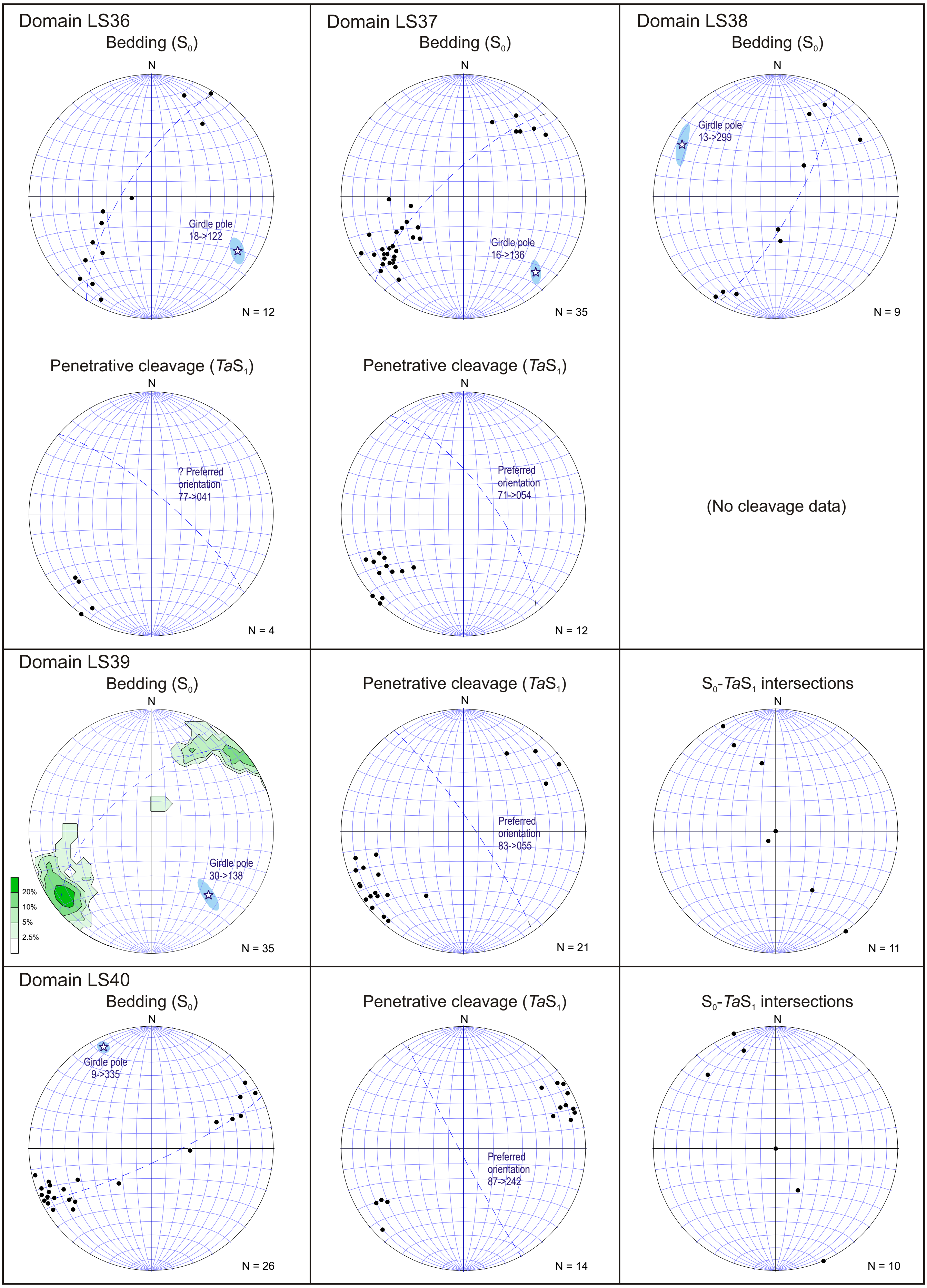


**Figure 19g**

*Lower hemisphere equal-area stereograms of structural data from the Lone Star Siltstone. Domains as in Figure 17. Statistical uncertainties on girdle poles and preferred orientations are shown where appropriate by blue fields.*

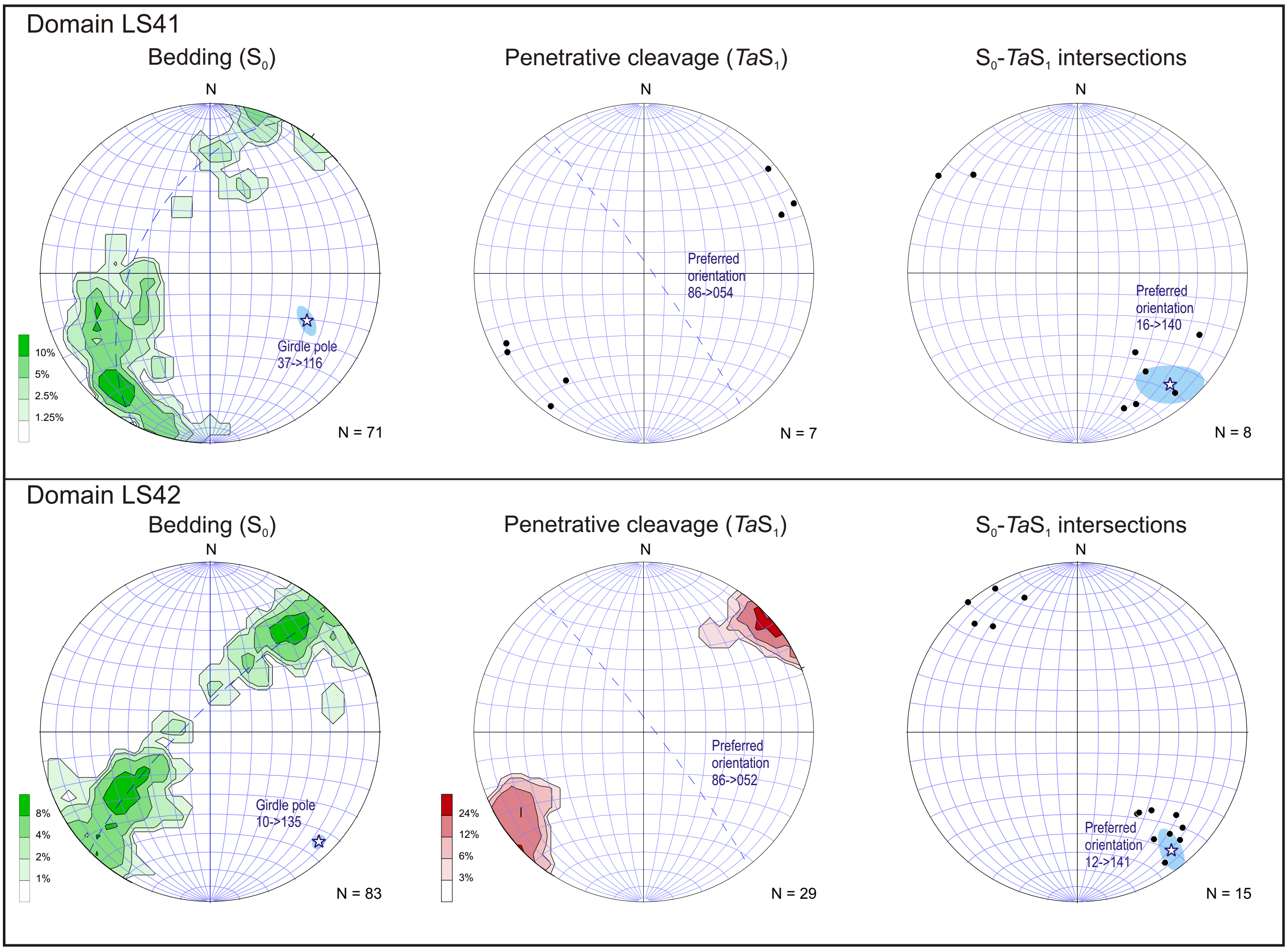


**Figure 19h**

*Lower hemisphere equal-area stereograms of structural data from the Lone Star Siltstone. Domains as in Figure 17. Statistical uncertainties on girdle poles and preferred orientations are shown where appropriate by blue fields.*

## Sideling Sandstone

Structural cross sections through the Sideling Sandstone allow a similar interpretation to that obtained from the Lone Star Siltstone. The northern part of the outcrop belt (sections 9 and 10, fig. 10) shows relatively open, upright folds (with sub-vertical axial plane penetrative cleavage, see domains SS2 and SS3, fig. 20), which are considered to be dominantly $TaD_1$–?$TaD_2$ structures. By contrast, sections 12 and 13 through the southern part of the belt show tighter folds with distinct southwesterly vergence (fig. 10*m,n*), interpreted as due to a greater influence of $TaD_3$ deformation in this area.

Structural domain analysis in the relatively competent Sideling Sandstone required a smaller number of domains to adequately characterise orientational variation. Results are shown in stereographic format in Figure 20, and summarised for each domain in Figure 21, in which several medium-scale effects are evident. As with the cross sections, the influence of $TaD_3$ is more prominent in the southernmost domains, with northeast-dipping penetrative cleavage being dominant here. In domains SS4 and SS6 southeast of Nabowla, fold and to some extent cleavage trends are rotated to sub-parallelism with the western margin of the Diddleum Granodiorite (fig. 21), consistent with shouldering aside of structures due to forceful emplacement of the intrusive rock. These two domains also appear to show a steepening of fold plunges compared to domains further away from the granodiorite. Domain SS1 (based on a re-plotting of legacy data from Jennings, 1967) shows very atypical data patterns on the stereograms; hinge lines to folds in bedding are dominantly sub-vertical, but distributed in a partial girdle pattern approximately parallel to the preferred orientation of penetrative cleavage, which is itself fairly consistent but seemingly rotated clockwise away from the regional trend towards parallelism with the nearby western margin of the Diddleum Granodiorite, concealed a short distance away to the east (fig. 21). This unusual geometry has previously been ascribed to rotations associated with intrusion of the granodiorite (Williams *et al.*, 1989). Finally, bedding data from domain SS2, south of Bridport, shows with reasonable confidence that folds in bedding have hinge line orientations close to 'regional', yet scant cleavage data suggest a preferred orientation 28° clockwise from 'regional' and possibly transecting the folds (fig. 20*b*, 21).

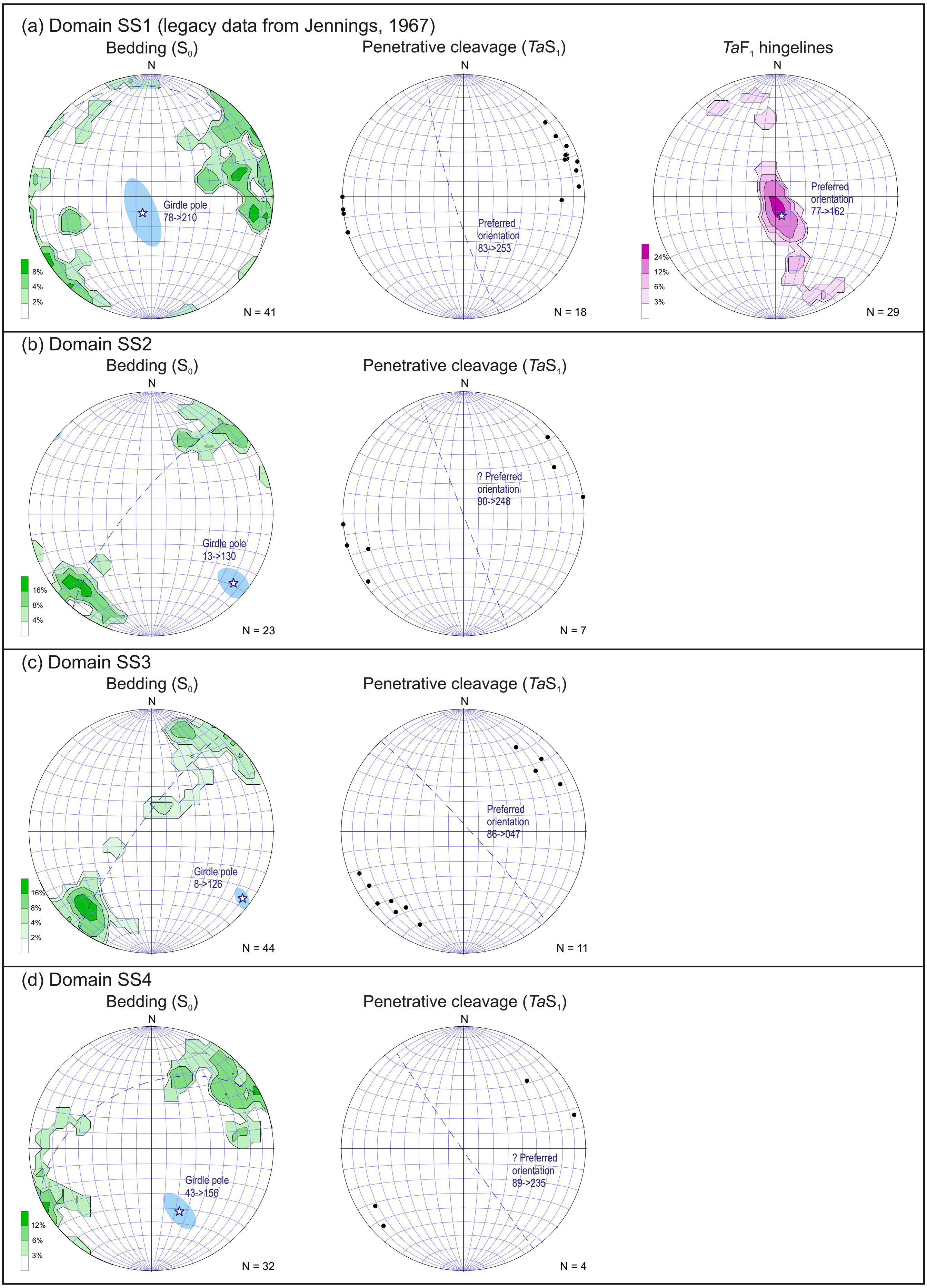


**Figure 20 (a–d)**

*Lower hemisphere equal-area stereograms of structural data from the Sideling Sandstone. Domains as in Figure 17. Statistical uncertainties on girdle poles and preferred orientations are shown where appropriate by blue fields.*

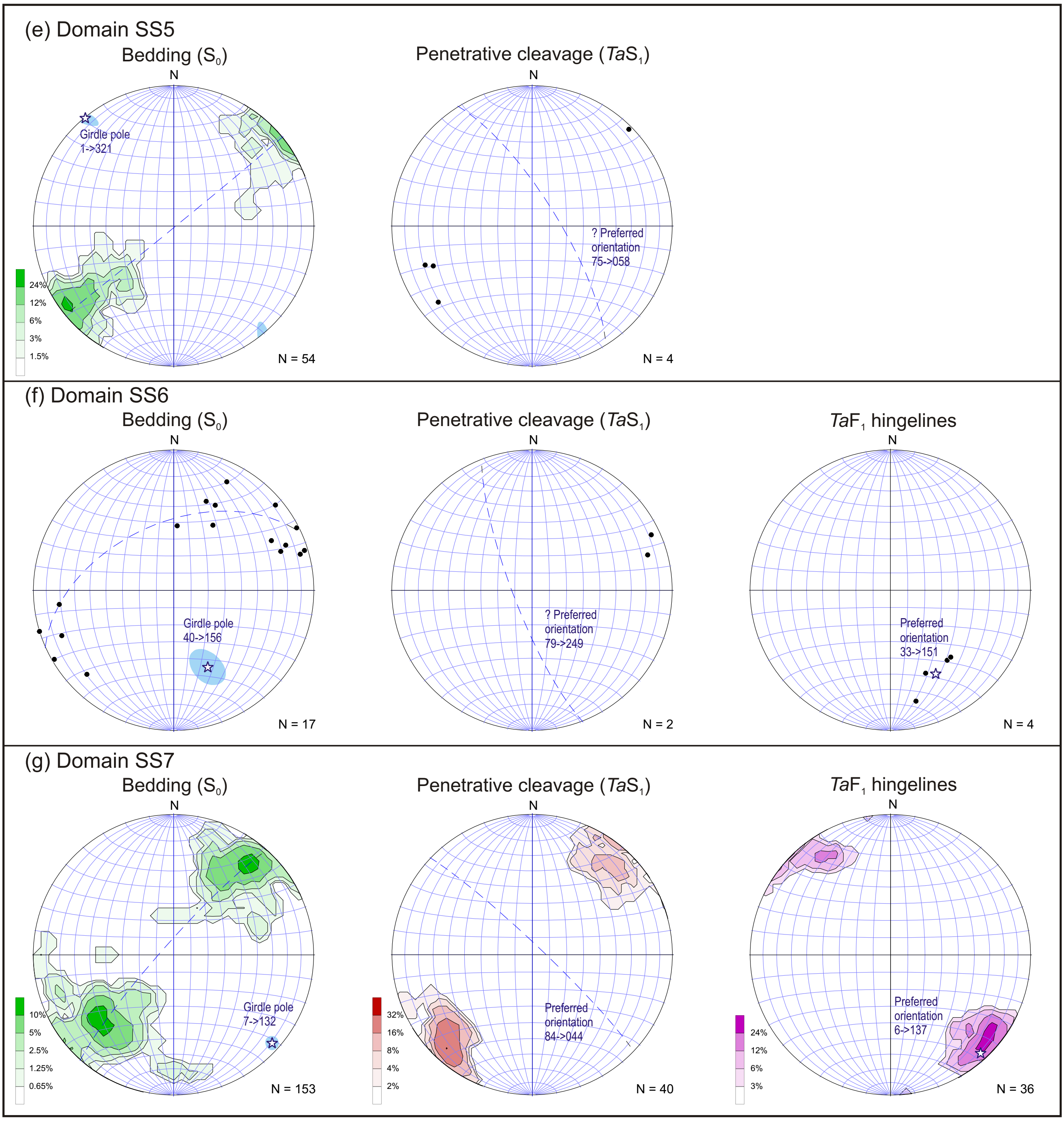


**Figure 20 (e–g)**

*Lower hemisphere equal-area stereograms of structural data from the Sideling Sandstone. Domains as in Figure 17. Statistical uncertainties on girdle poles and preferred orientations are shown where appropriate by blue fields.*

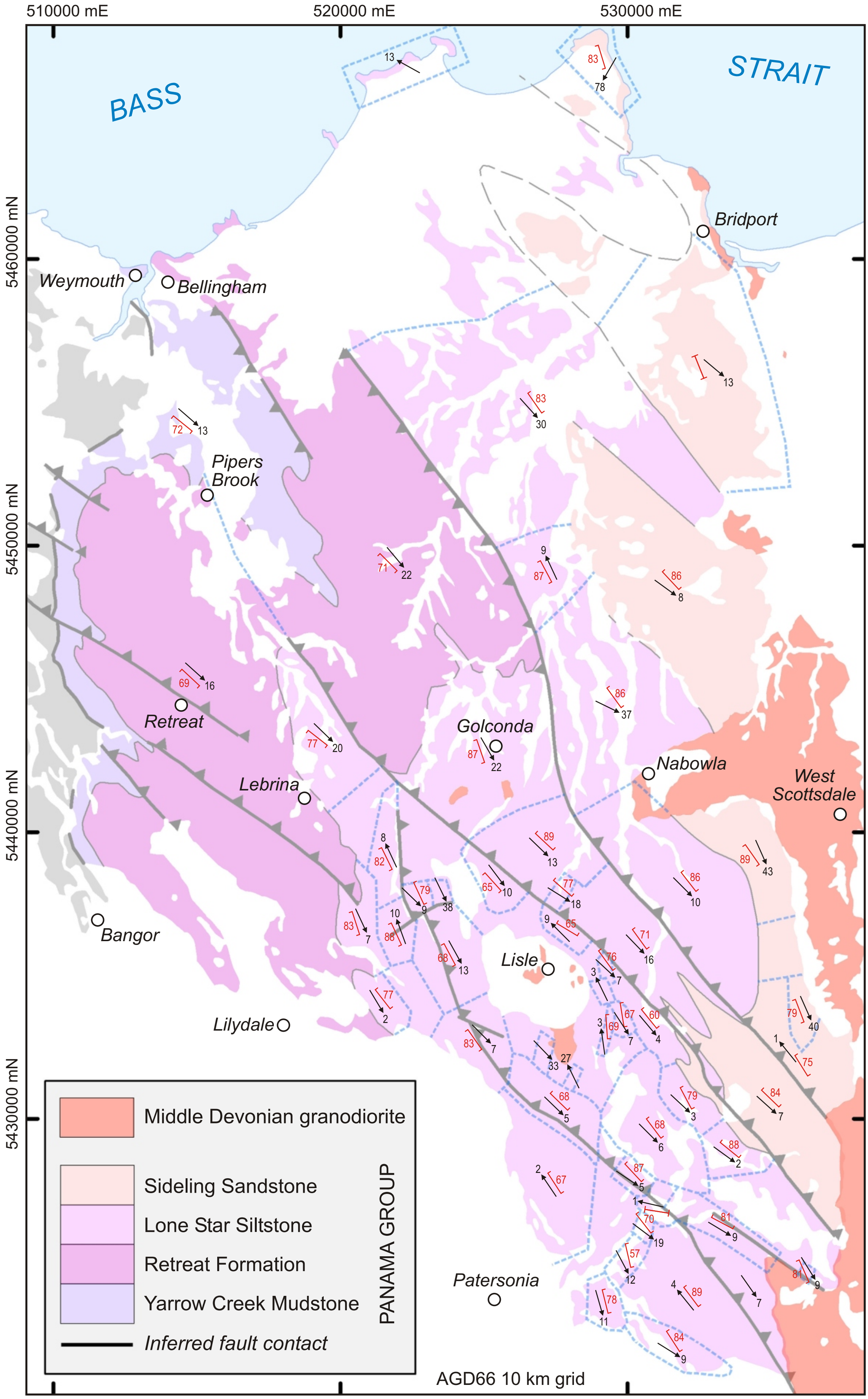


**Figure 21**

*Summary map showing statistically preferred orientations of axes to folds in bedding (black arrows with plunges), and of penetrative cleavage (red symbols with dips), in all structural domains in the Panama Group, derived from stereographic analysis of bedding and cleavage data.*

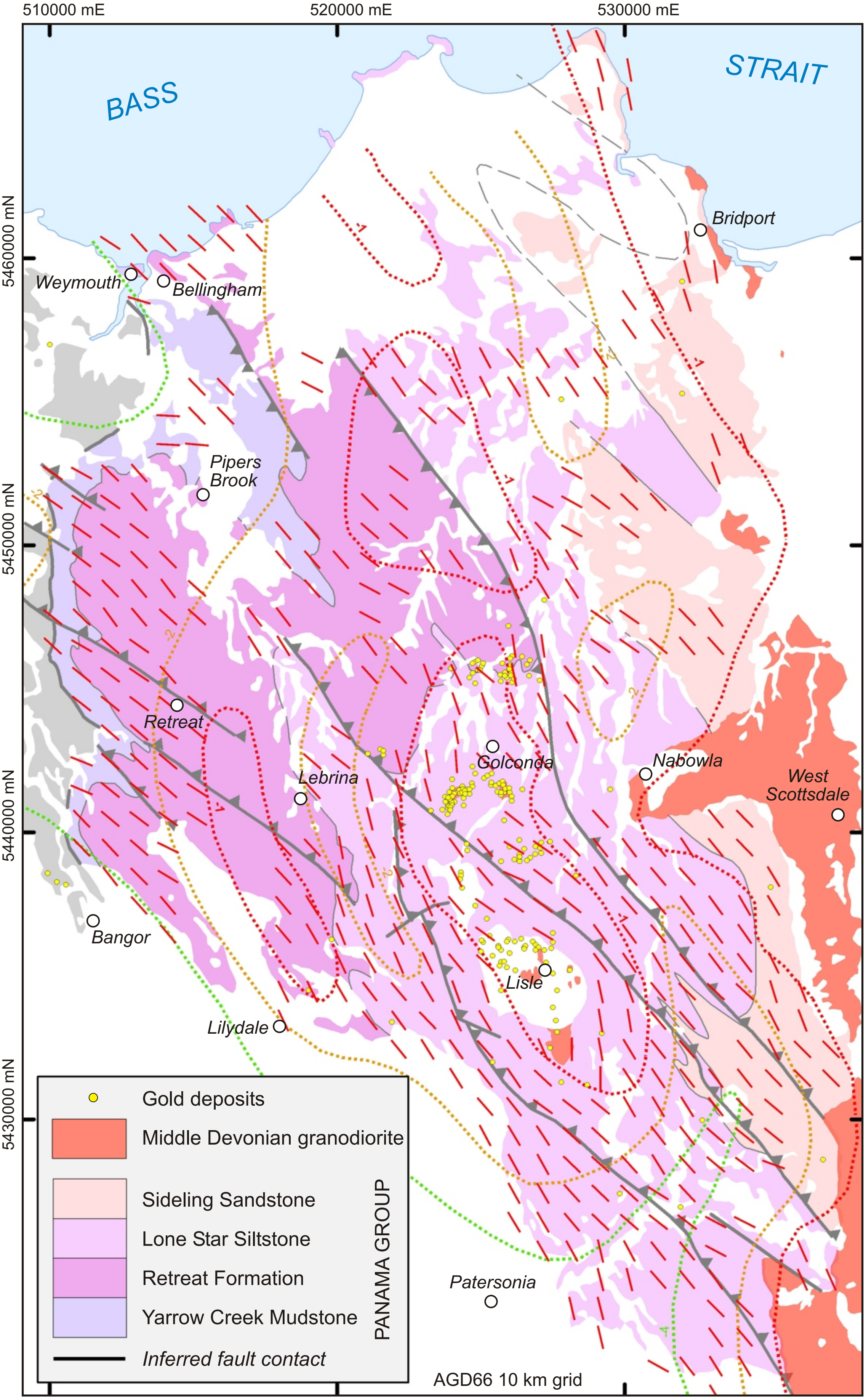


**Figure 22**

*Map showing the result of spatial averaging (on 1 km grid) of 738 measurements of penetrative cleavage in the Panama Group, presented as strikes of resultant average orientations. Dotted lines shown for reference are isobaths in kilometres depth to top of Devonian granitoid (from gravity-based model of Leaman and Richardson, 2003).*

## Structural effects of granitoid intrusion

The structural analysis presented above has identified deflections of structural trends that could be attributed to strain associated with forceful emplacement of the Lisle and Diddleum granodiorites. To examine this further, it is worth reviewing the current evidence on the age and internal structural characteristics of these granitoids. The Lisle Granodiorite is poorly outcropping and deeply weathered, and does not currently have a reliable radiometric age. The best data for the crystallisation age of the Diddleum Granodiorite is a SHRIMP U-Pb age of 390   2 Ma (Black *et al*., 2005). This is close to and partially overlaps with a Rb-Sr age of 388   1 Ma for the St Marys Porphyry (near Tasmania's east coast), the crystallisation of which separates older and younger Devonian deformation phases (Turner *et al*., 1986) which equate respectively with $Ta\mathrm{D}_{1-2}$ and $Ta\mathrm{D}_3$ in the terminology of this report — with the rider that regional deformation fronts can migrate progressively across a terrane, and thus vary in absolute age from one side to another. It is unlikely that intrusion of the Diddleum Granodiorite post-dated $Ta\mathrm{D}_3$, but it may have been post-tectonic or perhaps partially syn-tectonic with the earlier Devonian deformations.

Previous evidence for the internal foliation characteristics of these granodiorites is somewhat inconclusive regarding foliation origin, and this is a potential candidate for further work. Marshall (1969) regarded these intrusive rocks as post-orogenic, based partly on an absence of what he termed "secondary tectonic foliation". However he noted the uncommon presence of a weak foliation due to planar preferred orientation of biotite and hornblende, which was attributed to flow during granitoid emplacement. Marshall (1969) also noted the presence of a definite planar preferred orientation of xenoliths in the granodiorite, despite the paucity of primary foliation. Later work by Turner (in McClenaghan *et al*., 1982), on similar granodiorites along the eastern margin of the Scottsdale Batholith, identified a single dominant biotite-hornblende grain-defined foliation which varies considerably in intensity, being well developed within a few kilometres of the batholith margin. The latter observation is perhaps suggestive of a primary flow foliation. Taheri *et al*. (2004) referred to the Diddleum Granodiorite as one of three early, foliated biotite-hornblende bodies in the Scottsdale Batholith, and included it in a group of compositionally similar granodiorites across northeast Tasmania, many of which are distinguished by having a tectonic foliation parallel to a foliation in the Mathinna Supergroup country rocks. This generalisation may perhaps apply more to the early granodiorites in the Blue Tier Batholith than those in the Scottsdale Batholith. The poorly outcropping Lisle Granodiorite has had relatively little investigation. Samples collected by Roach (1994) showed little macroscopic or petrographic variability, all consisting of medium-grained equigranular hornblende-biotite granodiorite; no mention was made of foliation in the rock and included photomicrographs show no apparent deformation textures. The petrographic and geochemical investigation by Bottrill (1996*b*) of the Lisle Granodiorite intersected in diamond drilling revealed fresh, equigranular granitoids with some variation from granodiorite to tonalite, plus xenoliths of quartz diorite and some more siliceous granodioritic to aplitic dykes. No foliation could be detected, excepting some local weak veining. Chemical and petrophysical characteristics of the Lisle Granodiorite support a conclusion that this is a separate and distinct body from the Diddleum pluton (Roach, 1994), and so it cannot be assumed that it shares the latter's radiometric age.

All evidence considered, it seems likely that both the Diddleum Granodiorite and the Lisle Granodiorite were intruded post-$Ta\mathrm{D}_{1-2}$, but that neither body carries any substantial pervasive tectonic grain foliation associated with $Ta\mathrm{D}_3$. The structures that are deflected adjacent to the western margin of the Diddleum pluton due to its forceful emplacement, particularly on the coast northwest of Bridport, were dominantly $Ta\mathrm{D}_{1-2}$ structures prior to pluton emplacement. Similarly deflected structures around the form of the Lisle Granodiorite, and in the area between it and an inferred concealed pluton to the west, had in part been reactivated and reorientated to SW vergence/NE dips during $Ta\mathrm{D}_3$ prior to disturbance due to pluton emplacement at the structural level represented by the present ground surface. There is some evidence to suggest that $Ta\mathrm{D}_3$ deformation partially overlapped with granitoid emplacement at this structural level in the Lisle area.

# METAMORPHISM

## Granitoid-related contact metamorphism

The Sideling Sandstone and/or Lone Star Siltstone have been contact metamorphosed in areas adjacent to the western margin of the Scottsdale Batholith and surrounding the granodiorite bodies in the Lisle area. The metamorphism is recognised by a recrystallised texture and by the development of mineral spots. Spotting is best developed in the siltstone, while metamorphic effects are more difficult to recognise in the sandstone. The limit of the metamorphic aureole is marked by the onset of spotting in the siltstone or clear signs of recrystallisation in sandstone. The width of the aureole along the western margin of the Scottsdale Batholith is generally about one to 2.5 kilometres at ground level. This variation may reflect the 3-D orientation of the granite contact, with the ground width being least where it is steepest and greatest where it is shallowest. A small outlying area of aureole recognised in an incised creek at 534171/5438864 may indicate that the granite is close to the surface in that area.

In thin section the hornfels close to the granite surface has a recrystallised texture with loss of original sedimentary grain boundaries and without any mineral alignment due to cleavage. The mineralogy is quartz-biotite-cordierite-K feldspar-plagioclase with minor ilmenite and chlorite. The cordierite occurs in poorly defined optically continuous single-crystal patches. It is difficult to distinguish from quartz but its presence has been confirmed by XRD. The presence of cordierite indicates that the rocks close to the granite boundary attained the hornblende hornfels facies. Further from the granite, abundant oval spots consist of pale brown biotite. Here the quartz clasts in the matrix still retain their original sedimentary grain boundaries and a foliation defined by biotite and muscovite is slightly flattened around the spots.

# GEOPHYSICS

## Introduction

Following the *TasExplore* airborne geophysical data acquisition, the area of Mathinna Supergroup rocks covered by this report is now completely covered by 200 m line-spacing, 80 m terrain clearance, total magnetic intensity and 3-channel (K-Th-U) radiometric data. *TasExplore* also added a substantial number of new ground stations to upgrade the existing gravity data coverage. Images of the new and/or updated data are presented here at about 1:400 000 scale in Figure 23, in which the coverages are masked to show only responses within the areas of Mathinna Supergroup outcrop. *TasExplore* included the calculation, jointly with Geoscience Australia, of new 3-D potential field edges ('worms') based on the new and/or updated gravity and TMI data, and these are presented in Figure 24, which also shows responses outside the Mathinna Supergroup outcrop areas.

## Gravity

### *Anomalies and features*

The revised residual gravity coverage shows several broad-scale features as well as a better resolution of second-order anomalies due to the increased ground station density (fig. 23*a*). The most notable feature is a large positive anomaly in the western part of the area, which shows a high degree of coincidence with the area underlain by Ordovician Tippogoree Group rocks. This could be partially due to a net positive density contrast of these rocks against the Panama Group, but this seems unlikely to be the sole reason given the actual lithologies present. It is perhaps possible that the high-strain Turquoise Bluff Slate is somewhat denser than typical Panama Group rocks; this is difficult to investigate with currently available physical property data, as Roach (1994) has shown that density measurements from Mathinna Supergroup surface outcrop samples are unreliable, but there are few measurements from more reliable drill core or mine dump samples west of the Scottsdale Batholith. It seems more likely that this anomaly mostly represents the response of a rock unit structurally underlying the Turquoise Bluff Slate, that was relatively uplifted at the same time that the latter unit was elevated to its current structural level. This would imply a source in basement to the Mathinna Supergroup, but not Cambrian ultramafic rocks as there is no matching magnetic anomaly to accompany the gravity feature.

It is notable that the eastern 'fade-off' of the anomaly merges into the western part of the surface outcrop area of the Panama Group (fig. 23*a*), consistent with the source being underneath the Tippogoree Group but limited by an eastward-dipping structure; this would be compatible with the interpretation favoured in this report for the structural relationship between the Tippogoree and Panama groups. Planned 3-D inversion modelling, and/or a reflection seismic survey, may resolve the issue. While not greatly obvious in Figure 23*a* due to the masking, the northeastern margin of this anomaly is a relatively sharp NNW-trending linear which could represent the northward continuation of the major *Ta*$D_3$ SW-vergent thrust fault which has been mapped passing northeast of the Lisle Granodiorite.

Further east, the outcrop area of the Retreat Formation appears to show a noticeable degree of correspondence with a negative gravity anomaly (fig. 23*a*), particularly if the overlap of the large positive anomaly further west is filtered out. It is also notable that the largest negative amplitude of this anomaly corresponds with the more northeastward of the two structural domains in the Retreat Formation (domain RF2), in which the depth to structural base (depth of folding) in the unit is substantially greater than in domain RF1 (compare profiles 3 and 6, fig. 10). This suggests that the negative anomaly is at least partially due to a negative density contrast of the sandstone-rich Retreat Formation against the enclosing Panama Group units. Density data presented by Roach (1994) from 64 drill core or mine dump samples, mostly within the Panama Group and correlates, show only a minor difference in median density between sandstone (2.74 t/m$^3$) and siltstone (2.76 t/m$^3$), although the sandstone data show a distinctly broader spread with more densities in the 2.67–2.72 t/m$^3$ range, while the more compact siltstone spectrum shows substantially more densities in the 2.73–2.80 t/m$^3$ range. The distinction between Mathinna Supergroup pelites and sandstones is even more pronounced in the data of Goh (2008), obtained from drill core of Panama Group correlates to the southeast, which indicated an average density of 2.69 t/m$^3$ in sandstone v. 2.76 t/m$^3$ in siltstone and shale. It thus seems feasible that the Retreat Formation may have sufficient negative density contrast to affect the residual gravity anomaly pattern.

Further east and stratigraphically above the top of the Retreat Formation, a general area of positive gravity anomalism appears to show a high degree of correspondence with the outcrop area of the Lone Star Siltstone (fig. 23*a*). Here the issue is complicated by proximity to Middle Devonian granodiorite intrusive rocks with their associated and potentially substantial contact metamorphic effects on the mineralogy of pelites in the Lone Star Siltstone. It is notable that positive gravity anomalism is stronger in the southern half of the Lone Star Siltstone outcrop belt, where granodiorite is exposed in several cupolas and modelled at shallow depths under a sizeable part of the area (see fig. 22). Second order positive gravity anomalies in the Lone Star Siltstone in this area also show a suggestion of an annular pattern around the Lisle Granodiorite (fig. 23*a*), consistent with a contact metamorphic origin.

Information about density changes due to contact metamorphism of Mathinna Supergroup rocks is sparse. Leaman and Symonds (1975) showed density figures from across northeast Tasmania which suggest about a 6.5% increase in density between average bulk Mathinna Supergroup and the mid-range for contact-metamorphosed pelites; density measurements in the Rossarden–Storys Creek area in Leaman (1975) show a 2% positive differential for the same comparison in that area, while calculations based on gravity modelling of granitoid contacts in the Ringarooma–Boobyalla area in Leaman (1977) indicate a minimum 0.9–1.7% increase in the density of bulk Mathinna Supergroup rock when it is contact metamorphosed. Apart from these considerations, noticeably persistent positive gravity anomalism in the Lone Star Siltstone remote from granitoid contacts suggests that at least part of the signature is due to positive density contrast of the unit against the enclosing sandstone-rich formations. This impression is reinforced by at least a tendency in the data towards relatively negative gravity anomalism once the lower contact of the Sideling Sandstone is crossed (fig. 23*a*), although this could be solely due to the encroaching gravity signature of the adjacent Scottsdale Batholith.

### *Worms*

3-D potential field edges ('worms'), based on upward continuation heights ranging from 350 to 23 431 m, have been calculated from the updated residual gravity coverage (fig. 24*a*). A myriad of features are present in the worm patterns, only some of which are likely to be of relevance to internal features of the Mathinna Supergroup. One group of features which may be important is a family of sets of more or less east-west trending worms which appear to be intermittently present at various locations across the whole area (fig. 24*a*). The reason these may be significant is that one such worm set passes close to Lefroy and is parallel in strike to the dominant reef trend associated with gold mineralisation there. Several similar east-west trending worm sets are present in the Mathinna Supergroup between Lefroy and Bangor to the southeast (fig. 24*a*), and intriguingly they step progressively eastward between these two points in the same manner shown on a smaller scale by the Lefroy goldfield reefs, which occupy a NNW-trending corridor (Groves, 1965; see *Gold Mineralisation* below). Similar sets of east-west trending gravity worms are present in the Lone Star Siltstone in the Golconda–Nabowla–Lisle triangle (fig. 24*a*) and in the area of Lone Star Siltstone southeast of the Lisle Granodiorite. A prominent east-west trending worm set is also present in an area of mostly superficial cover ENE of Bellingham at about the northing of Bridport (fig. 24*a*). The widespread occurrence of these east-west trending worm sets is possibly indicative of the presence of a structural grain of that trend in sub-Mathinna Supergroup basement, and which may have had an influence on the development of the Lefroy gold reef structures.

A prominent NNW-trending gravity worm set extending from just west of Pipers Brook to the coast and offshore into Bass Strait (fig. 24*a*) reflects the relatively abrupt northeast termination of the large positive anomaly over the Tippogoree Group, visible in the residual gravity data image (fig. 23*a*). The worm geometry emphasises the linear nature of this edge and reinforces the impression of connection with the $TaD_3$ thrust fault passing northeast of the Lisle Granodiorite. Worm migration with upward continuation further suggests a sympathetic northeastward dip to this feature (fig. 24*a*). The probable deep source of this feature implies it is primarily to do with a structure in the sub-Mathinna Supergroup basement, in particular the large body of Cambrian ultramafic rocks interpreted at depth by Roach (1994). The $TaD_3$ thrust northeast of Lisle has its own subtle expression in the worm data, not so much in worm sets parallel to it but in a number of worm sets which terminate against it (fig. 24*a*).

## Magnetics

### *Anomalies and features*

In a conventional colour-draped shaded-intensity display, the straight TMI data yields a fairly 'flat' and uninteresting image over much of the area, even when optimised for the local amplitude range and with additional custom processing to enhance the finer details (fig. 23*b*). This is due to a large overall amplitude range together with the fact that much of the signal is in short wavelength, very small amplitude responses within the Mathinna Supergroup.

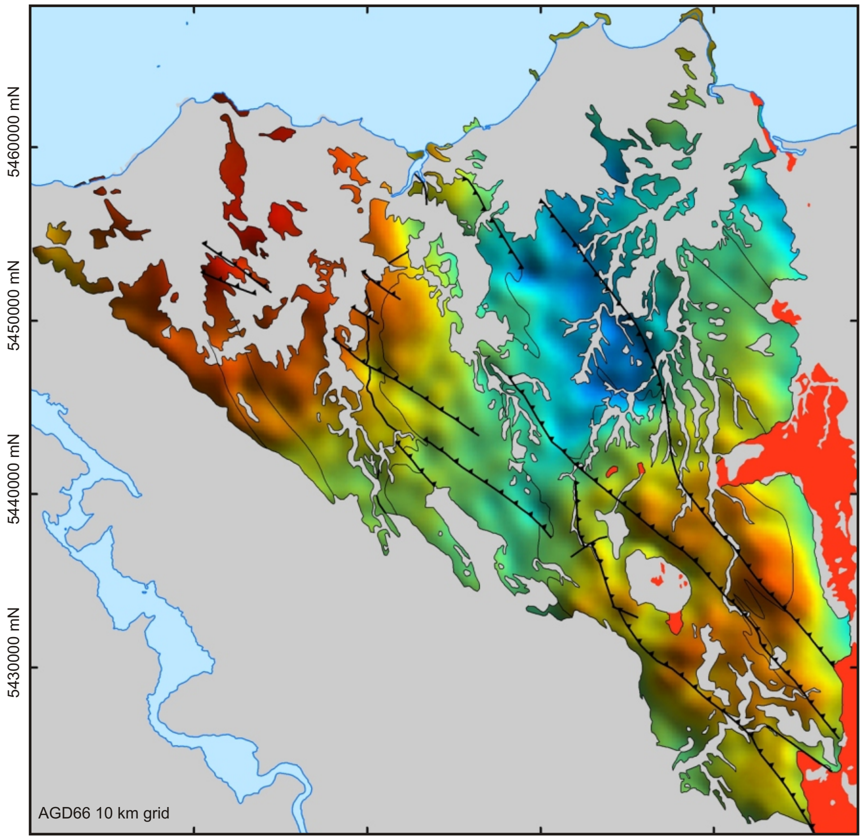


*(a) Colour-drape image of residual gravity data.*

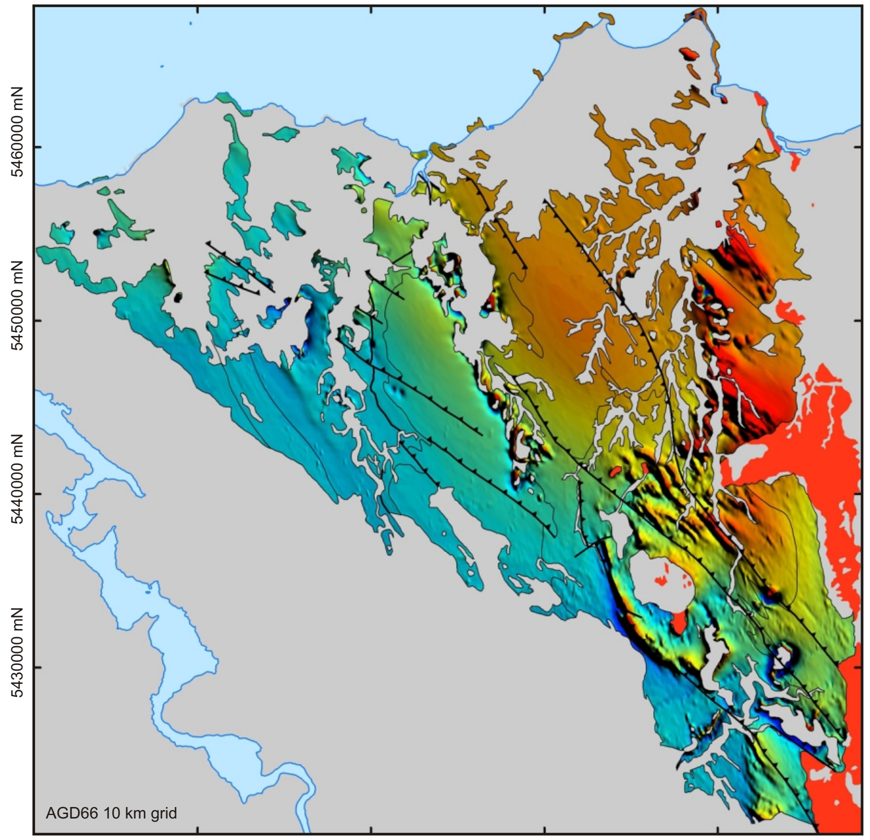


*(b) Colour-drape image of airborne 200 m line-spacing total magnetic intensity (TMI) data.*

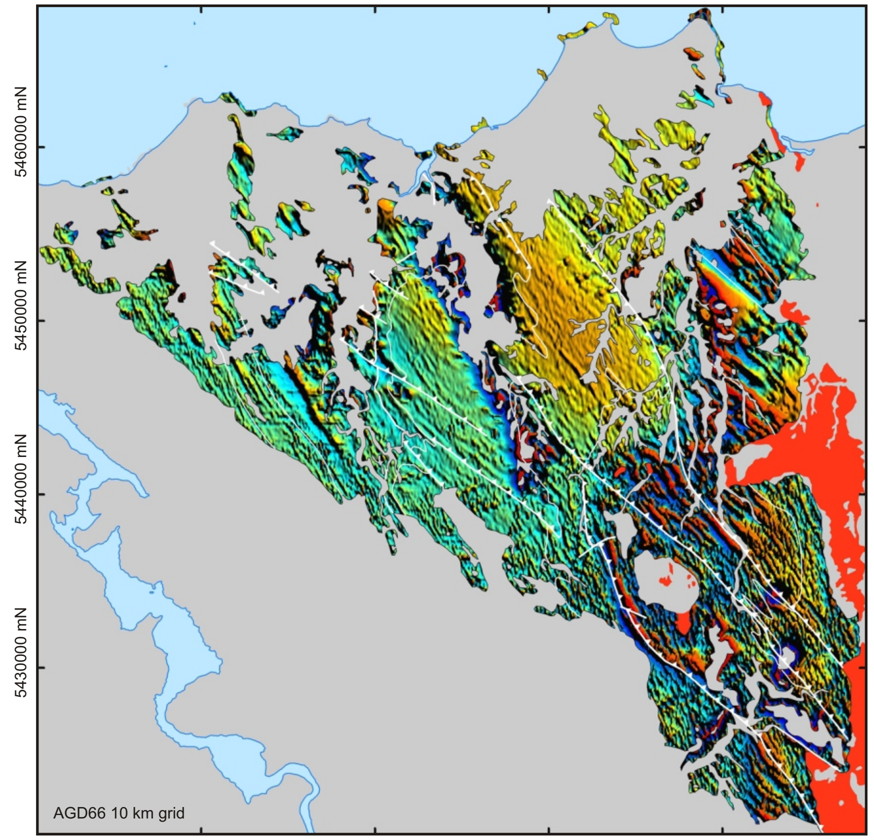


*(c) Colour-drape image of 1st vertical derivative calculation of TMI data (TMI_vd1).*

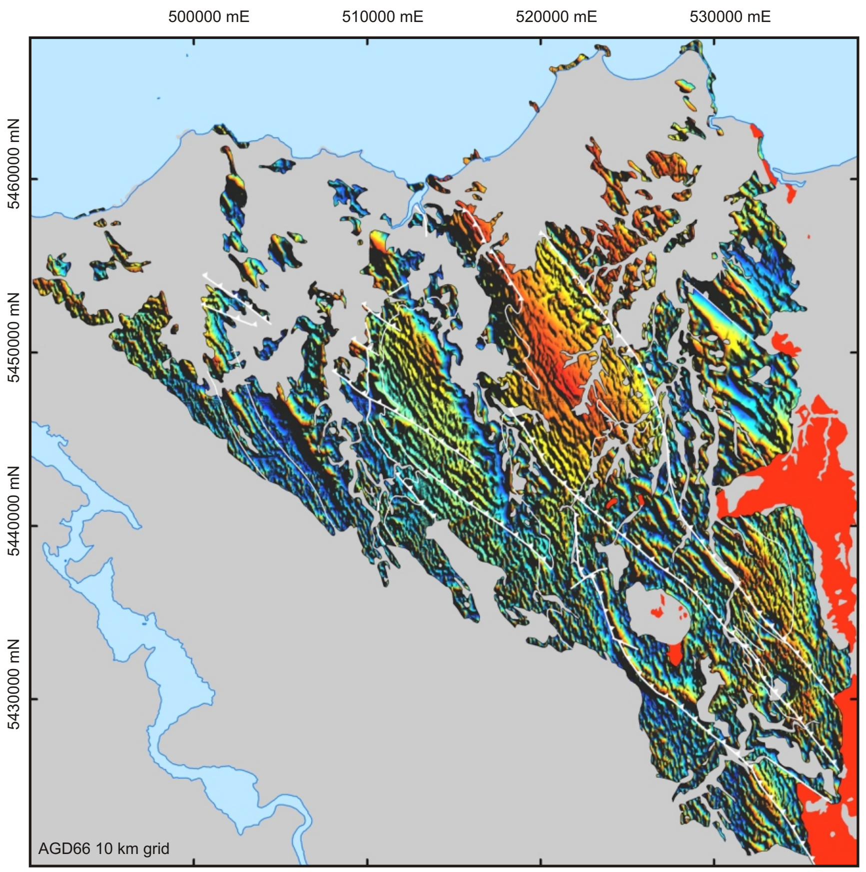


*(d) Colour drape image of tilt angle derivative, reduced-to-pole calculation of TMI data (TMI_tdr_rtp).*

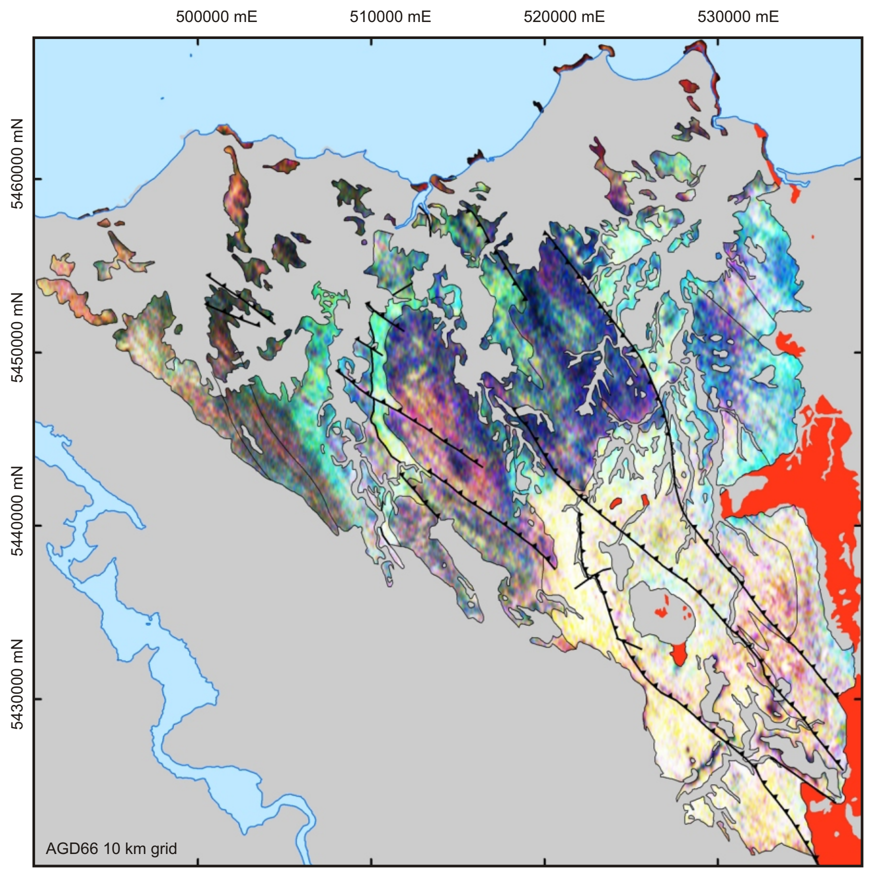


*(e) K-Th-U_RGB image of airborne 200 m line-spacing 3-channel radiometric data.*

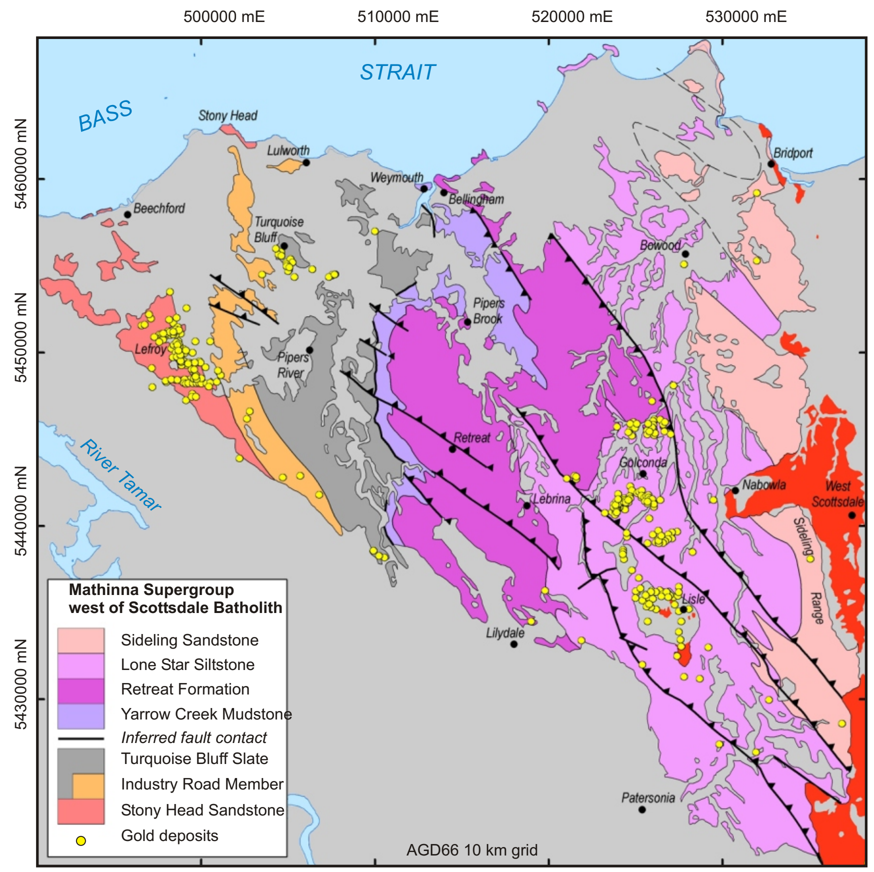


*(f) TasExplore revised mapping of Mathinna Supergroup for reference, with gold deposits and geographic locations overlain.*

**Figure 23**

*Images of new or updated geophysical coverages following TasExplore project data acquisition for the area west of the Scottsdale Batholith, masked to show only responses within outcropping Mathinna Supergroup rocks, and with Middle Devonian granodiorite outcrop (red), revised faults and geological boundaries overlain.*

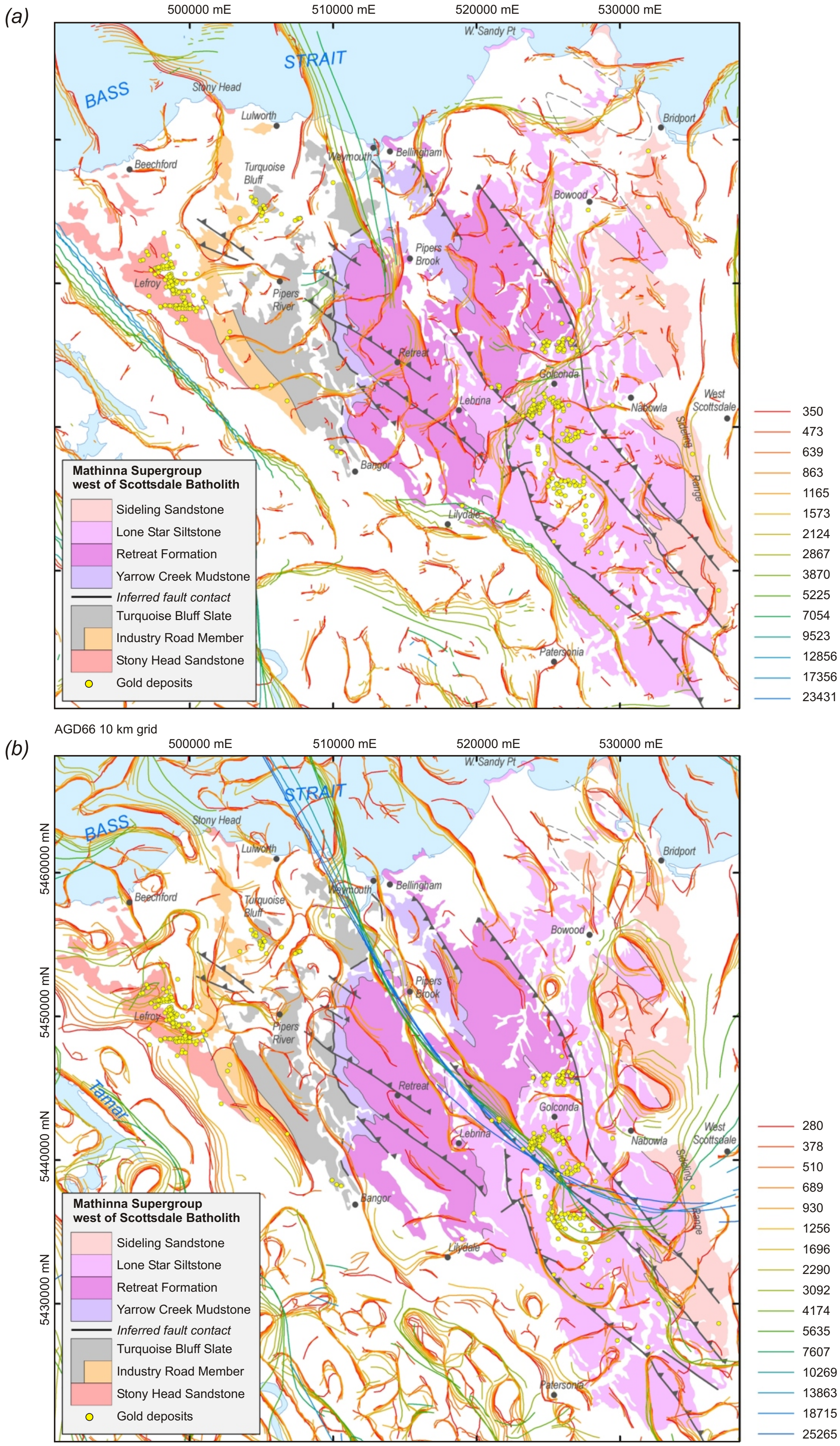


**Figure 24**

*3-D potential field edge (Worm) data, colour-contoured for upward continuation height, for new or revised geophysical datasets covering the area between the River Tamar and the Scottsdale Batholith, with TasExplore revised geological mapping shown as background image: (a) worms based on residual gravity data; (b) worms based on total magnetic intensity data.*

The only really obvious feature in the straight TMI is the presence of high-amplitude, relatively short-wavelength linear to curvilinear positive anomalies, mostly within the Lone Star Siltstone in proximity to the Diddleum and Lisle granodiorites and in the Golconda–Nabowla–Lisle triangle, where these two bodies are in closest proximity to each other (fig. 23*b*) and where granodiorite has been modelled at less than one kilometre depth between Golconda and Lisle (fig. 22; Leaman and Richardson, 2003). These anomalies are almost certainly an expression of contact metamorphic effects (and/or granitoid-related alteration) in the Lone Star Siltstone, an interpretation reinforced to some extent by the tendency towards an annular pattern around the surface outcrop form of the Lisle Granodiorite (fig. 23*b*). It is notable that in a number of areas the positive anomalism extends further away from the granitoid contacts than the mapped limit of observed metamorphic spotting in the country rocks, and so some of it may be sourced in contact metamorphic rocks at depth above a locally relatively shallowly dipping granitoid contact rather than from a surface source. There is a distinct tendency for this positive anomalism to be more prevalent in the Lone Star Siltstone than in the Sideling Sandstone. This is particularly evident in an anticlinal core of Lone Star Siltstone some nine kilometres south of Bridport (fig. 23*b,f*), and is presumably due to the greater propensity of this pelitic unit for contact metamorphic mineral growth.

Within the pattern of positive anomalies in the Golconda–Nabowla–Lisle triangle, corridors are evident which in part have been interpreted as the expression of two major NW-trending faults which transect this part of the area (fig. 23*b*). These corridors are in part 'lines of absence' against which curvilinear positive anomalies terminate in some cases, and some of the latter have shapes suggestive of large-scale tight fold closures, an impression supported by local mesoscopic structural data (vicinity of 527500/5438800, Lisle 1:25 000 map sheet: Woolward and McClenaghan, 2010).

The task of extracting greater information about the internal structure of the Mathinna Supergroup away from contact metamorphic effects has required further processing of the TMI data. Of the techniques tried, the two most useful proved to be a standard first vertical derivative calculation (TMI_vd1, fig. 23*c*) and a more involved tilt angle derivative, reduced-to-pole calculation (TMI_tdr_rtp, fig. 23*d*). The TMI_vd1 version produced a substantial increase in the clarity of subtle short-wavelength low-amplitude anomalies in the Mathinna Supergroup, and it became evident that at least some of these are likely sourced in sedimentary units in the sequence. NW-trending linears in the Stony Head Sandstone and the Industry Road Member are strata-parallel in trend, and linears in the westernmost domain (RF1) of the Retreat Formation show offsets on mapped *Ta*$D_3$ thrust faults which strongly suggest that the linears are strata-parallel (fig. 23*c*). On the other hand, some NW-trending linears in the eastern domain (RF2) of the Retreat Formation seem more likely to be sourced on faults. The TMI_vd1 treatment also substantially increased the discrimination of structures within the contact metamorphosed parts of the Lone Star Siltstone.

The TMI_tdr_rtp calculation was also very useful in enhancing subtle linear features in the magnetic data (fig. 23*d*). This treatment tends to further de-emphasise differences in anomaly amplitude while further enhancing the clarity of any linear feature in the data regardless of its prominence. The anomaly features evident are similar to those in the TMI_vd1 image, but some subtle features are more easily identified in the TMI_tdr_rtp data.

### Worms

3-D potential field edges ('worms'), based on upward continuation heights ranging from 280 to 25 265 m calculated from the latest TMI data coverage, are presented in Figure 24*b*. As with the gravity worms, a myriad of features are present in the TMI worm patterns, only some of which are likely to be of relevance to sources within the Mathinna Supergroup, particularly as edge effects related to the numerous bodies of Tertiary basalt in the area can be emphasised by the worm calculation process.

The most prominent first-order feature in the TMI worms is a large, arcuate set of deep-seated worms passing from offshore in Bass Strait, through a point just west of Pipers Brook then southeastward to the southern part of the Sideling Range (fig. 24*b*), before continuing eastward out of the area. This is the worm expression of the southwestern edge of the large Noland Bay–Anderson Bay positive magnetic anomaly, previously modelled by Roach (1994) as due to a gently northeast-dipping slab of Cambrian ultramafic rocks at some six kilometres depth, beneath the structural base of the Mathinna Supergroup section (fig. 2*c*).

Amongst second-order features are a family of northwest-trending worm sets at various points across the area, some of which show a correspondence with unit boundaries or other mapped structures within the Mathinna Supergroup. Some examples visible on Figure 24*b* are:

- A prominent southwest-migrating worm set coincident with the upper contact of the Industry Road Member with the rest of the Turquoise Bluff Slate, northwest of Bangor. The implied southwesterly source dip contradicts that shown on the structural profile (fig. 10*b*), but a paucity of local structural control here allows some flexibility on the interpretation.
- An *en echelon* set of slightly curvilinear NW-trending worm sets in the Retreat Formation north and south of Retreat, with geometry suggesting that they are sourced by a stratigraphic horizon which has been offset on *Ta*$D_3$ thrust faults.
- A pair of NW-trending worm sets passing either side of Pipers Brook and straddling the first-order deeper feature described above. Either one of these could represent the northwestward continuation of the major *Ta*$D_3$ thrust passing northeast of the Lisle Granodiorite.
- Worm sets with some NW-trending components showing a spatial relationship with the contact between the Lone Star Siltstone and the Sideling Sandstone on major fold limbs east of the Bowood–Golconda line.
- A NW-trending worm set extending from northwest of Bowood to a point on the coast just west of West Sandy Point, where previous observations indicate the

presence of a shear zone in the Lone Star Siltstone (pers. comm. Dr. R. F. Berry, ARC Centre of Excellence in Ore Deposits, University of Tasmania, 2008).

Although not as prominent as in the gravity data, there is also a family of sets of east-west trending TMI worms present at a number of locations across the area (fig. 24*b*). The most obvious of these is in a corridor in the Lefroy–Pipers River area, and also continuing west from Lefroy under post-Mathinna Supergroup cover. The fact that worm sets of this trend are present in both gravity and magnetic data in the Lefroy area reinforces a likely link with structural control on the gold mineralisation. Other east-west worm sets are present in the Lilydale area, north of Golconda, and in parts of the offshore coverage in Bass Strait (fig. 24*b*).

## Radiometrics

### *Anomalies and features*

The new *TasExplore* airborne 3-channel radiometric data, when displayed in K-Th-U RGB format (fig. 23*e*), reveals a highly varied pattern of responses, which after ground follow-up have proven to show a high degree of correlation with lithological variations within and between rock units in the now redefined formal stratigraphy of the Mathinna Supergroup. This correlation made the radiometric data a substantially useful tool for guiding remapping in this part of the Eastern Tasmanian terrane, and incidentally means that some comments on radiometric properties have already been included in the *Stratigraphy* section above. In some cases these are reiterated or summarised here.

The oldest unit in the stratigraphy, the Stony Head Sandstone, appears to show a relatively bright pale-coloured signature in the K-Th-U RGB image (fig. 23*e*), an unexpected response given the high proportion of quartz-rich sandstone in its sequence. It is possible that the signature may be due to a component of micaceous minerals, both as clastic material and within the well-developed 'stripy' cleavage, or perhaps due to a heavy trace mineral assemblage which is different from the Panama Group sandstone. As mentioned previously, the overlying unit, the Industry Road Member, has a slightly darker overall pattern on the radiometric image but with a distinct strata-parallel dark-light striping due to interlayered fine-grained quartz-rich sandstone and slaty pelite (fig. 6, 23*e*). The radiometric signature of the rest of the Turquoise Bluff Slate above the top of the Industry Road Member is more complicated. A band of low radiometric response in the lower part of the sequence (fig. 6, 23*e*) may be due to scree and soil creep from the ridge-forming Industry Road Member migrating downslope towards the generally lower ground occupied by the rest of the Turquoise Bluff Slate. East of this, in the centre of the Turquoise Bluff Slate outcrop belt, is a relatively bright mottled white-yellow-blue pattern in the image (fig. 6, 23*e*), which could represent the 'typical' radiometric response of the formation. Interestingly, the western margin of this zone is coincident with a relatively low-amplitude linear magnetic anomaly which is just visible in the straight TMI image (fig. 23*b*), but more so in images of the TMI_vd1 and TMI_tdr_rtp calculations (fig. 23*c,d*). Intriguingly, most of the belt between this anomaly and the top of the Industry Road Member is almost totally free of magnetic anomalism. As mentioned earlier in this report, the eastern part of the Turquoise Bluff Slate outcrop belt (east of the radiometrically 'bright' central belt) is characterised by a mottled dark-light pattern in the radiometric image (fig. 6, 23*e*), believed to be due to masking of the otherwise 'bright' pelitic response by weathering out and concentration into the soil profile of the commonly observed quartz veins associated with the high strain state of the slate.

As noted earlier, the lowest unit of the Panama Group, the Yarrow Creek Siltstone, is characterised by a bright light-coloured pattern in the K-Th-U RGB image, which makes it stand out from the adjoining units (fig. 6, 23*e*). In this case, relatively lower strain and less quartz veining in the unit mean that the response of the pelitic lithologies is less likely to be masked by vein quartz in the soil profile. The overlying Retreat Formation shows a prominently dark overall pattern on the image, consistent with its high content of quartz-rich sandstone. There are also second-order systematic internal variations in the radiometric pattern within the formation, consisting of darker and lighter areas whose geometry suggests they reflect lithological variations which represent real stratigraphic subdivisions within the unit (fig. 6, 23*e*). Outcrop lithology spatial data confirm that the lighter areas correspond to parts of the formation with higher proportions of siltstone and mudstone, and darker areas to more sandstone-rich parts. It is notable that the northeasternmost of the two structural domains (RF2) in the formation appears to be more sandstone-rich and may have been located closer to the main depositional axis within the submarine fan complex(es). Within the other, southwestern domain (RF1), the radiometric data is discriminating enough to pick out a relatively thin unit with a bright signature, which parallels the lower formation boundary and shows offsets on *Ta*$D_3$ thrust faults of the same sense as offsets noted in TMI worms in the same area (compare fig. 6 with fig. 24*b*).

Stratigraphically above the Retreat Formation, the lower part of the Lone Star Siltstone in the southern half of its outcrop belt shows an exceptionally bright, yellow-white signature on the K-Th-U RGB image (fig. 6, 23*e*). Geological mapping has shown that this corresponds to the most pelitic part of the formation which is relatively free of sandstone beds. It is uncertain how much of this lower unit is present in the western part of the northern half of the Lone Star Siltstone outcrop belt, where the formation is in fault contact with the Retreat Formation, and its radiometric signature is more subdued than in the southern area. This may be partially due to a greater prevalence of superficial Tertiary gravel deposits in the northern area, not all of which are included in the pre-*TasExplore* younger-cover polygon coverage used to mask Figure 6 and Figure 23*e*. Further east and up-section, the radiometric signature of the Lone Star Siltstone steadily becomes less bright and more mottled (fig. 6, 23*e*), likely due to a combination of two factors; increasing proportions of sandstone beds in the sequence, and contact metamorphic and/or alteration effects in proximity to outcropping and subjacent granodiorites.

Considering the relatively high proportion of quartz-rich sandstone in its section, the Sideling Sandstone shows a surprising lack of contrast in its K-Th-U RGB radiometric signature against the adjacent Lone Star Siltstone (fig. 6, 23*e*).

Overall there is a discernibly darker tone to its signature. The absence of a dark signature like that of the Retreat Formation could possibly be due to contact metamorphic effects associated with the Diddleum Granodiorite, but this is perhaps unlikely as it would imply significant metasomatism. Other explanations could include a higher overall proportion of pelite compared with the Retreat Formation, or the resistant nature of the contact metamorphosed rocks creating high, more steeply dissected ground preventing the accumulation of a thick quartz sand-rich soil cover on the unit and thus allowing the signature of the minor pelite component to show more prominently. One area of Sideling Sandstone, relatively remote from granitoid contacts at the northwestern end of a southeast-plunging syncline SSE of Bowood, does show a prominently dark signature (fig. 23*e*,*f*). Intriguingly this corresponds with an area of relatively lower ground. *TasExplore* remapping here found a greater extent of Tertiary basalt and other cover than depicted on the pre-*TasExplore* coverage used for the masks in Figure 23, and it is possible that the dark signature may be due to the presence of a veneer of sub-basalt Tertiary gravel in this area.

# GOLD MINERALISATION

Lode gold deposits hosted by the Mathinna Supergroup in the River Tamar–Scottsdale area occur in five main goldfield areas (fig. 4) which can be grouped into two distinct provinces, corresponding to two distinct genetic styles. The two western goldfields (Lefroy and Back Creek) are primarily orogenic, structurally-hosted gold vein deposits which are relatively remote from known or inferred granitoids. The other three main goldfield areas (Lisle, Panama–Golconda and Denison) show a strong spatial association with the outcropping and subjacent body of the Lisle Granodiorite, modelled from gravity interpretation (fig. 22; Bottrill *et al*., 1994; Roach, 1994; Callaghan and Reid, 2005; Leaman and Richardson, 2003), and some recent mineral exploration in these areas has been based on a primary intrusion-related model (Callaghan and Reid, 2005). There are associated alluvial gold deposits in Tertiary deep leads and/or Quaternary sediments in, and adjacent to, all of the goldfields. The summary here is largely based on a number of previous Tasmania Department of Mines or Mineral Resources Tasmania reports, particularly those produced during the NetGold project of the early 1990s, and later work by Reed (2002; 2004). Interpretation of *TasExplore* project geophysical data and subsequent ground follow-up has provided further insights into controls on gold mineralisation.

## Orogenic gold: Lefroy–Back Creek goldfields

Gold mining started in the Lefroy area in 1869 and about fifty mines operated in the area on some thirty lines of reef, mostly to shallow depth, but had largely finished by the start of the 20th century. Total lode gold production from Department of Mines statistics has been estimated at 5170 kg, mostly prior to 1900, with only 230 kg recovered since that date, plus an estimated 155 kg from alluvial deposits (Bottrill *et al*., 1994). The mined lode ores reportedly averaged 30 g/t Au (Noldart and Threader, 1965; McClenaghan, 1994). Such high grade ore was found to be rare below 90–120 m depth, and there was reportedly a marked decrease in grade below 30 m in many of the smaller mines which were consequently not worked to greater depths (Noldart *in* Gee and Legge, 1979). A mid-1990s drilling program on the Pinafore–Chum reefs showed grades generally below one g/t Au (Keele, 1996), but later drilling found some high grade zones (e.g. one metre @ 42 g/t; unpublished ASX reports). As only 4% of the recorded lode gold production of 5170 kg since 1883 was recovered after 1900 (Noldart *in* Gee and Legge, 1979), it seems likely that 19th century practices such as hand sorting of ore prior to crushing would have biased long-term grade figures (Dr G. R. Green, Mineral Resources Tasmania, pers. comm.). In 2006, Lefroy Resources Limited announced an Inferred Resource, potentially mineable by open-cut methods, of 616 000 tonnes of 2.5 g/t gold and this is probably more typical of average reef material.

Lode gold at Lefroy is hosted in an array of steeply-dipping, planar quartz reefs which occupy a set of sub-parallel, almost east-west trending mineralised faults (fig. 25*a*) with a preferred strike orientation of 084° (standard deviation 7°) based on measurements from the map in Groves (1965). The largest reef, the Volunteer near the southern end of the array, has abandoned workings over a strike length of about 1500 m (Groves, 1965), but the host structure appears to be discernible in airborne magnetic data over a length of about ten kilometres (Reed, 2002). The reef array is about four kilometres wide across reef strike, positioned close to the top of the Stony Head Sandstone, and arranged *en echelon* parallel to the contact with the overlying Industry Road Member (fig. 25*a*). The reefs mostly dip to the south although some smaller reefs dip north. Repeated movement along the fault planes has produced slickensiding, breccia and mylonitic pug, and overprinting quartz veins. Fault shear zones may be up to 60 m wide and reefs may occur anywhere in the zone. These reefs or fracture zones can be traced on the surface up to about 1.5 km and were proved to be continuous to a depth of at least 380 m (Bottrill *et al*., 1994). The gold is limited in economic quantities both laterally and at depth although present in trace amounts throughout the lodes.

Geochemical zoning of Au and As in soils about the lodes was noted by Keele (1996), and van Moort and Russell (2005) also noted an association with Mo, Ca and other elements, plus some geochemical and Electron Spin Resonance variations in quartz in mineralised areas that could be useful indicators of mineralisation.

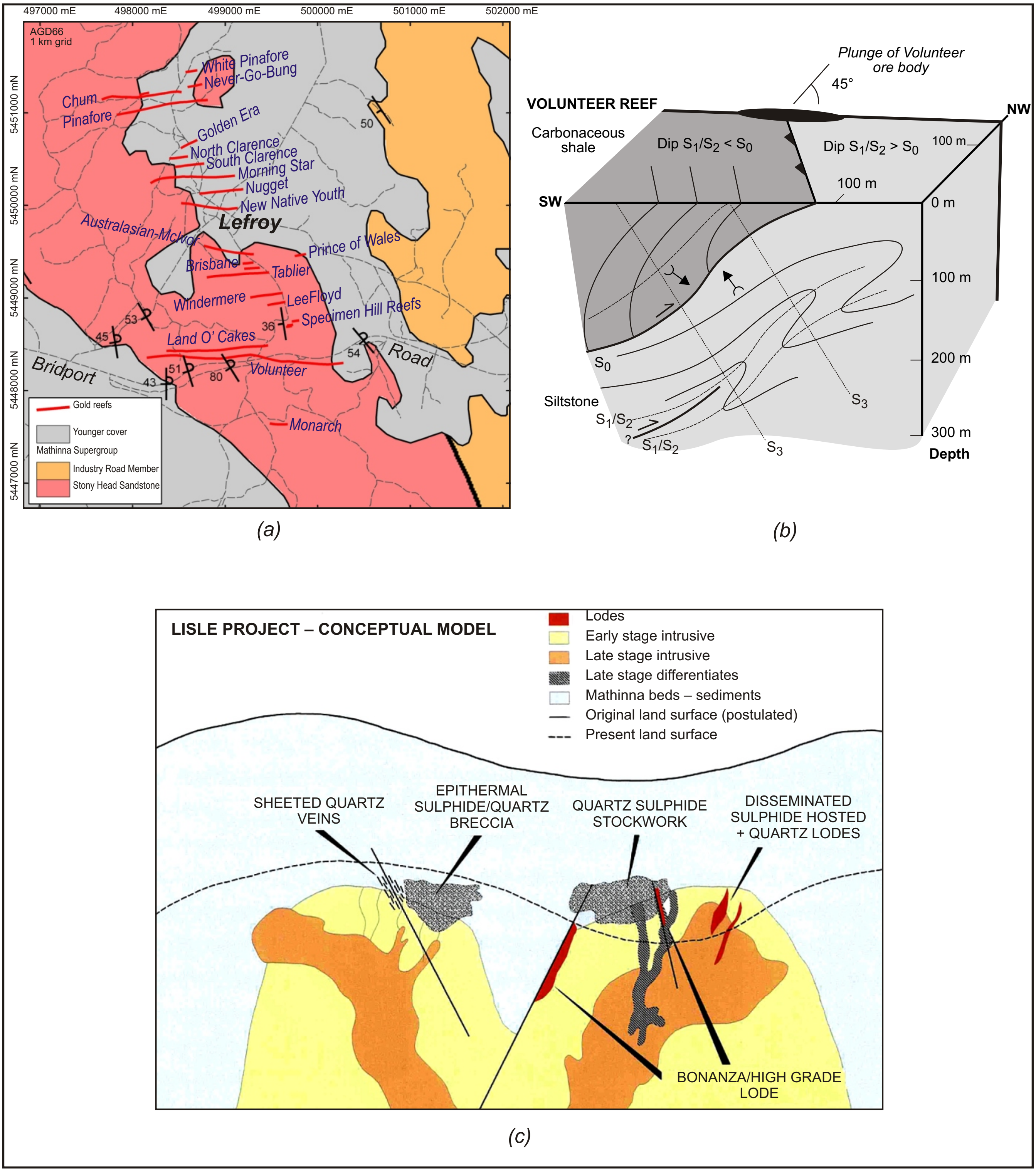


**Figure 25**

*Contrasting styles of gold mineralisation in the Lefroy and Lisle areas: (a) map showing surface projection of the main reefs at Lefroy from Groves (1965), reprojected onto TasExplore revised geology map; (b) block diagram from Reed (2002) showing interpreted structure in the vicinity of the Volunteer lode at Lefroy, and the coincidence between the plunge of the lode (in the plane of the reef) and the intersection of the reef with a pre-mineralisation BeD$_1$ / D$_2$ thrust; (c) a conceptual model for intrusion-related gold mineralisation in the Golconda–Panama goldfields, by Callaghan and Reid (2005).*

The ore mineralogy at Lefroy was summarised by McClenaghan (1994) as follows. The gold is generally associated with vughy quartz on the footwall and/or hanging wall of the fractures. Associated minerals were reported as stibnite, cervantite (an antimony oxide formed by oxidation of stibnite), and more rarely pyrite, chalcopyrite and arsenopyrite. Common vitreous white quartz is generally non-auriferous. Sulphide-hosted gold was exemplified in the Clarence mine, where free gold was extremely rare but pyrite assayed up to 673 g/t Au. A pocket of pyrite ore at the 800 ft (245 m) level in the New Pinafore mine assayed 50.5 g/t Au, and is one of the few known concentrations of gold found below 120 m in the field. Recent studies suggest that stibnite is generally rare in the lodes but some quartz-sulphide mineralisation was found to contain small amounts of free gold with arsenopyrite, chalcopyrite, tetrahedrite, bournonite, galena, sphalerite and pyrite (Bottrill, 1996*a*). Meneghinite was also reported in the lodes by Russell and van Moort (1992), and overall the lodes are generally quite Sb-rich compared with the Beaconsfield mine and other gold deposits in Tasmania.

Reef orientation at Lefroy is at a relatively high angle (70°) to the axial trend of the dominant semi-recumbent *Be*$D_1$ folds in the area, which have a preferred plunge of 8° to 154° based on *TasExplore* field data (fig. 13*a*). Together with other orogenic gold mineralisation in northeast Tasmania, the Lefroy deposits are considered coeval with the last major Devonian regional deformation event, labelled *Ta*$D_3$ in this report (equivalent to $D_3$ of Reed, 2002). *TasExplore* data from the Stony Head Sandstone suggest that the Lefroy reefs are at a somewhat higher angle (77°) to *Ta*$D_3$ folds, for which combined intersection lineation and hinge line data indicate a preferred axial orientation of 7° to 161° (fig. 13*e*), consistent with a preferred orientation of axial planar *Ta*$S_3$ crenulation cleavage dipping 63° to 070° (fig. 13*d*). If it is assumed that the principal compressive stress ( $_1$) during *Ta*$D_3$ at Lefroy was horizontal and aligned at about 070° (orthogonal to the strike of *Ta*$S_3$ cleavage), and that $_2$ was vertical, then the 14° horizontal angle between $_1$ and the preferred reef strike could allow for a significant component of extension across the reefs as well as a component of sinistral wrench movement as proposed by Reed (2002). It appears that the angle between $_1$ and the preferred reef trend at Lefroy may be less than half the optimum 30° angle suggested by Reed (2002) based on pre-*TasExplore* data. This, together with the existence in both gravity and magnetic data of prominent east-west trending worm sets running through the Lefroy area and further southeast towards Lilydale (fig. 24), suggests a degree of reef control from *Ta*$D_3$ reactivation of older (Cambrian?) basement structures with this same trend.

At a more detailed scale, Reed (2002) identified a further level of structural control which acts to limit the extent of high-grade ore zones at Lefroy. Within the Volunteer Reef, the main Volunteer lode plunges 45° to the west within the reef, coinciding with the intersection with the reef of a *Ta*$D_1$ southwest-dipping thrust fault which separates overturned pelite in the hanging wall from right-way-up quartz-rich siltstone in the footwall (fig. 25*b*). Reed also noted a relationship between arching of ore shoots within the Chum and Pinafore reefs and folding of pre-*Ta*$D_3$ structures, resulting in curvilinear intersections between *Be*$D_1$–$D_2$ thrusts (and folded sedimentary contacts) and the *Ta*$D_3$ reefs. The exact mechanism by which this control operates is not totally clear, but as Reed (2000) notes there is a definite association between changes in lithology and locations of gold mineralisation — the controls here could include competency, porosity, geochemistry/mineralogy, or combinations of these, as well as structural geometry.

The Back Creek goldfield (fig. 4), although mostly comprising alluvial deposits hosted in four Tertiary deep leads, also includes a number of gold-bearing quartz reefs hosted in Mathinna Supergroup rocks (Noldart *in* Marshall, 1969; McClenaghan, 1994). Total gold production to 1907 was in the range of 280–311 kg (McClenaghan, 1994). The goldfield appears to be positioned in the vicinity of the contact between the Industry Road Member of the Turquoise Bluff Slate and the overlying, dominantly pelitic main body of the latter formation (fig. 4), i.e. at a higher stratigraphic level than the Lefroy goldfield. Measurement of the eight reefs on the map in Broadhurst (1935) shows a preferred east-west orientation, with a standard deviation of 9°about an average trend of 090°. Six of the reefs occur in a roughly *en echelon* fashion within a narrow NNW-trending belt which is more or less parallel to lithological contacts and strike of bedding in the host sequence. From a structural point of view the Back Creek reefs show a high degree of similarity to those at Lefroy.

The predominant feature of the Lefroy mining field is the consistent decline in gold values below the 90–120 m levels, and, in many of the smaller mines the marked decrease at only 30 m, although quartz may fill the lode channel. The New Pinafore and Volunteer mines were extended to depths of 370 m and 380 m respectively but yielded very little gold although the lode channel in each case was distinct. Gold values generally declined from about 30 g/t in the upper levels to less than 3 g/t at depth. The decline in gold values was attributed to a process of surface enrichment, which is unproven and appears unlikely in this geological environment. In the New Golden Gate mine at Mathinna, for example, the original workings were abandoned at shallow depth, as with most of the early mines in the area, but were later re-opened and reached a final depth of about 600 m, with average grades of 26 g/t persisting. This suggests a high potential for more gold reserves at depth below other mines and 'barren' veins, although the gold distribution is obviously erratic.

## Intrusion-related gold

Several historical goldfield areas cluster about the Lisle–Golconda area (fig. 4) and include primary vein, stockwork and disseminated deposits plus substantial alluvial workings (Bottrill, 1994). As noted above, their strong spatial association with domal structures in a mostly concealed body of Middle Devonian granodiorite (fig. 22) has led to some thought that these deposits are fundamentally intrusion-related (Callaghan and Reid, 2005). The intrusive rocks are variable hornblende-biotite-magnetite-sulphide bearing diorite and granodiorite with relatively sharply defined contact metamorphic aureoles varying from 800 m to about five kilometres in map width depending on the dip of the intrusive contact (McClenaghan *et al*., 1982; Bottrill, 1996*b*; Bottrill *et al*., 1994). The metamorphosed Panama Group rocks in the aureole are locally very rich in sekaninaite ('Fe-cordierite'), biotite, recrystallised quartz, muscovite and chlorite, and quartz and greisen veins, migmatites and granitic dykes locally occur in the aureole near the contact (Bottrill *et al*., 1994). It is notable that the Lone Star Siltstone when contact metamorphosed typically undergoes a substantial increase in grain size due to new mineral growth, possibly leading to mistaken identification of 'sandstone' in the contact aureoles in some of the historical literature.

## *Lisle goldfield*

Gold production from the Lisle goldfield was predominantly alluvial and may have amounted to nearly ten tonnes (Bottrill *et al*., 1994), although official figures are considerably lower as much of the initial production was apparently taken interstate for sale (Noldart *in* Marshall, 1969). The alluvial workings included alluvium and eluvium in a basin-shaped depression which may represent an old lake bed of Tertiary age (Marshall, 1969). The topographic depression is the result of a negatively-weathering and poorly outcropping cupola of granodiorite surrounded by ridges of erosion-resistant contact metamorphosed Lone Star Siltstone.

The lacustrine sediments, and carbonaceous horizons underlying talus, produced relatively pure, free, angular (crystalline?) gold (Noldart *in* Marshall, 1969), suggesting a secondary origin (Bottrill, 1986; Bottrill *et al*., 1994). Some gold grains are highly porous and/or colloform, while some have silver-rich cores and silver-depleted rims (Bottrill, 1991; Roach, 1991), confirming that some gold is detrital and some reprecipitated (Bottrill *et al*., 1994). Auriferous quartz was extremely rare in both alluvial and bedrock occurrences. Twelvetrees (1909) found few veins and only limited evidence of free gold in the contact aureole rocks surrounding the Lisle basin. Inclusions of mica, rutile and magnetite, with little quartz, in the gold grains suggest that the gold was more likely to have been disseminated in the hornfels or granitoids than in quartz veins, while rare gold-limonite composites in placers suggest that gold-bearing pyrite may have originally been present (Bottrill, 1986). Some gold was found in small quartz veins in the granitic rock underlying the alluvial sediments (Thureau, 1882; Montgomery, 1894), while some possible stratabound mineralisation has been reported but poorly described (Callaghan and Reid, 2005). Drilling by the Tasmania Department of Mines revealed very minor quartz-carbonate-pyrite alteration zones in the magnetite-pyrite bearing granodiorite, with trace gold (to 0.05 g/t Au; Bottrill, 1996*b*). TasGold Limited reported more significant drill intersections at the Potoroo prospect of 106.5 m of 0.19 g/t Au, including 6.9 m of 1.8 g/t Au, 44 m of 0.4 g/t Au, 26 m of 0.6 g/t Au and 34 m of 0.3 g/t Au (Reid and Callaghan, 2004; McNeil, 2004).

Recent explorers have also found gold mineralisation in quartz veins related to faults in the granodiorite, with ferroan carbonates, pyrite, arsenopyrite, galena, molybdenite and chalcopyrite and accompanying intense silica-sericite alteration; they envisage a Pogo or Fort Knox style of intrusive-hosted mineralisation (Callaghan and Reid, 2005).

## *Golconda, Panama and Cradle Creek goldfields*

Lode gold in the Golconda and Panama goldfields is hosted in quartz-sulphide veins, stockworks and disseminations within the granodiorite intrusive rocks, and structurally-controlled veins in metamorphosed Panama Group rocks within the contact aureole. Some veins are zoned from edge to centre (albite quartz calcite sulphides apatite); gold is Ag-rich (electrum) and associated with maldonite(?) and chalcopyrite (Bottrill, 1996*c*). Other sulphide minerals include arsenopyrite and pyrite with lesser galena, sphalerite, pyrrhotite (mostly altered to pyrite + marcasite), bismuthinite, stibnite and molybdenite, and geochemically the mineralisation has a Au-Ag-Bi-Mo association (Callaghan and Reid, 2005; Bottrill, 1996*c*). Historical hard-rock mining in the Golconda and Panama goldfields produced head grades in the 8 to 15 g/t range (Taheri and Bottrill, 2005). Reconnaissance geochemical surveys in the Panama field have indicated minor gold in hornfels (up to 3 g/t Au) and some very gold-rich quartz-sulphide veins (up to 210 g/t Au; Bottrill *et al*., 1994; Bottrill, 1996*b*). A recent conceptual exploration model for intrusion-related gold mineralisation in the Golconda–Panama area is shown in Figure 25*c*.

Stockwork-hosted gold mineralisation (to about 1 g/t) has been reported in arenites at Bessells Reward mine in the Cradle Creek goldfield (Roach, 1991) (fig. 4). Minor gold veins occur in other parts of the district such as the St Patricks River–Myrtlebank area, and Lebrina, but have had little detailed investigation (Bottrill, 1994).

## *Denison goldfield: hybrid deposits?*

The genesis of the Denison goldfield, north of Golconda, is a somewhat more complex story, with elements suggesting it may represent a hybrid between the Panama–Golconda intrusion-related deposits and the Lefroy orogenic deposits. Historical workings at Denison are reported to have been on a series of parallel ENE-WSW trending quartz reefs in which gold was associated with pyrite, arsenopyrite and galena (Reid, 1926; Noldart *in* Marshall, 1969). A biotite-rich rock, which occurs with one lode (in the Wiangatta mine), is a possible lamprophyre (R. S. Bottrill, pers. comm.) that could indicate the potential for Wood's Reef style mineralisation. Mining on the Denison field was short-lived due to narrow veins, short productive sections, irregular distribution of gold, and interruption of veins by faults (Noldart *in* Marshall, 1969). The reported reef trend appears to be based on magnetic azimuth, and when corrected to grid north the ten reefs on the map in Reid (1926) show an average trend of 083° (standard deviation 10°), almost identical to the reef trend at Lefroy, reinforcing the similarity between the two goldfields (Bottrill *et al*., 1994) and further suggesting a common underlying (mid-crustal?) structural control.

In addition to the known spatial relationship between the Denison goldfield and the northern end of the concealed elongate overall form of the Lisle Granodiorite (or a separate pluton contiguous with the latter), *TasExplore* remapping has shown that the goldfield also has a strong spatial relationship with the stratigraphic contact between the Retreat Formation and the overlying Lone Star Siltstone (fig. 22). Projection of the map in Reid (1926) onto the revised mapping shows that deposits in the goldfield straddle the stratigraphic contact, with some reefs hosted in each formation. The average reef trend is approximately parallel to the overall trace of the formation contact through the goldfield, although in detail the contact is curvilinear due to second-order folding. There is thus at least one further potential control on the localisation of deposits in this goldfield compared with the Golconda–Panama–Lisle fields. The apparent significance of a sandstone-pelite contact in the Mathinna Supergroup in localising gold mineralisation in this case is reminiscent of similar controls previously recognised in orogenic gold deposits at Lefroy and in the Alberton–Mangana lineament (Reed, 2002; 2004).

According to Bierlein *et al.* (2005) gold mineralisation at Denison is sandstone-hosted and stockwork to disseminated style, with wallrock alteration including silicification, minor sericite and disseminated pyrite arsenopyrite porphyroblasts. They report that the sandstone is intensely fractured and criss-crossed with a network of massive quartz veinlets, but that there is no consistent correlation between the degree of veining/fracturing and gold grades, leading to a suggestion that the disseminated gold pre-dated (largely barren) vein emplacement. They conclude that the Denison goldfield lies outside the contact aureole of the Lisle Granodiorite, based on the absence of typical contact-metamorphic minerals present in hornfelsed Mathinna Supergroup rocks exposed in the Lisle and Golconda goldfield areas. However the fact remains that gravity interpretation indicates that a body of granitoid, contiguous in 3-D form with the Lisle Granodiorite, extends at depths of 1–1.5 km below the Denison goldfield (fig. 22). In an attempt to constrain the age of gold mineralisation, Bierlein *et al.* (2005) separated magmatic biotite from a monzodiorite dyke hosting auriferous gold veins at Denison East. These veins are associated with strong hydrothermal alteration, and intense metasomatism of the primary mineral assemblage. A $^{40}Ar/^{39}Ar$ plateau age of 385.4 2.0 Ma was interpreted as a maximum age constraint on hydrothermal alteration of the dyke and the timing of gold mineralisation. This age would be consistent with a syn-*Ta*$D_3$ timing for the gold. The mineralisation style was considered to be similar to the low grade but bulk-mineable deposit at Fosterville, Victoria (McConachy and Swensson, 1990).

## Other deposits of note

At the Whiting prospect (537010/5428780), in the St Patricks River valley 11 km southeast of the centre of the Lisle goldfield (fig. 4), patches of Au-Ag-As rich, semi-massive, quartz-poor sulphide mineralisation are concentrated along a silicified, sulphidic shear zone up to about one metre wide, in hornfelsed siltstone and sandstone of the Sideling Sandstone close to a granitoid contact (in the Scottsdale batholith). The mineralisation contains arsenopyrite (<30%), pyrite, sphalerite, chalcopyrite, galena, Ag-sulphosalts (polybasite, freibergite and pyrarygyrite) and free gold (Bottrill, 2005). The mineralisation is also disseminated within the wallrocks, with kaolinite, sericite, quartz and chlorite. The mineralisation is relatively rich in silver sulphosalts which suggests an epithermal style of mineralisation, and is thus possibly unique in northeast Tasmania. However it appears to lack typical epithermal textures and there are also similarities to the hornfels-hosted, massive to disseminated arsenopyrite-rich gold mineralisation in granite contacts at the Stawell gold mine (Magdala decline), Victoria (Miller and Wilson, 2002); this deposit requires more investigation.

# SUMMARY AND DIRECTIONS FOR FURTHER WORK

Prior to the *TasExplore* project, the 1:25 000 scale digital geological map coverage of the subject area of this report was compiled from legacy data derived from outdated geological maps originally published at 1:63,360 scale, and for which data collection programs had been designed with that output scale in mind. One outcome of the *TasExplore* work is that at least the part of this area underlain by Mathinna Supergroup rocks has now been upgraded to a geological mapping standard closer to 'primary' first-edition 1:25 000 scale; further refinement was not possible within the strict time and budget constraints of Initiative Project funding, and some mapping uncertainties remain.

The new work has also enabled the recognition and formalisation of a more detailed stratigraphic subdivision of the Mathinna Supergroup, which in the type area now consists of six formations, three of them new and replacing the previous Bellingham Formation. Also significant is the discovery of six new Late Silurian graptolite fossil localities in the Panama Group, substantially increasing the known age controls on the sequence. The assessment that all of the new fossil localities probably come from the same horizon as the previously discovered Late Silurian locality at Golden Ridge (Rickards *et al*., 1993) provides the first-recognised terrane-wide marker horizon in the Mathinna Supergroup, traceable at the time of this report over a point-to-point distance of some 80 km across northeast Tasmania.

The revised stratigraphic framework and improved map coverage should provide a useful basis for further sedimentary research. Examples of possible research include a stratigraphic, sedimentological and provenance comparison of the three major sandy turbidite complexes (Stony Head Sandstone, Retreat Formation and Sideling Sandstone); and a geochemical comparison of the pelites (Turquoise Bluff Slate, Yarrow Creek Mudstone and Lone Star Siltstone), or of the units of the Tippogoree Group versus the Panama Group.

The new mapping has led to the interpretation of a fault contact between the Tippogoree and Panama groups, a return to the previous interpretation of Turner (1980). The new data also lend support to the interpretation of Reed (2002) that the early recumbent folds and associated high-strain foliation(s) in the Tippogoree Group belong to a period of early Silurian deformation, correlated with the Benambran Orogeny of mainland Australia and pre-dating deposition of the Panama Group. This interpretation implies an unconformable relationship between the Tippogoree and Panama groups, although if indeed the two groups are anywhere in erosional contact the undisturbed unconformity is probably not presently exposed. The body of evidence to date is consistent with an interpretation of the fault contact as an early, extensional growth fault which was active during Panama Group deposition, and which has subsequently been partially inverted, folded and obliquely cross-faulted during Devonian compressional deformation events. Further investigation of this contact relationship could benefit from detailed structural fabric studies and associated radiometric dating, more detailed sampling for metamorphic grade comparison across the contact, and at a larger scale, reflection seismic transects to better constrain the 3-D geometry of the contact.

A more complex structural history is now apparent in the Mathinna Supergroup. The inferred Benambran structures in the Tippogoree Group may be dual-phase, but it was not possible to confirm the previously reported presence of two tectonic foliations contributing to the high-strain fabric axial planar to the early northeast-vergent recumbent folds; this is a potential area for further investigation. The Devonian structural history is now recognised as at least three-phase. *Ta*$D_1$ and *Ta*$D_2$ produced a succession of widespread northeast-vergent to upright folds with moderately to steeply southwest-dipping axial surfaces, axial planar penetrative and rarely crenulation cleavage, and associated northeast-directed thrust faults. *Ta*$D_3$, which increases in intensity towards the southwestern part of the area, produced markedly southwest-vergent open to close folds with moderately to steeply northeast-dipping axial surfaces. These structures overprinted the earlier structures in some areas, producing folds with axial planar crenulation cleavage, but particularly in the southern part of the Lone Star Siltstone outcrop belt the final structures appear to be substantially the result of reactivation and reorientation of earlier *Ta*$D_1$–$D_2$ folds and cleavages. A possible additional, post-*Ta*$D_3$ phase of folding is suggested by the presence of partial girdle patterns on stereoplots of *Ta*$S_3$ crenulation cleavage orientations.

Although little additional fieldwork was done on the Devonian granitoids in this project, existing radiometric data on the crystallisation age of the Diddleum Granodiorite suggest that it was intruded post-*Ta*$D_{1\text{–}2}$ (but perhaps partially syn-tectonic with the latter part of that deformation history), and pre-*Ta*$D_3$. Although there are previous reports of grain-defined foliation in the Diddleum Granodiorite, there seems a strong possibility that this is a primary, igneous flow-related feature, and that the pluton lacks post-crystallisation tectonic foliation. This implies that *Ta*$D_3$ did not produce pervasive, grain-scale foliation in the Diddleum Granodiorite. The Lisle Granodiorite may have reached the presently exposed structural level slightly later, late syn to post-*Ta*$D_3$, consistent with petrographic descriptions by Roach (1994), but SHRIMP dating of igneous zircons in this body would be useful to confirm its age relationships. What has become increasingly clear following the *TasExplore* work is that the intrusion of the Lisle and Diddleum plutons involved a substantial component of forceful rather than passive emplacement, shown by examples of substantial deflection and displacement of pre-existing (*Ta*$D_{1\text{–}2}$ or *Ta*$D_3$) structures in Mathinna Supergroup country rocks around the margins of the upwelling plutons.

Devonian gold deposits in the Mathinna Supergroup in the River Tamar–Scottsdale area fall into two main categories. Vein-related gold mineralisation at Lefroy and Back Creek is considered to be part of a larger family of orogenic gold deposits coeval with the last major phase of Devonian deformation, or *Ta*D$_3$ in the terminology applied here. The other main group of deposits, in the Lisle–Panama–Golconda–Denison goldfields area, shows a strong spatial relationship with the mostly concealed subjacent form of the Lisle Granodiorite, and so may be more fundamentally intrusion-related. If so, these deposits may have a late syn-TaD$_3$ to post-*Ta*D$_3$ timing.

While the *TasExplore* project scope did not include substantial further detailed local groundwork on the gold deposits, some further insights into controls on the mineralisation have been possible. Measurements on a published detailed map of the Lefroy goldfield show that the angle between *Ta*D$_3$- $_1$ and the preferred reef trend (084° 7°) may be less than half the optimum 30° angle for reef formation, suggested by Reed (2002) based on pre-*TasExplore* data. This, together with the existence in both gravity and magnetic data of prominent east-west trending worm sets running through Lefroy, and elsewhere across the River Tamar–Scottsdale region, suggests that reef formation may have been partially controlled by *Ta*D$_3$ reactivation of older east-west trending structures in the pre-Mathinna Supergroup basement. The latter could be Cambrian structures, perhaps transfer faults or lateral ramps associated with the emplacement of Early Cambrian mafic-ultramafic complexes which are inferred to underlie the Mathinna Supergroup.

Further east, interpretation of the Lisle–Panama–Golconda–Denison lode gold now perhaps has the additional complication of substantial intrusion-related deformation associated with forceful emplacement of the Lisle Granodiorite; this process alone may have created structural acceptor sites for mineralising fluids migrating outward from the intrusive rocks. The Denison goldfield may be considered a hybrid between the Lefroy–Back Creek style and the intrusion-related style of deposit; measurements on an historical map show a preferred reef trend of 083° ± 10°, almost identical to that at Lefroy and suggesting a common underlying (mid-crustal?) structural control. The lithological contact between the sandstone-dominant Retreat Formation and the overlying pelitic Lone Star Siltstone also appears to have been an important control on localisation of the Denison mineralisation, further reinforcing the importance of lithological controls on mineralisation noted by Reed (2002; 2004).

## Acknowledgements

The report content was substantially improved following review and comment from a number of MRT colleagues, particularly Geoff Green, Mark Duffett and Mike Vicary. Geoff Green provided overall project management and guidance for the duration of the *TasExplore* Project, of which the study reported here was one component. Shane Heawood of MRT's Mornington Core Store complex is thanked for competent and helpful field assistance during the fieldwork.

The Launceston Field Naturalists Club, and Annette Vains of the Queen Victoria Museum and Art Gallery, are thanked for drawing attention to a previous Late Silurian graptolite collection from the Lone Star Siltstone. The late Dr Tatyana Koren, and Dr Anna Suyarkova, of the A. P. Karpinsky Russian Geological Research Institute (VSEGEI), St Petersburg, are thanked for providing expert advice on species identification and biozone assignment of the Late Silurian graptolite faunas.

# REFERENCES


BANKS, M. R. 1962. Silurian and Devonian systems, *in:* SPRY, A.; BANKS, M. R. (ed.). The geology of Tasmania. *Journal of the Geological Society of Australia* 9(2):177–187.

BANKS, M. R.; SMITH, E. A. 1968. A graptolite from the Mathinna Group, north-eastern Tasmania. *Australian Journal of Science* 31:118–119.

BAILLIE, P. B.; POWELL, C. MCA.; BANKS, M. R.; HILLS, P. B. 1989. The Eastern Tasmanian Terrane, *in:* BURRETT, C. F.; MARTIN, E. L. (ed.). Geology and mineral resources of Tasmania. *Special Publication Geological Society of Australia* 15:234–237.

BARTON, T. J. 1999*a*. Crustal structure of northern Tasmania based upon a deep seismic transect, *in:* JESSELL, M. (ed.). Last conference of the Millenium. *Abstracts Geological Society of Australia* 53:3–4.

BARTON, T. J. 1999*b*. *Crustal structure of northern Tasmania, Australia*. M.Sc. thesis, Monash University.

BHATIA, M. R. 1983. Plate tectonics and geochemical composition of sandstones. *Journal of Geology* 91:611–627.

BHATIA, M. R.; CROOK, K. A. W. 1986. Trace element characteristics of graywackes and tectonic setting discrimination of sedimentary basins. *Contributions to Mineralogy and Petrology* 92:181–193.

BIERLEIN, F. P.; FOSTER, D. A.; GRAY, D. R.; DAVIDSON, G. J. 2005. Timing of orogenic gold mineralisation in northeastern Tasmania: implications for the tectonic and metallogenic evolution of Palaeozoic SE Australia. *Mineralium Deposita* 39:890–903.

BLACK, L. P.; CALVER, C. R.; SEYMOUR, D. B.; REED, A. 2004. SHRIMP U-Pb detrital zircon ages from Proterozoic and Early Palaeozoic sandstones and their bearing on the early geological evolution of Tasmania. *Australian Journal of Earth Sciences* 51:885–900.

BLACK, L. P.; MCCLENAGHAN, M. P.; KORSCH, R. J.; EVERARD, J. L.; FOUDOULIS, C. 2005. Significance of Devonian–Carboniferous igneous activity in Tasmania as derived from U-Pb SHRIMP dating of zircon. *Australian Journal of Earth Sciences* 52:807–829.

BOTTRILL, R. S. 1986. Mineralogy of gold-bearing concentrates from Synfields Lease (Tasmanian Alluvials), Lisle goldfield. *Unpublished Report Department of Mines Tasmania* 1986/66.

BOTTRILL, R. S. 1991. Alluvial gold. *Mineral Resources of Tasmania* 11.

BOTTRILL, R. S. 1994. The Lisle–Golconda–Denison goldfield (including some adjacent gold mining areas). *Unpublished Report Department of Mines Tasmania* 1994/01.

BOTTRILL, R. S. 1996*a*. The ore petrology of some samples from the Lefroy goldfield, *in:* KEELE, R. A. 1996. *Annual report for gold exploration over EL1/95 – Lefroy, N.E. Tasmania*. Lefroy Gold Mines Pty Ltd [TCR 96-3852].

BOTTRILL, R. S. 1996*b*. Diamond drilling in the Lisle Valley. *Record Tasmanian Geological Survey* 1996/04.

BOTTRILL, R. S. 1996*c*. Petrography of some samples from the Lisle–Golconda goldfield, *in:* DUNCAN, D. MCP. *Exploration Licence 2/92 'Lisle'. Annual report on exploration activity July 1995 to June 1996*. Macmin NL [TCR 96-3895].

BOTTRILL, R. S. 2005. *Petrological studies: Whiting prospect.* Unpublished Report Mineral Resources Tasmania to Cala Resources M056/05.

BOTTRILL, R. S.; TAHERI, J.; KEELE, R. A. 1994. A field guide to gold deposits in northeastern Tasmania. *Report Mineral Resources Tasmania* 1994/19.

BROADHURST, E. 1935. Lefroy and Back Creek goldfields. *Bulletin Geological Survey Tasmania* 42.

CALLAGHAN, T.; REID, R. 2005. Golconda goldfield, *in:* TAHERI, J.; BOTTRILL, R. S. Devonian granites and associated mineralisation in northeast and northwest Tasmania. *Record Geological Survey Tasmania* 2005/03:48–53.

COCKER, J. D. 1982. Rb-Sr geochronology and Sr isotopic composition of Devonian granitoids, eastern Tasmania. *Journal Geological Society Australia* 29:139–158.

COOKSON, I. C. 1937. The occurrence of fossil plants at Warrentinna, Tasmania. *Papers and Proceedings Royal Society of Tasmania* 1936:73–78.

GEE, R. D.; LEGGE, P. J. 1979. Geological atlas 1:63,360 series. Sheet 30 (8215N). Beaconsfield (2nd edition). *Explanatory Report Geological Survey Tasmania*.

GOH, H. K. H. 2008. *Properties of north eastern Tasmanian rocks for geothermal exploration: Petrophysical, geochemical and thermal characteristics of the Mathinna Group and Devonian granites.* B.Sc. (Hons) thesis, University of Tasmania, Hobart.

GOSCOMBE, B. D.; FINDLAY, R. H.; MCCLENAGHAN, M. P.; EVERARD, J. L. 1994. Multi-scale kinking in northeast Tasmania: crustal shortening at shallow crustal levels. *Journal of Structural Geology* 16:1077–1092.

GRAY, D. R.; FOSTER, D. A. 1997. Orogenic concepts — application and definition: Lachlan Fold Belt, eastern Australia. *American Journal of Science* 297:859–891.

GROVES, D. I. 1965. Geology of the Lefroy goldfield. *Technical Report Department of Mines Tasmania* 9:59–76.

HERRON, M. M. 1988. Geochemical classification of terrigenous sands and shales from core or log data. *Journal of Sedimentary Petrology* 58:820–829.

JENNINGS, D. J. 1967. *Geological Atlas 1:63,360 Series. Zone 7 Sheet 23 (8316S). Noland Bay*. Department of Mines Tasmania.

KEELE, R. A. 1996. *Annual report for gold exploration over EL1/95 – Lefroy, N.E. Tasmania*. Lefroy Gold Mines Pty Ltd [TCR 96-3852].

KEELE, R. A.; TAYLOR, B.; DAVIDSON, G. J. 1995. Relationships between Devonian thrusting and gold mineralization in northeastern Tasmania, *in:* COOKE, D. R.; KITTO, P. A. (ed.). Contentious issues in Tasmanian geology. *Abstracts Geological Society of Australia* 39:69–72.

LEAMAN, D. E. 1975. Gravity survey of the Rossarden–Storys Creek region. *Technical Report Department of Mines Tasmania* 19:55–81.

LEAMAN, D. E. 1977. Gravity survey of north-eastern Tasmania. Analysis of pluton margins. *Unpublished Report Department of Mines Tasmania* 1977/26.

LEAMAN, D. E.; RICHARDSON, R. G. 2003. A geophysical model of the major Tasmanian granitoids. *Record Geological Survey Tasmania* 2003/11.

LEAMAN, D. E.; SYMONDS, P. A. 1975. Gravity survey of north-eastern Tasmania. *Paper Geological Survey Tasmania* 2.

MARSHALL, B. 1969. Geological Atlas 1 Mile Series. Zone 7 Sheet 31 (8315N). Pipers River. *Explanatory Report Geological Survey Tasmania*.

MARSHALL, B.; BARTON, C. M.; JENNINGS, D. J.; NAQVI, I. H. 1965. *Geological Atlas 1:63,360 Series. Zone 7 Sheet 31 (8315N). Pipers River*. Department of Mines Tasmania.

MCCLENAGHAN, M. P. 1994. A summary of the Beaconsfield, Lefroy, Back Creek and Gladstone goldfields. *Report Mineral Resources Tasmania* 1994/03.

MCCLENAGHAN, M. P.; HIGGINS, N. C. 1993. The age and intrusive relationships of granitoids of the Blue Tier Batholith, north-east Tasmania. *Report Mineral Resources Tasmania* 1993/33.

McClenaghan, M. P.; Turner, N. J.; Baillie, P. W.; Brown, A. V.; Williams, P. R.; Moore, W. R. 1982. Geology of the Ringarooma–Boobyalla area. *Bulletin Geological Survey Tasmania* 61.

McConachy, G .W.; Swensson, C. G. 1990. Fosterville gold field, *in:* Hughes, F. E. (ed.). Geology of the mineral deposits of Australia and Papua New Guinea. *Monograph Serial Australasian Institute of Mining and Metallurgy* 14:1297–1298.

McNeil, P. A. 2004. *Long gold intersection drilled at the Potoroo prospect, NE Tasmania*. TasGold Limited Report to the Australian Stock Exchange, 16 August 2004.

Miller, J. M.; Wilson, C. J. L. 2002. The Magdala lode system, Stawell, southeastern Australia: Structural style and relationship to gold mineralization across the western Lachlan Fold Belt. *Economic Geology* 97:325–349.

Montgomery, A. 1894. Report on certain portions of the Lisle goldfield. *Unpublished Report Department of Mines Tasmania* 1861–1920:44–51.

Noldart, A. J.; Threader, V. M. 1965. Gold deposits of Tasmania, *in:* McAndrew, J. (ed.). The geology of Australian ore deposits. *Proceedings 8th Commonwealth Mining and Metallurgy Congress* 1:518–521. Australasian Institute of Mining and Metallurgy.

Patison, N. L.; Berry, R. F.; Davidson, G. J.; Taylor, B. P.; Bottrill, R. S.; Manzi, B.; Ryba, J.; Shepherd, R. E. 2001. Regional metamorphism of the Mathinna Group, northeast Tasmania. *Australian Journal of Earth Sciences* 48:281–292.

Powell, C. McA.; Baillie, P. W. 1992. Tectonic affinity of the Mathinna Group in the Lachlan Fold Belt. *Tectonophysics* 214:193–209.

Powell, C. McA.; Baillie, P. W.; Conaghan, P. J.; Turner, N. J. 1993. The mid-Palaeozoic turbiditic Mathinna Group, northeast Tasmania. *Australian Journal of Earth Sciences* 40:169–196.

Reed, A. R. 2001. Pre-Tabberabberan deformation in eastern Tasmania: a southern extension of the Benambran orogeny. *Australian Journal of Earth Sciences* 48:785–796.

Reed, A. R. 2002. Formation of lode-style gold mineralisation during Tabberabberan wrench faulting at Lefroy, eastern Tasmania. *Australian Journal of Earth Sciences* 49:879–890.

Reed, A. R. 2004. Gold mineralisation and the regional Palaeozoic structure of the Mathinna Supergroup, eastern Tasmania. *Record Geological Survey Tasmania* 2004/01.

Reid, A. M. 1926. The Golconda gold mining district. *Bulletin Geological Survey Tasmania* 37.

Reid, R.; Callaghan, T. 2004. *EL2/92 Lisle: Annual Report July 2003–August 2004*. TasGold Limited [TCR 04-5057].

Rickards, R. B.; Banks, M. R. 1979. An Early Devonian monograptid from the Mathinna Beds, Tasmania. *Alcheringa* 3:307–311.

Rickards, R. B.; Davidson, G. J.; Banks, M. R. 1993. Silurian (Ludlow) graptolites from Golden Ridge, NE Tasmania. *Memoirs Association Australasian Palaeontologists* 15:125–135.

Roach, M. 1991. *Six monthly report – Lisle area for Billiton Australia*. Centre for Ore Deposits and Exploration Studies, University of Tasmania [TCR 91-3296A].

Roach, M. J. 1994. *The regional geophysical setting of gold mineralisation in northeast Tasmania*. Ph.D. thesis, University of Tasmania, Hobart.

Roser, B. P.; Korsch, R. J. 1986. Determination of tectonic setting of sandstone–mudstone suites using $SiO_2$ content and $K_2O/Na_2O$ ratios. *Journal of Geology* 94:635–650.

Roser, B. P.; Korsch, R. J. 1988. Provenance signatures of sandstone-mudstone suites determined using discriminant function analysis of major element data. *Chemical Geology* 67:119–139.

Russell, D. W.; van Moort, J. C. 1992. Mineralogy and stable isotope geochemistry of the Beaconsfield, Salisbury and Lefroy goldfields. *Bulletin Geological Survey Tasmania* 70:208–226.

Taheri, J.; Bottrill, R. S. 2005. Devonian granites and associated mineralisation in northeast and northwest Tasmania. *Record Geological Survey Tasmania* 2005/03.

Taheri, J.; Keele, R. A.; Bottrill, R. S.; Callaghan, T.; McClenaghan, M. P.; McDonald, G.; Reed. A. 2004. Mineralisation, structure and granites, northeast Tasmania. *Field Guide 17th Australian Geological Convention*. A1. Geological Society of Australia.

Thompson, D. 2000. *The geology of the Sideling Range*. B.Sc. (Hons) thesis, University of Tasmania, Hobart.

Thureau, G. 1882. Report on the mineral resources and on the permanency of the Lisle gold field. *House of Assembly Paper Tasmania* 1882 (46).

Turner, N. J. 1980. Composite geological profile across Tasmania. *Unpublished Report Department of Mines Tasmania* 1980/38.

Turner, N. J.; Black, L. P.; Higgins, N. C. 1986. The St Marys Porphyrite — a Devonian ash-flow and its feeder. *Australian Journal of Earth Sciences* 33:201–218.

Twelvetrees, W. H. 1909. The Lisle Goldfield. *Bulletin Geological Survey Tasmania* 4.

van Moort, J. C.; Russell, D. W. 2005. Lefroy and Beaconsfield gold mines, Tamar region, Tasmania, *in:* Butt, C. R. M.; Cornelius, M.; Scott, K. M.; Robertson, I. D. M. (ed.). *Regolith expression of Australian ore systems — A compilation of geochemical case histories and conceptual models*. 276–278. Cooperative Research Centre for Landscape Environments and Mineral Exploration.

Walker, R. G.; Mutti, E. 1973. Turbidite facies and facies associations, *in: Turbidites and deep-water sedimentation.* Short Course Notes Society of Economic Paleontologists and Mineralogists, Pacific Section. 119–157.

Williams, E. 1978. Tasman Fold Belt System in Tasmania. *Tectonophysics* 48:159–205.

Williams, E. 1989. Fold related mesoscopic structures in the Mathinna beds: Field relationships compared with text-book relationships. *Report Department of Mines Tasmania* 1989/41.

Williams, E.; McClenaghan, M. P.; Collins, P. L. F.; *et al.* 1989. Mid-Palaeozoic deformation, granitoids and ore deposits, *in:* Burrett, C. F.; Martin, E. L. (ed.). Geology and mineral resources of Tasmania. *Special Publication Geological Society of Australia* 15:238–292.

Woolward, I. R.; McClenaghan, M. P. 2010. *Geological Atlas 1:25 000 scale digital series. Sheet 5243. Lisle*. Mineral Resources Tasmania.

# APPENDIX 1
## ASUD stratigraphic definitions

| DEFINITION CARD | |
|---|---|
| **NAME OF UNIT:** Industry Road Member | **STATE(S):** Tasmania |
| **STATUS OF UNIT:** New name | **RANK:** Member |
| **PROPOSER:** David Seymour, Mineral Resources Tasmania | **DATE:** 03/09/2010 |
| **RESERVED IN STRATIGRAPHIC UNITS DATABASE:** YES | |
| **PROPOSED PUBLICATION:**<br>Seymour, D. B.; Woolward, I. R.; McClenaghan, M. P. 2011. Stratigraphic revision and re-mapping of the Mathinna Supergroup between the River Tamar and the Scottsdale Batholith, northeast Tasmania. *Mineral Resources Tasmania, 1:25 000 Scale Digital Geological Map Series Explanatory Report* 4.<br>Possibly also AJES. | |

| |
|---|
| **DERIVATION OF NAME:** Named after a section of Industry Road centred on about: GDA94 Zone 55, 503040 mE, 5446355 mN |
| **SYNONYMY, UNIT NAME HISTORY:** None |
| **CONSTITUENT UNITS:** None |
| **PARENT UNIT:** Turquoise Bluff Slate (of the Tippogoree Group, of the Mathinna Supergroup) |
| **TYPE LOCALITY:** The unit is generally not well exposed. The best exposures may occur within the Australian Army Stony Head Artillery Range, but due to severe access restrictions this is not considered suitable as a type area. Intermittent representative exposures of the unit occur on Industry Road between 502525 mE, 5445380 mN and 503405 mE, 5447600 mN (GDA94 Zone 55), and this is nominated as the type area. |
| **CONFIDENTIAL TYPE LOCALITY?:** No |
| **DESCRIPTION AT TYPE LOCALITY:** Interbedded phyllitic slate and foliated very fine-grained quartz-rich sandstone, with almost-recumbent large-scale $D_1$ folds and associated intensely developed gently dipping axial plane penetrative cleavage. This new member represents a transition package between the underlying Stony Head Sandstone and the rest of the Turquoise Bluff Slate. |
| **LITHOLOGY:** The slate component is similar to the lithology which dominates the rest of the Turquoise Bluff Slate. It is typically dark grey and indistinctly bedded internally, probably partly due to the high strain associated with the intense penetrative cleavage, which commonly shows a phyllitic sheen on the foliation surfaces. The other component interbedded with the slate typically comprises quartzose siltstone to fine-grained quartz-rich sandstone with a somewhat less intense penetrative cleavage typically at a low angle to bedding. Sedimentary structures indicating facing are typically scant, perhaps partly due to the high strain state. |
| **THICKNESS:** Estimated from structural profile sections, about 1200–1300 m. |
| **FOSSILS:** None known. |
| **DIASTEMS OR HIATUSES:** None known. |
| **RELATIONSHIPS & BOUNDARY CRITERIA:** Contact sections are not particularly well exposed, but it is likely that this unit has conformable and transitional contacts with both the underlying Stony Head Sandstone, and the overlying main body of the parent Turquoise Bluff Slate. |
| **DISTINGUISHING OR IDENTIFYING FEATURES:** Mainly the geomorphic expression: the mix of resistant quartz-rich lithologies and more easily weathered pelitic slate give the unit a distinctive topographic pattern of parallel strike ridges which distinguish it from the underlying and overlying units, particularly visible in high-resolution DEM or LiDAR data and to a lesser extent in aerial photography. |
| **AGE & EVIDENCE:** Probably Early Ordovician. The youngest detrital zircons in the underlying Stony Head Sandstone are less than 500 Ma in age (Black *et al*., 2004). A graptolite of Early–Middle Ordovician age occurs in the main body of the Turquoise Bluff Slate a short interval above the top of the Industry Road Member (Banks and Smith, 1968). |
| **CORRELATION WITH OTHER UNITS:** No known correlates elsewhere within the outcrop area of the Mathinna Supergroup as at March 2010. |

| REGIONAL ASPECTS/GENERAL GEOLOGICAL DESCRIPTION: |
|---|
| **EXTENT:** Currently mapped geographic extent comprises a slightly discontinuous 1.7 km wide outcrop belt extending from near the township of Lulworth on the Bass Strait coast in the north, some 30 km in (folded) strike length to the southern end of the Den Ranges (GDA94 Zone 55, 508160 mE, 5439635 mN) in the south. |
| **GEOMORPHIC EXPRESSION:** Generally elevated ground, with a distinctive topographic pattern of parallel strike ridges. |
| **THICKNESS VARIATIONS:** Mapping to date suggests the unit is relatively constant in thickness. |
| **STRUCTURE AND METAMORPHISM:** Structural style is early large-scale almost-recumbent NE-vergent folds with gently dipping well developed to intense penetrative axial plane cleavage, overprinted by later, smaller-scale, steeply inclined SW-vergent open folds with axial plane crenulation cleavage selectively developed in the slaty lithologies. Metamorphism is anchizonal (200–300°C, sub-greenschist facies) according to Patison *et al.* (2001). |
| **ALTERATION AND MINERALISATION:** The unit hosts about seven scattered historical small mines and prospects targeting gold-bearing quartz reef systems. |
| **GEOPHYSICAL EXPRESSION:** Nothing particularly distinctive, but a subdued striped dark-light pattern is evident on K-Th-U RGB images of airborne radiometric data, presumably due to the interlayered slate and quartz-rich lithologies in the unit. |
| **GEOCHEMISTRY:** No data. |
| **GENESIS/DEPOSITIONAL ENVIRONMENT:** Deep marine, distal turbidite to possibly marginal submarine fan. |
| **COMMENTS:** |
| **REFERENCES:**<br>Banks, M. R.; Smith, E. A. 1968. A graptolite from the Mathinna Group, north-eastern Tasmania. *Australian Journal of Science* 31:118–119.<br>Black, L. P.; Calver, C. R.; Seymour, D. B.; Reed, A. 2004. SHRIMP U-Pb detrital zircon ages from Proterozoic and Early Palaeozoic sandstones and their bearing on the early geological evolution of Tasmania. *Australian Journal of Earth Sciences* 51:885–900.<br>Patison, N. L.; Berry, R. F.; Davidson, G. J.; Taylor, B. P.; Bottrill, R. S.; Manzi, B.; Ryba, J.; Shepherd, R. E. 2001. Regional metamorphism of the Mathinna Group, northeast Tasmania. *Australian Journal of Earth Sciences* 48:281–292. |

| DEFINITION CARD | |
|---|---|
| **NAME OF UNIT:** Yarrow Creek Mudstone | **STATE(S):** Tasmania |
| **STATUS OF UNIT:** New name | **RANK:** Formation |
| **PROPOSER:** David Seymour, Mineral Resources Tasmania | **DATE:** 03/09/2010 |
| **RESERVED IN STRATIGRAPHIC UNITS DATABASE:** YES | |
| **PROPOSED PUBLICATION:** Seymour, D. B.; Woolward, I. R.; McClenaghan, M. P. 2011. Stratigraphic revision and re-mapping of the Mathinna Supergroup between the River Tamar and the Scottsdale Batholith, northeast Tasmania. *Mineral Resources Tasmania, 1:25 000 Scale Digital Geological Map Series Explanatory Report* 4.<br>Possibly also AJES. | |

| | |
|---|---|
| **DERIVATION OF NAME:** Yarrow Creek headwaters: GDA94 Zone 55, 510905 mE, 5452175 mN | |
| **SYNONYMY, UNIT NAME HISTORY:** None | |
| **CONSTITUENT UNITS:** None | |
| **PARENT UNIT:** Panama Group (of the Mathinna Supergroup) | |
| **TYPE LOCALITY:** A 1350 m long traverse of Lewis Road between points 511320 mE, 5444235 mN and 511990 mE, 5444945 mN (GDA94 Zone 55). See 1:25 000 scale topographic map series, sheet 5044: RETREAT, and Mineral Resources Tasmania digital geology equivalent. | |
| **CONFIDENTIAL TYPE LOCALITY?:** No | |
| **DESCRIPTION AT TYPE LOCALITY:** Dominantly thin-bedded mudstone, with subordinate cross-laminated siltstone. | |
| | **LITHOLOGY:** Thin bedded clastic sedimentary sequence, bed thickness <30 cm. Dominant lithology is cleaved grey mudstone, with subordinate to minor pale-weathering beds of quartz-rich siltstone to very fine-grained sandstone, commonly cross-laminated, and occasional beds of fine-grained quartz-rich sandstone. Ratio of grey mudstone : quartz-rich siltstone + sandstone is ~ 2.7:1. |
| | **THICKNESS:** Approximately 900 m (but base is probably faulted). |
| | **FOSSILS:** None |
| | **DIASTEMS OR HIATUSES:** None known |
| | **RELATIONSHIPS & BOUNDARY CRITERIA:** Contact with underlying Turquoise Bluff Slate is an inferred fault or faulted unconformity. Contact with overlying Retreat Formation appears conformable. |
| | **DISTINGUISHING OR IDENTIFYING FEATURES:** This is a pelitic clastic sedimentary unit which consistently occupies the interval between the Turquoise Bluff Slate and the Retreat Formation. Its most distinguishing feature is a geophysical one, i.e. a bright white signature on K-Th-U RGB images of airborne radiometric data, contrasting with the dark signatures of the two adjacent units. |
| **AGE & EVIDENCE:** Probably Silurian. It is the lowest unit of the redefined Panama Group, a conformable sequence of four formations in which the third formation from the base contains Late Silurian (Ludlow) graptolites. It is in fault or faulted unconformity contact with the underlying Turquoise Bluff Slate which contains Early Ordovician graptolites. | |
| **CORRELATION WITH OTHER UNITS:** Correlates probably exist elsewhere within the Mathinna Supergroup outcrop area but none have been identified at this stage. | |

| REGIONAL ASPECTS/GENERAL GEOLOGICAL DESCRIPTION: |
|---|
| **EXTENT:** Currently mapped geographic extent comprises a more or less continuous 0.5–4 km wide outcrop belt extending from Weymouth on the Bass Strait coast in the north, some 27 km in (folded) strike length to 2 km north of Bangor in the south. |
| **GEOMORPHIC EXPRESSION:** Subdued but undulating topography. |
| **THICKNESS VARIATIONS:** Variations are probably largely due to (inferred) faulted lower contact. Calculated or estimated minimum thicknesses vary from about 380 m to about 1015 m (about 900 m at type section). |
| **STRUCTURE AND METAMORPHISM:** Structural style is upright to steeply inclined, close to tight folds typically with well developed axial planar penetrative slaty cleavage. Later folds with axial planar crenulation cleavage present in some areas. Metamorphism is anchizonal (200–300°C, sub-greenschist facies) according to Patison *et al.* (2001). |
| **ALTERATION AND MINERALISATION:** None. |
| **GEOPHYSICAL EXPRESSION:** Distinctive bright white signature on K-Th-U RGB images of airborne radiometric data, i.e. equally strong signal in all three channels. |
| **GEOCHEMISTRY:** No data. |
| **GENESIS/DEPOSITIONAL ENVIRONMENT:** Deep marine, distal turbidite-influenced. |
| **COMMENTS:** |
| **REFERENCES:**<br>Patison, N. L.; Berry, R. F.; Davidson, G. J.; Taylor, B. P.; Bottrill, R. S.; Manzi, B.; Ryba, J.; Shepherd, R. E. 2001. Regional metamorphism of the Mathinna Group, northeast Tasmania. *Australian Journal of Earth Sciences* 48:281–292. |

| DEFINITION CARD | |
|---|---|
| **NAME OF UNIT:** Retreat Formation | **STATE(S):** Tasmania |
| **STATUS OF UNIT:** New name | **RANK:** Formation |
| **PROPOSER:** David Seymour, Mineral Resources Tasmania | **DATE:** 03/09/2010 |
| **RESERVED IN STRATIGRAPHIC UNITS DATABASE:** YES | |
| **PROPOSED PUBLICATION:** Seymour, D. B.; Woolward, I. R.; McClenaghan, M. P. 2011. Stratigraphic revision and re-mapping of the Mathinna Supergroup between the River Tamar and the Scottsdale Batholith, northeast Tasmania. *Mineral Resources Tasmania, 1:25 000 Scale Digital Geological Map Series Explanatory Report* 4.<br>Possibly also AJES. | |

| |
|---|
| **DERIVATION OF NAME:** Named after the small settlement of Retreat: GDA94 Zone 55, 514480 mE, 5444050 mN |
| **SYNONYMY, UNIT NAME HISTORY:** None |
| **CONSTITUENT UNITS:** None |
| **PARENT UNIT:** Panama Group (of the Mathinna Supergroup) |
| **TYPE LOCALITY:** The main type area is nominated as Bare Hill Road and its spur roads, between the intersection with Golconda Road (GDA94 Zone 55: 520700 mE, 5443170 mN) and a point some 5.6 km to the north (GDA94 Zone 55: 521565 mE, 5448730 mN), along which representative folded sections through the more sandstone-rich parts of the formation are exposed. Folded reference sections exposing parts of the formation with more interbedded siltstone-mudstone are intermittently exposed on Retreat Road between a point (GDA94 Zone 55: 513860 mE, 5445420 mN) some 1.5 km north of Retreat, to the intersection with Bridport Road some 7 km to the north (GDA94 Zone 55: 512780 mE, 5452270 mN). |
| **CONFIDENTIAL TYPE LOCALITY?:** No |
| **DESCRIPTION AT TYPE LOCALITY:** Interbedded turbiditic medium to fine-grained quartz-rich sandstone with generally minor interbedded siltstone-mudstone. Reference sections on Retreat Road show a higher proportion of interbedded siltstone-mudstone, and lower proportion of medium-grained sandstone. |
| **LITHOLOGY:** Sandstone-rich parts of the formation (e.g. in the type area) contain graded beds up to 2 m thick of quartz-rich medium to fine-grained sandstone commonly showing Bouma A-B-C bed subdivisions, with interbedded combinations of typically thinner-bedded quartzose siltstone (commonly cross laminated), laminated mudstone and shale. These sections typically have ratios = 2:1 of sandstone:siltstone-mudstone-shale. Less sandstone-rich sections (e.g. in the reference area) are thinner bedded (= 0.5 m) and typically comprise interbedded fine to very fine-grained quartz-rich sandstone, siltstone, grey mudstone and shale with ratios of sandstone:siltstone-mudstone-shale of about 1:1, although some outcrops may show a paucity or absence of sandstone. Some sandstone beds and bed sequences in these sections are massive or plane laminated, but are lacking in grading or other classical Bouma turbidite bed structures. |
| **THICKNESS:** Estimated from structural profiles: about 1050 m. |
| **FOSSILS:** None |
| **DIASTEMS OR HIATUSES:** None known |
| **RELATIONSHIPS & BOUNDARY CRITERIA:** Map relationships, bedding measurements and facing evidence indicate apparently conformable relationships with both the underlying Yarrow Creek Mudstone and the overlying Lone Star Siltstone. Both contacts are probably abrupt transitions (i.e. over a few metres of section). |
| **DISTINGUISHING OR IDENTIFYING FEATURES:** The Retreat Formation is distinguished from the underlying and overlying formations largely by its high percentage of turbiditic quartz-rich sandstone beds. The other main distinguishing characteristic is a geophysical one – i.e. a dark (approaching black) signature on K-Th-U RGB images of airborne radiometric data, which is probably partly due to a paucity of response in all three channels due to the high quartz sandstone content and partly due to the quartz sand-rich soils which derive from weathering of the unit and blanket its outcrop area. |
| **AGE & EVIDENCE:** Probably Silurian. The overlying Lone Star Siltstone contains Late Silurian (Ludlow) graptolites, and the Panama Group, which this unit is part of, is in fault or faulted unconformity contact with the underlying Turquoise Bluff Slate which contains Early Ordovician graptolites.<br><br>**CORRELATION WITH OTHER UNITS:** Correlates possibly exist elsewhere within the Mathinna Supergroup outcrop area but none have been confirmed at this stage. |

| **REGIONAL ASPECTS/GENERAL GEOLOGICAL DESCRIPTION:** |
|---|
| **EXTENT:** Currently mapped geographic extent comprises a more or less continuous, sinuous outcrop belt up to 8 km wide, extending from near Bellingham on the Bass Strait coast in the north, some 29 km to near Lilydale in the south. |
| **GEOMORPHIC EXPRESSION:** Undulating, elevated to hilly ground. Generally more positive geomorphic expression than immediately underlying or overlying units. |
| **THICKNESS VARIATIONS:** Faulted contacts against adjacent units in several areas make assessment of variations in stratigraphic thickness difficult. Structural profile sections suggest stratigraphic thickness may be reasonably consistent. |
| **STRUCTURE AND METAMORPHISM:** Structural style is upright to steeply inclined, generally open to close folds with variably developed axial planar sandstone cleavage (showing conjugate geometry in some outcrops), and well developed axial planar penetrative slaty cleavage in the finer-grained lithologies. Later folds with axial planar crenulation cleavage in the finer-grained lithologies present in some areas. Metamorphism is anchizonal (200–300°C, sub-greenschist facies) according to Patison *et al.* (2001). |
| **ALTERATION AND MINERALISATION:** Devonian gold mineralisation in the Denison Goldfield is spatially associated with the contact between this unit and the overlying Lone Star Siltstone. |
| **GEOPHYSICAL EXPRESSION:** Distinctive dark signature on K-Th-U RGB images of airborne radiometric data, i.e. weak signal in all three channels. |
| **GEOCHEMISTRY:** No data |
| **GENESIS/DEPOSITIONAL ENVIRONMENT:** Marine, probably largely deposited in one or more sandy submarine fan complexes. |
| **COMMENTS:** |
| **REFERENCES:** Patison, N. L.; Berry, R. F.; Davidson, G. J.; Taylor, B. P.; Bottrill, R. S.; Manzi, B.; Ryba, J.; Shepherd, R. E. 2001. Regional metamorphism of the Mathinna Group, northeast Tasmania. *Australian Journal of Earth Sciences* 48:281–292. |

| DEFINITION CARD | |
|---|---|
| **NAME OF UNIT:** Lone Star Siltstone | **STATE(S):** Tasmania |
| **STATUS OF UNIT:** New Name | **RANK:** Formation |
| **PROPOSER:** I. R. Woolward | **DATE:** 02/06/2010 |
| **RESERVED IN STRATIGRAPHIC UNITS DATABASE:** YES | |
| **PROPOSED PUBLICATION:** Seymour, D. B.; Woolward, I. R.; McClenaghan, M. P. 2011. Stratigraphic revision and re-mapping of the Mathinna Supergroup between the River Tamar and the Scottsdale Batholith, northeast Tasmania. *Mineral Resources Tasmania, 1:25 000 Scale Digital Geological Map Series Explanatory Report* 4. Possibly also AJES. | |

**DERIVATION OF NAME:** Named from the 'Lone Star Ridge' (GDA94 Zone 55: 524512 mE, 5435393 mN) over which it is the dominant bedrock.

**SYNONYMY, UNIT NAME HISTORY:** Along with the Retreat Formation and Yarrow Creek Mudstone, replaces the Bellingham Formation (Strat. No. 1426, of the former Mathinna Group).

**CONSTITUENT UNITS:** None.

**PARENT UNIT:** Panama Group (of the Mathinna Supergroup).

**TYPE LOCALITY:** Exposure throughout the unit is variable, and extensive outcrops are rare. Exposure at the type locality is intermittent. The tightly folded section lies east of the Sideling Range, between points 528962 mE, 5423313 mN and 532302 mE, 5431363 mN (GDA94, zone 55), on the Tasman Highway, and includes south Targa Hill Road and Myrtle Bank Road. See 1:25 000 scale topographic map series, sheets 5242: PATERSONIA and 5243: LISLE, as well as Mineral Resources Tasmania digital geology equivalents.

**CONFIDENTIAL TYPE LOCALITY?:** No

**DESCRIPTION AT TYPE LOCALITY:** The west of the traverse is dominated by a basal unit comprising cleaved, upright folded, variably bioturbated marine siltstone with significant shale and mudstone. Thin planar laminations are typical, but may be obscured by deformation, bioturbation or weathering. Units of massive, medium to thick-bedded sandstone, rarely lenticular, become more common eastwards towards the overlying Sideling Sandstone.

**LITHOLOGY:** The thinly laminated siltstone is typically thin bedded and fine to medium-grained, although may form slabby medium beds approaching and within hornfelsed zones. Fine-grained lithologies are micaceous, and although locally weakly deformed on long fold limbs, elsewhere they assume a slaty cleavage with a phyllitic sheen. Significant black shale is rare, typically pyritic and locally graptolite-bearing. Bioturbation, soft sediment deformation, rare isolated cross beds and mud drapes have been observed in the basal unit. The sandstone is mostly fine-grained with a significant groundmass. Sorting is typically poor. Sedimentary structures associated with sandstone deposition are uncommon but increase in frequency up sequence.

**THICKNESS:** As estimated from structural profiles: approximately 1 km in the type area. Estimation is poorly constrained due to complex folding and probable interruption by faults.

**FOSSILS:** Identifications of graptolites from five new localities are yet to be confirmed but initial observations indicate assemblages are probably Ludlow in age. The graptolites outcrop in dark pyritic shale and fine-grained siltstone around the top of the basal unit. Similar ages have been attributed to graptolites at Boags Ridge and at Golden Ridge in Mathinna Supergroup sediments in NE Tasmania. Within the type section, graptolites are located at 530791 mE, 5426628 mN (GDA94, zone 55), on the Tasman Highway. Significant but variable trace fossils and bioturbation are present within the formation and are concentrated in fine-grained siltstone in the basal unit. Examples of burrows, faecal pellets and bedding obscured by bioturbation may be found at 529095 mE, 5423824 mN (GDA94, zone 55), on the Tasman Highway. The as yet unconfirmed presence of *Chondrites* of the *Nereites* ichnofacies indicates a deep marine environment for the lower part of the formation.

**DIASTEMS OR HIATUSES:** None known

**RELATIONSHIPS & BOUNDARY CRITERIA:** Map relationships and bedding measurements indicate a conformable transitional boundary with the overlying Sideling Sandstone. Away from the type area, the boundary is often poorly exposed. The boundary with the underlying Retreat Formation is typically exposed as a relatively abrupt transition over several metres, and is probably conformable, although the contrast of the unit descriptions allows the possibility of an unconformity.

**DISTINGUISHING OR IDENTIFYING FEATURES:** The basal siltstone and its distinctive yellow signature on ternary radiometric images is readily distinguished from the underlying sandstone-dominant Retreat Formation. The ratio of siltstone to sandstone decreases towards the top of the Lone Star Siltstone, and the transitional boundary with the overlying Sideling Sandstone is defined as the point where the sandstone dominates siltstone. Younger units overlying and intruding the formation lack the well defined penetrative slaty cleavage and fold style of the Lone Star Siltstone.

**AGE & EVIDENCE:** Late Silurian, based on presence of probable Ludlow graptolite fossils. The conformably overlying Sideling Sandstone contains Lower Devonian plant fossils. The formation is intruded by the Scottsdale Batholith and the Lisle Granodiorite, both of which are probably Middle Devonian.

**CORRELATION WITH OTHER UNITS:** Correlates possibly exist east of the Scottsdale Batholith, but none have been confirmed at this stage.

**REGIONAL ASPECTS/GENERAL GEOLOGICAL DESCRIPTION:** The dominance of siltstone over sandstone, the presence of bioturbation, Ludlow graptolites and deep marine mudstone, and a distinctive yellow signature on ternary radiometric images may distinguish the Lone Star Siltstone from other formations in the Mathinna Supergroup.

**EXTENT:** The currently mapped geographic extent comprises a sinuous folded horizon from near Fordington on the Bass Strait coast approximately 45 km SSE to the Mt Barrow Falls State Reserve.

**GEOMORPHIC EXPRESSION:** Ranging from undulating to steep terrain. Elevated ground south of the Lisle granodiorite. Generally lower than surrounding units. The effects of subsequent events prevent the formation from being distinguished by geomorphology alone.

**THICKNESS VARIATIONS:** Cross sections and preliminary modelling indicate a typical total average thickness of up to 1.5 km. This varies considerably due to interruption by faulting throughout the formation, and the possibility of submarine fan complexes along the transitional contact of the overlying Sideling Sandstone. Estimations are hampered by extensive post-Devonian cover of the formation south of the Lone Star Siltstone.

**STRUCTURE AND METAMORPHISM:** Folds are classified as typically upright to steeply inclined, shallowly plunging and close. Fold closures are rarely observed, but stereonet evidence indicates they may be chevrons, particularly in areas with no sandstone. A well developed axial planar penetrative slaty cleavage predominates. Metamorphism is anchizonal (200–300°C, sub-greenschist facies) according to Patison *et al.* (2001).

**ALTERATION AND MINERALISATION:** This formation hosts the Lisle–Golconda goldfields. Most of the goldfields are spatially closely related to small, geomorphically subdued, probably Middle Devonian granodiorite cupolas. 95% of gold in the goldfields was won from alluvial workings (Roach, 1992). Devonian gold mineralisation in the Denison Goldfield is located at the contact between this formation and the underlying Retreat Formation.

**GEOPHYSICAL EXPRESSION:** Where exposure is more extensive towards the south the basal siltstone is distinguished by a high potassium and thorium signature on K-Th-U RGB images of airborne radiometric data. Expression is variable at intermediate intensity of all three channels where the proportion of sandstone increases towards the transitional boundary with the overlying Sideling Sandstone. High frequency linear magnetic anomalies occur locally adjacent to metamorphic aureoles, and may indicate magnetic marker units within the beds (Roach, 1994).

**GEOCHEMISTRY:** Using the geochemical classification of Herron (1988), the siltstone can be classified as wacke or shale, and the sandstone as litharenite. The formation has a passive margin tectonic setting, based on the geochemical classifications of Roser and Korsch (1986), and Bhatia and Crook (1986). The Lone Star Siltstone falls dominantly in the field for rocks with a quartzose sedimentary provenance, using the geochemical classification of Roser and Korsch (1988).

**GENESIS/DEPOSITIONAL ENVIRONMENT:** Marine, based on presence of graptolites, bioturbation and local turbidites within a passive margin setting (see geochemistry). The basal siltstone and shale of the formation is distal, and forms a relatively passive environment between the sandy submarine fan complexes of the underlying Retreat Sandstone and the increasing sandy sheet flows to the east, which lead up to further sandy submarine fan complexes of the overlying Sideling Sandstone.

**COMMENTS:**

**REFERENCES:**


Bhatia, M. R.; Crook, K. A. W. 1986. Trace element characteristics of graywackes and tectonic setting discrimination of sedimentary basins. *Contributions to Mineral and Petrology* 92:181–193.

Herron, M. M. 1988. Geochemical classification of terrigenous sands and shales from core or log data. *Journal of Sedimentary Petrology* 58:820–829.

Patison, N. L.; Berry, R. F.; Davidson, G. J.; Taylor, B. P.; Bottrill, R. S.; Manzi, B.; Ryba, J.; Shepherd, R. E. 2001. Regional metamorphism of the Mathinna Group, northeast Tasmania. *Australian Journal of Earth Sciences* 48:281–292.

Roach, M. J. 1992. Geology and geophysics of the Lisle–Golconda goldfield, northeast Tasmania. *Bulletin Geological Survey Tasmania* 70:189–198.

Roser, B. P.; Korsch R. J. 1986. Determination of tectonic setting of sandstone-mudstone suites using $SiO_2$ content and $K_2O/Na_2O$ ratio. *Journal of Geology* 94:635–650.

Roser, B. P.; Korsch, R. J. 1988. Provenance signatures of sandstone-mudstone suites determined using discriminant function analysis of major element data. *Chemical Geology* 67:119–139.

| DEFINITION CARD | |
|---|---|
| **NAME OF UNIT:** Sideling Sandstone | **STATE(S):** Tasmania |
| **STATUS OF UNIT:** Variation of published name | **RANK:** Formation |
| **PROPOSER:** Dr Marcus McClenaghan, Mineral Resources Tasmania | **DATE:** 03/09/2010 |
| **RESERVED IN STRATIGRAPHIC UNITS DATABASE:** YES | |
| **PROPOSED PUBLICATION:** Seymour, D. B.; Woolward, I. R.; McClenaghan, M. P. 2011. Stratigraphic revision and re-mapping of the Mathinna Supergroup between the River Tamar and the Scottsdale Batholith, northeast Tasmania. *Mineral Resources Tasmania, 1:25 000 Scale Digital Geological Map Series Explanatory Report* 4.<br>Possibly also AJES. | |

| | |
|---|---|
| **DERIVATION OF NAME:** The Sideling Range GDA94 Zone 55, 535310 mE, 5435180 mN, 11 kilometres southwest of Scottsdale in northeast Tasmania. | |
| **SYNONYMY, UNIT NAME HISTORY:** Replacement of Sidling Sandstone which was accidentally formalised and mis-spelled and also replaces the informal Sidling sandstone. Previous database entry (Strat. No. 34172) identifying Sidling Sandstone as a formal unit was in error and based on a few erroneous uses in figures in a publication by A. R. Reed, in which most uses in the body of the text were the correct, informal 'Sidling sandstone'. | |
| **CONSTITUENT UNITS:** Not subdivided. | |
| **PARENT UNIT:** Panama Group, which is part of the Mathinna Supergroup. | |
| **TYPE LOCALITY:** Traverse along the Tasman Highway between points 535610 mE, 5431680 mN and 536310 mE, 5434683 mN (GDA94, zone 55) where the highway crosses the Sideling Range about 15 kilometres southwest of Scottsdale in northeast Tasmania. See 1:25 000 scale topographic map series, sheet 5243: LISLE, and Mineral Resources Tasmania digital geology equivalent. | |
| **CONFIDENTIAL TYPE LOCALITY?:** No | |
| **DESCRIPTION AT TYPE LOCALITY:** Massive fine-grained, tightly folded pale-grey sandstone beds with minor interbeds of siltstone, as prominent roadside outcrops. | |
| | **LITHOLOGY:** Dominantly turbiditic, fine and very fine-grained sandstone with interbedded siltstone. |
| | **THICKNESS:** At least 1500 m (top not exposed). |
| | **FOSSILS:** Contains Early Devonian plant remains. |
| | **DIASTEMS OR HIATUSES:** None known. |
| | **RELATIONSHIPS & BOUNDARY CRITERIA:** The unit has a conformable transitional contact with the underlying Lone Star Siltstone. Top is not exposed. In map view the unit is bounded to the east by an intrusive contact with the Diddleum Granodiorite (of the Scottsdale Batholith). |
| | **DISTINGUISHING OR IDENTIFYING FEATURES:** The dominance of fine-grained sandstone over siltstone distinguishes the formation from the underlying Lone Star Siltstone. |
| **AGE & EVIDENCE:** Early Devonian based on containing plant fossils of that age (Cookson, 1937; Banks, 1962), being intruded by middle Devonian granodiorite of the Scottsdale Batholith, and overlying the Lone Star Siltstone which contains late Silurian (Ludlow) graptolites. | |
| **CORRELATION WITH OTHER UNITS:** Uncertain correlation with sandstone-dominated sequences to the east of the Scottsdale Batholith. | |
| **REGIONAL ASPECTS/GENERAL GEOLOGICAL DESCRIPTION:** The dominance of fine-grained sandstone over siltstone has been used to distinguish the formation from the underlying Lone Star Siltstone. | |
| **EXTENT:** The formation extends to the north adjacent to the Sottsdale Batholith as far as the coast near Bridport and also for about 5 km southeast of the type locality on the Tasman Highway. | |
| **GEOMORPHIC EXPRESSION:** Undulating, elevated to hilly ground which is similar to that of the adjacent unit. | |
| **THICKNESS VARIATIONS:** Unknown variations in thickness. | |
| **STRUCTURE AND METAMORPHISM:** Structural style is upright to steeply inclined, generally open to close folds with an axial planar penetrative slaty cleavage in the finer-grained lithologies. Metamorphism is anchizonal (200–300°C, sub-greenschist facies) according to Patison *et al.* (2001), with hornblende hornfels facies adjacent to the Scottsdale Batholith. | |
| **ALTERATION AND MINERALISATION:** None. | |

**GEOPHYSICAL EXPRESSION:** Variable expression at intermediate intensity of all three channels on K-Th-U RGB images of airborne radiometric data.

**GEOCHEMISTRY:** Using the geochemical classification of Herron (1988) the sandstones are litharenite and the siltstones are wacke or shale.

**GENESIS/DEPOSITIONAL ENVIRONMENT:** Marine, probably largely deposited in one or more sandy submarine fan complexes. Based on geochemical classification the formation was deposited in a passive margin tectonic setting (Roser and Korsch, 1986) and had a quartzose sedimentary provenance (Roser and Korsch, 1988).

**COMMENTS:**

**REFERENCES:**

Banks, M. R. 1962. Silurian and Devonian systems, *in:* SPRY, A.; BANKS, M. R. (ed.). The geology of Tasmania. *Journal of the Geological Society of Australia* 9(2):177–187.

Cookson, I. C. 1937. The occurrence of fossil plants at Warrentinna, Tasmania. *Papers and Proceedings Royal Society of Tasmania* 1936:73–78.

Herron, M. M. 1988. Geochemical classification of terrigenous sands and shales from core or log data. *Journal of Sedimentary Petrology* 58:820–829.

Patison, N. L.; Berry, R. F.; Davidson, G. J.; Taylor, B. P.; Bottrill, R. S.; Manzi, B.; Ryba, J.; Shepherd, R. E. 2001. Regional metamorphism of the Mathinna Group, northeast Tasmania. *Australian Journal of Earth Sciences* 48:281–292.

Roser, B. P.; Korsch R. J. 1986. Determination of tectonic setting of sandstone-mudstone suites using $SiO_2$ content and $K_2O/Na_2O$ ratio. *Journal of Geology* 94:635–650.

Roser, B. P.; Korsch, R. J. 1988. Provenance signatures of sandstone-mudstone suites determined using discriminant function analysis of major element data. *Chemical Geology* 67:119–139.

## DEFINITION CARD (update)

| | |
|---|---|
| **NAME OF UNIT:** Panama Group | **STATE(S):** Tasmania |
| **STATUS OF UNIT:** Formal – ASUD Strat. No. 36814 | **RANK:** Group |
| **PROPOSER:** David Seymour, Mineral Resources Tasmania | **DATE:** 10/09/2010 |
| **RESERVED IN STRATIGRAPHIC UNITS DATABASE:** YES | |
| **PROPOSED PUBLICATION:** For update: Seymour, D. B.; Woolward, I. R.; McClenaghan, M. P. 2011. Stratigraphic revision and re-mapping of the Mathinna Supergroup between the River Tamar and the Scottsdale Batholith, northeast Tasmania. *Mineral Resources Tasmania, 1:25 000 Scale Digital Geological Map Series Explanatory Report* 4. | |

**DERIVATION OF NAME:** After Panama Ridge (GDA94 Zone 55, 523830 mE, 5440000 mN).

**SYNONYMY, UNIT NAME HISTORY:** Existing formal ASUD unit, Strat. No. 36814; this is an update for the Definition Card.

**CONSTITUENT UNIT:** Yarrow Creek Mudstone, Retreat Formation, Lone Star Siltstone, Sideling Sandstone, Scamander Formation. Note: Sideling Sandstone and Scamander Formation are partial lateral equivalents of each other.

**PARENT UNIT:** Mathinna Supergroup

**TYPE LOCALITY:** No single type locality specified. Refer to type locality information for constituent formations (see above).

**CONFIDENTIAL TYPE LOCALITY?:** No

**DESCRIPTION AT TYPE LOCALITY:** Alternating megasequences of dominantly thin-bedded mudstone-siltstone with minor or subordinate sandstone (Yarrow Creek Mudstone, Lone Star Siltstone) and quartz-rich sandstone-dominated turbidites deposited in submarine fan complexes (Retreat Formation, Sideling Sandstone, Scamander Formation).

**LITHOLOGY:** Thin-bedded mudstone-siltstone with generally minor fine-grained quartz-rich sandstone, or medium to thick-bedded quartz-rich sandstone (commonly classical Bouma turbidites) with generally minor interbedded shale-mudstone-siltstone.

**THICKNESS:** Estimated from structural sections, in the range 4500–6000 m (but top not exposed).

**FOSSILS:** Late Silurian (Ludlow) graptolites in Lone Star Siltstone; Late Silurian and Early Devonian plant fossils in Sideling Sandstone; Early Devonian plant fossils, graptolites and marine macrofossils in Scamander Formation.

**DIASTEMS OR HIATUSES:** None known.

**RELATIONSHIPS & BOUNDARY CRITERIA:** Inferred fault contact with, and inferred unconformable relationship with, Ordovician Turquoise Bluff Slate. Distinguished from high-strain recumbently folded generally non-turbiditic pelitic slate of the Turquoise Bluff Slate by an abrupt change to low-medium strain upright-folded turbidite-dominated facies of the Panama Group. Stratigraphic top not exposed, but is unconformably overlain by extrusive Middle Devonian St Marys Porphyry or intruded by Middle Devonian granitoids.

**DISTINGUISHING OR IDENTIFYING FEATURES:** Sandy turbidite-bearing megasequence containing Silurian to Early Devonian fossils and lacking Ordovician fossils and high-strain recumbent fold structures.

**AGE & EVIDENCE:** Inferred unconformable relationship with Ordovician Turquoise Bluff Slate. Contains Late Silurian graptolites, and Early Devonian plant, graptolite and marine macrofossils. Unconformably overlain by Middle Devonian extrusive St Marys Porphyry (Rb-Sr age 388 1 Ma, Turner *et al.*, 1986).

**CORRELATION WITH OTHER UNITS:** May occupy all of the Mathinna Supergroup outcrop area east of the currently known extent of the Tippogoree Group; however second-generation regional mapping (at 1:25 000 scale) needs to be completed to be sure of this.

| |
|---|
| **REGIONAL ASPECTS/GENERAL GEOLOGICAL DESCRIPTION:** |
| **EXTENT:** As noted above, may occupy all of the Mathinna Supergroup outcrop area east of the currently known extent of the Tippogoree Group in northeast Tasmania. |
| **GEOMORPHIC EXPRESSION:** Variable, from dissected undulating low to mid-level plateau country on the pelitic formations, to higher dissected hilly to ridge country on the sandstone-rich units and within contact metamorphic zones adjacent to mid-Devonian granitoids. |
| **THICKNESS VARIATIONS:** No information |
| **STRUCTURE AND METAMORPHISM:** Generally upright to steeply inclined open to close folds with a tendency to chevron morphology, associated moderately to steeply dipping thrust faults, and moderately developed axial plane cleavages. Regional metamorphic grade is dominantly anchizonal (200–300°C, sub-greenschist facies) (Patison *et al.*, 2001). Contact metamorphism in aureoles around mid-Devonian granitoids reaches hornblende hornfels facies. |
| **ALTERATION AND MINERALISATION:** The Panama Group is host to important orogenic gold mineralisation associated with the last major phase of Devonian deformation. |
| **GEOPHYSICAL EXPRESSION:** Variable. Characterised in some areas on K-Th-U (RGB) radiometric imagery by lack of response in all channels (i.e. dark image) over sandstone-rich units, and strong response in all channels (i.e. bright image) over pelite-rich units. However this is not a general rule, partially due to response modification by contact metamorphism. |
| **GEOCHEMISTRY:** On standard discrimination diagrams, geochemical signatures show clear indications of a dominantly passive margin sedimentary environment with a quartzose sedimentary provenance. |
| **GENESIS/DEPOSITIONAL ENVIRONMENT:** Marine, alternating between background to distal turbidite pelitic sedimentation, and sandy turbidite-dominated deposition in overlapping and coalescing submarine fan complexes. |
| **COMMENTS:** |
| **REFERENCES:**<br>Patison, N. L.; Berry, R. F.; Davidson, G. J.; Taylor, B. P.; Bottrill, R. S.; Manzi, B.; Ryba, J.; Shepherd, R. E. 2001. Regional metamorphism of the Mathinna Group, northeast Tasmania. *Australian Journal of Earth Sciences* 48:281–292.<br>Turner, N. J.; Black, L. P.; Higgins, N. C. 1986. The St Marys Porphyrite – a Devonian ash-flow and its feeder. *Australian Journal of Earth Sciences* 33:201–218. |

# APPENDIX 2
## Palaeontology and biostratigraphy

## Palaeontological identification reports on new graptolite fossil localities within the Lone Star Siltstone

***Dr Tatyana Koren and Dr Anna Suyarkova***
*A.P. Karpinsky Russian Geological Research Institute (VSEGEI)*
*74 Sredny Pr., St-Petersburg 199106, Russia*

*(with additional background information by D. B. Seymour)*

### *LOCALITY 1: Boags Ridge (542240/5411665, Ben Nevis 1:25 000 scale map sheet)*

This locality was discovered in 2005 during pre-*TasExplore* reconnaissance fieldwork by D. B. Seymour in an area of Mathinna Supergroup outcrop in the Burns Creek area, some 11.5 km southeast of the southeastern extremity of the area covered by the parent report of this Appendix. The Boags Ridge graptolites are hosted in a pyritic black shale interval, part of a sequence which is now considered to be a correlate of the Lone Star Siltstone. Species identifications within the assemblage are listed below, organised according to Registered Sample numbers within Mineral Resources Tasmania's rock sample collection and database.

| | |
|---|---|
| R012401 | *Pseudomonoclimacis* cf. *dalejensis* (Boucek)<br>*Monograptus* cf. *insignitus* (Pribyl)<br>Badly preserved and deformed rhabdosomes. |
| R012402 | *Monograptus insignitus* (Pribyl) |
| R012403 | *Bohemograptus* sp. nov. |
| R012404 | *Polonograptus* sp. indet. or *Egregiograptus* sp. indet.<br>(a fragment of the ventrally curved and broad rhabdosome up the slide)<br>*Pseudomonoclimacis dalejensis* (Boucek)<br>*Bohemograptus* sp. indet. (in the left corner down the slide) |
| R012405 | *Bohemograptus* sp. nov.<br>*Pseudomonoclimacis* cf. *dalejensis* (Boucek) |
| R012407 | *Bohemograptus* sp. nov.<br>Unidentifiable deformed monograptids |
| R012408 | *Pseudomonoclimacis dalejensis* (Boucek) |
| R012409 | *Monograptus insignitus* (Pribyl)<br>*Bohemograptus* sp. nov.<br>*Bohemograptus* cf. *tenuis* (Boucek) |
| R012410 | *Bohemograptus tenuis*<br>*Monograptus insignitus* (Pribyl) |
| R0124013 | *Linograptus posthumus* (R. Richter)<br>Unidentifiable deformed monograptids |
| R0124015 | *Bohemograptus* sp. nov.<br>*Bohemograptus tenuis*<br>Unidentifiable deformed monograptids |
| R0124017 | *Bohemograptus* sp. nov.<br>*Bohemograptus tenuis* (Boucek)<br>*Pseudomonoclimacis dalejensis* (Boucek) |
| R0124018 | *Bohemograptus tenuis*<br>*Bohemograptus* sp. nov.<br>*Monograptus insignitus* (Pribyl) |
| R0124019 | *Bohemograptus* sp. nov.<br>*Monograptus insignitus*<br>*Linograptus posthumus* (R. Richter) |
| R0124020 | *Linograptus posthumus* (R. Richter) |

| | |
|---|---|
| R0124022 | *Bohemograptus* sp. nov.<br>*Monograptus insignitus* (Pribyl)<br>*Linograptus posthumus* (R. Richter) |

### Age

Ludlow, middle part of the Ludfordian; stratigraphic interval above the top of the *Saetograptus leintwardinensis* Biozone. This interval most probably is an equivalent of the combined *B. tenuis–N. kozlowskii* Biozone (Koren *et al*., 1996). An exact correlation with the regional zonal sequences of the upper Ludlow of Southern Tien Shan, Prague Basin and Poland is difficult because of an absence of *Polonograptus* and *Neocucullograptus* zonal species in the graptolite assemblage from Boags Ridge. The graptolite assemblage is very similar to that from Golden Ridge (Rickards *et al*., 1993).

## LOCALITY 2: Lisle Road (529115/5439235, Lisle 1:25 000 scale map sheet)

This is one of four new graptolite localities discovered by I. R. Woolward in the Lone Star Siltstone in 2009 during the course of geological re-mapping of the Mathinna Supergroup as part of the *TasExplore* Project. Species identifications within the assemblage are listed below, organised according to Registered Sample numbers within Mineral Resources Tasmania's rock sample collection and database.

| | |
|---|---|
| R014479 | *Bohemograptus* sp. indet. |
| R014481 | *Bohemograptus* cf. *praecornutus* Urbanek |
| R014482 | *Bohemograptus* sp. nov. |
| R014483A, B | *Linograptus posthumus introversus* Rickards et Wright<br>*Bohemograptus* sp. indet.<br>*Pristiograptus* sp. indet. |
| R014484A, B | *Linograptus posthumus introversus* Rickards et Wright |
| R014485 | *Pristiograptus* sp. indet.<br>*Bohemograptus* sp. nov. (strongly deformed) |
| R014486 | *Bohemograptus* sp. nov.<br>*Bohemograptus* sp. indet. |
| R014487A, B | *Monograptus insignitus* (Pribyl) |
| R014488 | *Bohemograptus* sp. nov. |
| R014489 | *Monograptus insignitus* (Pribyl)<br>*Pseudomonoclimacis* cf. *dalejensis* (Boucek) |
| R014490 | *Bohemograptus* cf. *praecornutus* Urbanek<br>*Pseudomonoclimacis* cf. *dalejensis* (Boucek) |
| R014491 | *Bohemograptus* sp. indet.<br>*Monograptus* sp. indet. |
| R014492 | *Bohemograptus* sp. nov. |
| R014493, 14494 | *?Bohemograptus* sp. indet.<br>*?Monograptus* sp. indet.<br>Strongly deformed |
| R014495 | *Monograptus insignitus* (Pribyl)<br>*Bohemograptus* sp. indet. |

### Age

Ludlow, middle part of the Ludfordian. This interval most probably is an equivalent of the combined *B. tenuis–N. kozlowskii* Biozone (Koren *et al*., 1996). *Linograptus posthumus introversus* Rickards et Wright is known from the uppermost part of the Barnby Hills Shale of New South Wales, Australia (Rickards and Wright, 1997).

## References


Koren, T. N.; Lenz, A. C.; Loydell, D. K.; Melchin, M. J.; Storch, P.; Tellek, L. 1996. Generalized graptolite zonal sequence defining Silurian time intervals for global paleogeographic studies. *Lethaia* 29:59–60.

Rickards, R. B.; Davidson, G. J.; Banks, M. R. 1993. Silurian (Ludlow) graptolites from Golden Ridge, NE Tasmania. *Memoirs Association of Australasian Palaeontologists* 15:125–135.

Rickards, R. B.; Wright, A. J. 1997. Graptolites of the Barnby Hills Shale (Silurian, Ludlow), New South Wales, Australia. *Proceedings of the Yorkshire Geological Society* 51:209–227.

# APPENDIX 3
## Major and trace element analyses of samples from the Lone Star Siltstone and Sideling Sandstone

| Reg. No. | R014436 | R014437 | R014438 | R014439 | R014440 | R014441 | R014442 | R014443 | R0144448 |
|---|---|---|---|---|---|---|---|---|---|
| Field No. | 1124 | 60 | 672 | 674 | 677 | 673 | 692 | 697 | 700 |
| GDA94 mE | 525567 | 529952 | 528545 | 530798 | 531603 | 529921 | 530382 | 530383 | 523318 |
| GDA94 mN | 5432633 | 5433345 | 5428897 | 5426693 | 5422194 | 5433370 | 5443062 | 5443063 | 5436963 |
| $SiO_2$ | 71.50 | 54.02 | 68.27 | 72.30 | 66.32 | 65.81 | 70.87 | 69.11 | 66.73 |
| $TiO_2$ | 0.74 | 0.84 | 0.71 | 0.80 | 0.74 | 0.72 | 0.84 | 0.80 | 0.76 |
| $Al_2O_3$ | 14.25 | 23.60 | 14.54 | 15.33 | 15.88 | 17.44 | 16.03 | 18.02 | 16.95 |
| $Fe_2O_3$ | 1.42 | 6.70 | 1.64 | 2.08 | 3.41 | 4.28 | 1.40 | 2.16 | 5.66 |
| FeO | 1.1 | 0.7 | 4.1 | 0.1 | 2.4 | 1 | 0.3 | 0.2 | 0.2 |
| MnO | 0.03 | 0.13 | 0.08 | 0.01 | 0.09 | 0.11 | 0.01 | 0.03 | 0.02 |
| MgO | 1.47 | 1.75 | 2.43 | 0.68 | 2.28 | 1.34 | 0.49 | 0.37 | 0.46 |
| CaO | 0.09 | 0.01 | 0.04 | 0.03 | 0.03 | 0.01 | 0.01 | 0.01 | 0.01 |
| $Na_2O$ | 0.01 | 0.13 | 0.18 | 0.00 | 0.36 | 0.07 | 0.39 | 0.30 | 0.01 |
| $K_2O$ | 3.60 | 4.38 | 3.25 | 3.80 | 3.96 | 3.59 | 3.67 | 3.80 | 3.86 |
| $P_2O_5$ | 0.07 | 0.07 | 0.07 | 0.04 | 0.05 | 0.04 | 0.01 | 0.00 | 0.06 |
| $SO_3$ | 0.04 | 0.01 | 0.01 | 0.01 | 0.01 | 0.01 | 0.01 | 0.01 | 0.01 |
| $CO_2$ | 0.5 | 0.5 | 0.1 | 0.5 | 0.1 | 0.3 | 0.5 | 0.1 | 0.1 |
| $H_2O^+$ | 4.76 | 6.45 | 3.82 | 3.64 | 3.64 | 4.33 | 4.43 | 4.22 | 4.30 |
| TOTAL | 99.56 | 99.27 | 99.25 | 99.32 | 99.25 | 99.05 | 98.96 | 99.13 | 99.13 |
| LOI | 5.14 | 6.87 | 3.46 | 4.13 | 3.47 | 4.52 | 4.89 | 4.29 | 4.38 |
| As | -3 | -3 | 17 | 10 | -3 | -3 | -3 | 24 | -3 |
| Ba | 470 | 835 | 480 | 640 | 520 | 670 | 500 | 550 | 590 |
| Bi | -1 | -1 | 1 | -1 | 1 | -1 | -1 | -1 | 1 |
| Ce | 99 | 115 | 82 | 190 | 85 | 95 | 71 | 63 | 92 |
| Cl | 40 | 40 | 30 | 30 | 30 | 20 | 9250 | 8360 | 90 |
| Co | -2 | 15 | 6 | -2 | 18 | 12 | -2 | -2 | 3 |
| Cr | 90 | 115 | 84 | 84 | 88 | 98 | 99 | 97 | 97 |
| Cs | 9 | 10 | 6 | 8 | 11 | 7 | 6 | 4 | 10 |
| Cu | 9 | 62 | 16 | 23 | 21 | 60 | 6 | 14 | 31 |
| Ga | 20 | 27 | 21 | 20 | 21 | 23 | 21 | 23 | 22 |
| La | 55 | 105 | 43 | 99 | 53 | 58 | 36 | 32 | 42 |
| Mo | 5 | -1 | -1 | 1 | -1 | -1 | 1 | -1 | -1 |
| Nb | 19 | 18 | 17 | 18 | 18 | 17 | 21 | 20 | 18 |
| Nd | 43 | 67 | 31 | 80 | 34 | 47 | 27 | 28 | 30 |
| Ni | 11 | 45 | 29 | 9 | 38 | 34 | 5 | 21 | 12 |
| Pb | 58 | 37 | 10 | 22 | 17 | 33 | 38 | 19 | 19 |
| Rb | 180 | 290 | 175 | 185 | 200 | 170 | 145 | 125 | 200 |
| S | 3200 | 0 | 0 | 0 | 0 | 0 | 200 | 100 | 0 |
| Sb | -2 | -2 | -2 | 7 | 2 | 3 | 4 | 5 | 2 |
| Sc | 14 | 20 | 14 | 13 | 15 | 17 | 19 | 20 | 17 |
| Sn | 3 | 6 | 4 | 4 | 4 | 5 | 5 | 5 | 4 |
| Sr | 19 | 45 | 21 | 48 | 34 | 34 | 44 | 44 | 31 |
| Th | 19 | 19 | 17 | 19 | 17 | 19 | 22 | 22 | 18 |
| U | 5 | 5 | 4 | 6 | 3 | 5 | 5 | 4 | 5 |
| V | 135 | 135 | 115 | 120 | 110 | 125 | 130 | 110 | 125 |
| W | 4 | 2 | 3 | 5 | 3 | 4 | 5 | 3 | 4 |
| Y | 45 | 37 | 34 | 38 | 31 | 27 | 28 | 30 | 24 |
| Zn | 26 | 135 | 83 | 18 | 105 | 85 | 14 | 68 | 36 |
| Zr | 210 | 190 | 210 | 270 | 190 | 170 | 240 | 195 | 190 |

| Reg. No. | R014445 | R014446 | R014447 | R014448 | R014449 | R014450 | R013517 | R013519 | R013520 |
|---|---|---|---|---|---|---|---|---|---|
| Field No. | 701 | 705 | 912 | 1235 | 692+10 | 767 | MNET46 | MNET48 | MNET49 |
| GDA94 mE | 521750 | 529214 | 523836 | 523824 | 530382 | 531417 | 532837 | 535242 | 535532 |
| GDA94 mN | 5436713 | 5434539 | 5432480 | 5432467 | 5443062 | 5433471 | 5449875 | 5431142 | 5433568 |
| $SiO_2$ | 66.52 | 66.85 | 68.05 | 70.25 | 34.84 | 70.60 | 68.37 | 80.68 | 83.26 |
| $TiO_2$ | 0.81 | 0.67 | 0.67 | 0.63 | 0.30 | 0.65 | 0.71 | 0.56 | 0.5 |
| $Al_2O_3$ | 20.50 | 16.45 | 15.27 | 14.82 | 7.68 | 14.42 | 15.73 | 9.59 | 8.68 |
| $Fe_2O_3$ | 0.97 | 0.46 | 2.04 | 0.93 | 44.43 | 1.84 | 0.4439 | 1.2213 | 0.5613 |
| FeO | 0.1 | 5.9 | 0.8 | 1.5 | 0.4 | 2.9 | 5.1 | 1.7 | 1.7 |
| MnO | 0.01 | 0.15 | 0.02 | 0.02 | 0.03 | 0.12 | 0.08 | 0 | 0 |
| MgO | 0.61 | 2.42 | 0.81 | 1.17 | 0.29 | 1.84 | 2.22 | 1.14 | 0.86 |
| CaO | 0.01 | 0.19 | 0.05 | 0.10 | 0.02 | 0.02 | 0.18 | 0.05 | 0 |
| $Na_2O$ | 0.00 | 0.64 | 0.61 | 0.82 | 0.36 | 0.36 | 0.92 | 0.4 | 0.24 |
| $K_2O$ | 4.20 | 4.21 | 3.65 | 3.12 | 1.14 | 3.33 | 4.1 | 2.23 | 1.76 |
| $P_2O_5$ | 0.00 | 0.08 | 0.06 | 0.03 | 1.04 | 0.05 | 0.1 | 0.11 | 0.12 |
| $SO_3$ | 0.01 | 0.01 | 0.01 | 0.01 | 0.02 | 0.01 | | | |
| $CO_2$ | 0.3 | 0.1 | 1 | 0.9 | 1.4 | 0.2 | 0.1 | 0.2 | 0.2 |
| $H_2O^+$ | 5.03 | 1.57 | 5.94 | 5.10 | 7.81 | 3.26 | 1.73 | 2.11 | 2.12 |
| TOTAL | 99.07 | 99.70 | 98.97 | 99.40 | 99.76 | 99.60 | 99.78 | 99.99 | 100 |
| LOI | 5.32 | 1.02 | 6.85 | 5.84 | 9.16 | 3.14 | 1.26 | 2.12 | 2.13 |
| As | 7 | -3 | 16 | 11 | 30 | -3 | -3 | -3 | 9 |
| Ba | 590 | 530 | 550 | 500 | 180 | 520 | 609 | 415 | 383 |
| Bi | -1 | -1 | -1 | -1 | 27 | 1 | -1 | -1 | -1 |
| Ce | 160 | 76 | 87 | 60 | 31 | 105 | 78 | 73 | 65 |
| Cl | 70 | 50 | 20 | 50 | 100 | 20 | 120 | 90 | 100 |
| Co | -2 | 14 | 3 | 2 | 5 | 11 | 14 | 9 | 6 |
| Cr | 110 | 94 | 130 | 150 | 72 | 85 | 99 | 71 | 67 |
| Cs | 10 | 16 | 14 | 14 | 5 | 8 | 13 | 8 | -3 |
| Cu | 13 | 22 | 13 | 9 | 58 | 51 | 31 | 17 | 15 |
| Ga | 24 | 21 | 21 | 20 | 23 | 19 | 20 | 12 | 11 |
| La | 68 | 53 | 48 | 36 | 53 | 54 | 49 | 33 | 23 |
| Mo | -1 | -1 | 1 | -1 | -1 | -1 | -1 | 1 | 1 |
| Nb | 18 | 14 | 15 | 14 | 5 | 15 | 15 | 14 | 13 |
| Nd | 51 | 32 | 46 | 23 | bdl | 53 | 38 | 30 | 27 |
| Ni | 9 | 36 | 13 | 18 | bdl | 31 | 36 | 30 | 26 |
| Pb | 33 | 23 | 25 | 22 | 125 | 20 | 14 | 14 | 8 |
| Rb | 220 | 210 | 185 | 160 | 73 | 170 | 199 | 106 | 77 |
| S | 0 | 0 | 400 | 100 | 1200 | 0 | 100 | 100 | 100 |
| Sb | 3 | -2 | 3 | 5 | -2 | 3 | -2 | 3 | 5 |
| Sc | 19 | 15 | 11 | 11 | 18 | 14 | 15 | 6 | 7 |
| Sn | 5 | 4 | 5 | 7 | 6 | 4 | 3 | 4 | 5 |
| Sr | 25 | 54 | 175 | 54 | 18 | 25 | 70 | 25 | 10 |
| Th | 19 | 14 | 16 | 13 | -2 | 16 | 15 | 14 | 13 |
| U | 5 | 4 | 4 | 3 | 4 | 4 | 4 | 4 | 3 |
| V | 105 | 110 | 210 | 170 | 57 | 105 | 119 | 63 | 59 |
| W | 4 | 2 | 4 | 3 | 12 | 3 | -2 | 3 | 3 |
| Y | 34 | 29 | 33 | 26 | 16 | 40 | 29 | 26 | 26 |
| Zn | 16 | 91 | 49 | 43 | 45 | 110 | 98 | 71 | 54 |
| Zr | 170 | 130 | 175 | 170 | 82 | 155 | 149 | 339 | 343 |

| Reg. No. | R013521 | R013522 | R013540 | R013541 | R013542 | R013549 | R013553 | R013554 |
|---|---|---|---|---|---|---|---|---|
| Field No. | MNET50 | MNET51 | MNET69 | MNET70 | MNET71 | MNET78 | MNET82 | MNET83 |
| GDA94 mE | 533089 | 532828 | 529177 | 532143 | 532359 | 530351 | 532827 | 530602 |
| GDA94 mN | 5435283 | 5436969 | 5434513 | 5453955 | 5453973 | 5443075 | 5431620 | 5432052 |
| $SiO_2$ | 70.34 | 67.8 | 65.56 | 83.05 | 87.21 | 67.07 | 60.73 | 65.36 |
| $TiO_2$ | 0.59 | 0.69 | 0.72 | 0.43 | 0.36 | 0.76 | 0.84 | 0.66 |
| $Al_2O_3$ | 14.32 | 15.5 | 17.34 | 8 | 6.58 | 18.22 | 20.03 | 15.88 |
| $Fe_2O_3$ | 2.4758 | 3.9713 | 0.815 | 1.0113 | 0.4279 | 3.3545 | 1.4304 | 1.445 |
| FeO | 2.2 | 1.7 | 5 | 1.7 | 1.1 | 0.5 | 3.6 | 5 |
| MnO | 0.13 | 0.11 | 0.2 | 0.07 | 0.03 | 0 | 0.07 | 0.23 |
| MgO | 2.02 | 1.84 | 2.4 | 1.16 | 0.57 | 0.62 | 2.51 | 2.58 |
| CaO | 0 | 0.03 | 0.34 | 0.05 | 0.08 | 0 | 0 | 0.12 |
| $Na_2O$ | 0.16 | 0.16 | 0.88 | 0.34 | 0.13 | 0.21 | 0.12 | 0.71 |
| $K_2O$ | 3.23 | 3.54 | 4.16 | 2.03 | 1.63 | 3.88 | 5.17 | 3.97 |
| $P_2O_5$ | 0.07 | 0.07 | 0.11 | 0.05 | 0.08 | 0.04 | 0.07 | 0.09 |
| $SO_3$ | | | | | | | | |
| $CO_2$ | 0.2 | 0.2 | 0.1 | 0.3 | 0.3 | 0.6 | 0.3 | 0.2 |
| $H_2O^+$ | 3.87 | 4.22 | 2.32 | 1.71 | 1.39 | 4.41 | 4.63 | 3.61 |
| TOTAL | 99.61 | 99.83 | 99.95 | 99.9 | 99.89 | 99.66 | 99.5 | 99.86 |
| LOI | 3.83 | 4.23 | 1.86 | 1.82 | 1.57 | 4.95 | 4.53 | 3.25 |
| As | -3 | 15 | 12 | -3 | 3 | 3 | 6 | -3 |
| Ba | 720 | 602 | 634 | 361 | 349 | 511 | 795 | 596 |
| Bi | -1 | 1 | 1 | -1 | -1 | -1 | 1 | -1 |
| Ce | 106 | 69 | 92 | 56 | 51 | 71 | 100 | 32 |
| Cl | 90 | 90 | 70 | 70 | 70 | 280 | 120 | 90 |
| Co | 11 | 9 | 20 | 8 | 4 | -2 | 8 | 14 |
| Cr | 76 | 92 | 99 | 50 | 40 | 100 | 124 | 87 |
| Cs | 9 | 7 | 15 | 14 | 6 | -3 | 13 | 12 |
| Cu | 35 | 26 | 22 | 9 | 17 | 9 | 25 | 28 |
| Ga | 19 | 21 | 23 | 10 | 7 | 21 | 25 | 21 |
| La | 58 | 42 | 60 | 29 | 16 | 34 | 66 | 35 |
| Mo | -1 | -1 | -1 | -1 | -1 | -1 | -1 | -1 |
| Nb | 13 | 16 | 14 | 11 | 9 | 18 | 16 | 15 |
| Nd | 35 | 26 | 38 | 20 | 18 | 24 | 50 | 20 |
| Ni | 32 | 38 | 41 | 15 | 13 | 3 | 28 | 37 |
| Pb | 20 | 23 | 31 | 13 | 11 | 27 | 31 | 9 |
| Rb | 161 | 190 | 196 | 150 | 84 | 157 | 258 | 196 |
| S | 100 | 100 | 100 | 200 | 100 | 100 | 100 | 100 |
| Sb | 2 | 7 | 2 | 3 | 3 | 3 | 3 | -2 |
| Sc | 14 | 15 | 17 | 8 | 5 | 16 | 19 | 14 |
| Sn | 5 | 6 | 5 | 3 | 2 | 4 | 6 | 4 |
| Sr | 22 | 22 | 88 | 15 | 15 | 37 | 41 | 28 |
| Th | 13 | 14 | 17 | 9 | 8 | 17 | 18 | 15 |
| U | 3 | 4 | 6 | 4 | 2 | 4 | 5 | 4 |
| V | 99 | 111 | 127 | 50 | 44 | 107 | 154 | 105 |
| W | 3 | 3 | 2 | -2 | 3 | 4 | 3 | -2 |
| Y | 28 | 20 | 29 | 24 | 24 | 27 | 34 | 17 |
| Zn | 95 | 107 | 108 | 44 | 21 | 21 | 82 | 98 |
| Zr | 134 | 155 | 140 | 206 | 215 | 178 | 160 | 137 |